8-3-2006

A Comparison of Change Detection Methods in an Urban Environment Using LANDSAT TM and ETM+ Satellite Imagery: A Multi-Temporal, Multi-Spectral Analysis of Gwinnett County, GA 1991-2000

Paul Alrik DiGirolamo

A COMPARISON OF CHANGE DETECTION METHODS IN AN URBAN ENVIRONMENT USING LANDSAT TM AND ETM+ SATELLITE IMAGERY: A MULTI-TEMPORAL, MULTI-SPECTRAL ANALYSIS OF GWINNETT COUNTY, GA 1991-2000

by

PAUL A. DIGIROLAMO

Under the Direction of Zhi-Yong Yin

ABSTRACT

Land cover change detection in urban areas provides valuable data on loss of forest and agricultural land to residential and commercial development. Using Landsat 5 Thematic Mapper (1991) and Landsat 7 ETM+ (2000) imagery of Gwinnett County, GA, change images were obtained using image differencing of Normalized Difference Vegetation Index (NDVI), principal components analysis (PCA), and Tasseled Cap-transformed images. Ground truthing and accuracy assessment determined that land cover change detection using the NDVI and Tasseled Cap image transformation methods performed best in the study area, while PCA performed the worst of the three methods assessed. Analyses on vegetative and vegetation changes from 1991-2000 revealed that these methods perform well for detecting changes in vegetation and/or vegetative characteristics but do not always correspond with changes in land use. Gwinnett County lost an estimated 13,500 hectares of vegetation cover during the study period to urban sprawl, with the majority of the loss coming from forested areas.

INDEX WORDS: Change Detection, Image Differencing, NDVI, Tasseled Cap, Principal Components Analysis, Landsat, Remote Sensing, Vegetation Index, Land Cover, Deforestation, Urban Sprawl

A COMPARISON OF CHANGE DETECTION METHODS IN AN URBAN ENVIRONMENT USING LANDSAT TM AND ETM+ SATELLITE IMAGERY: A MULTI-TEMPORAL, MULTI-SPECTRAL ANALYSIS OF GWINNETT COUNTY, GA 1991-2000

by

PAUL A. DIGIROLAMO

A Thesis Submitted in Partial Fulfillment of the Requirements for the Degree of

Master of Arts

Georgia State University

2006

A COMPARISON OF CHANGE DETECTION METHODS IN AN URBAN ENVIRONMENT USING LANDSAT TM AND ETM+ SATELLITE IMAGERY: A MULTI-TEMPORAL, MULTI-SPECTRAL ANALYSIS OF GWINNETT COUNTY, GA 1991-2000

by

PAUL A. DIGIROLAMO

Major Professor:	Dr. Zhi-Yong Yin
Committee:	Dr. Paul Knapp
	Dr. Truman Hartshorn

Electronic Version Approved:

Office of Graduate Studies
College of Arts and Sciences
Georgia State University
June 2006

DEDICATION

This thesis paper is dedicated to my parents, Mario and Gay DiGirolamo, without whose help and support my education would not have been possible. It is also dedicated to my sisters and brothers, Ann, Julia, Mark and Michael, and friend Melissa Beatty, as thanks for their support and encouragement in completing this project.

ACKNOWLEDGEMENTS

I would like to acknowledge the expertise and assistance of my committee members, Dr. Zhi Yong Yin, Dr. Paul Knapp and Dr. Truman Hartshorn, for their guidance and support in completing this thesis. I would also like to acknowledge all of the other talented teachers and professionals at Georgia State University that helped me to complete my program of study including Dr. John Allensworth, Dr. Jeremy Crampton, Dr. Jeremy Diem, Elaine Hallisey-Hendrix, Jeff McMichael, Dr. Dona Stewart, and Dr. Susan Walcott.

TABLE OF CONTENTS

LIST OF FIGURES

Page

LIST OF TABLES

Page

LIST OF ABBREVIATIONS

ABBREVIATION	MEANING
AOI	Area of Interest
ARC	Atlanta Regional Commission
ARIS	Atlanta Region Information System
BV	Brightness Values
CIR	Color Infrared
DEM	Digital Elevation Model
DN	Digital Number
DOQQ	Digital Orthorectified Quarter Quad
GCP	Ground Control Point
GIS	Geographic Information Systems
IR	Infrared
(Landsat) ETM+	Enhanced Thematic Mapper +
(Landsat) TM	Thematic Mapper
MSA	Metropolitan Statistical Area
NDVI	Normalized Difference Vegetation Index
NED	National Elevation Dataset
NOAA	National Oceanic and Atmospheric Administration
PCA	Principal Components Analysis
PDSI	Palmer Drought Severity Index
PIF	Pseudo-Invariant Feature

SAR	Synthetic Aperture Radar
SOV	Single Occupancy Vehicle
TCT	Tasseled Cap Transformation
UGA	University of Georgia
USGS	United States Geological Survey

CHAPTER ONE: INTRODUCTION AND LITERATURE REVIEW

1. Recent Research in Environmental Remote Sensing

Global and Regional Environmental Applications of Remote Sensing Data

Land cover change detection using remote sensing satellite imagery is a powerful tool for monitoring urbanization and the resulting loss of forest and agricultural land. Planners, lawmakers, community leaders, and others rely on accurate data in decision making and planning for future growth and development. Environmental quality is threatened in many urban areas around the globe by the rapid spread of low-density, automobile-oriented development known as urban sprawl. Public and political opinion is evolving as awareness of the environmental, economic, and social impacts of sprawl become clearer. Satellite imagery offers a unique multi-temporal, multi-spectral, and synoptic perspective on urbanization at regional scales (Lambin, 1999), providing valuable data for monitoring and assessment of change.

Many satellite platforms and sensors currently in use capturing earth imaging data are building a global library of earth surface data, particularly relevant in environmental "hot spots" such as the Amazon Basin, Africa and Madagascar, Southeast Asia, China and the American Pacific Northwest. Crucial conservation work is being done in these and other areas, and remote sensing data makes possible a unique perspective free of the constraints of political borders and topographic obstacles (Lillesand & Kiefer, 2000). Some of the most recent research and applications include projects ranging from global scale monitoring to intensive research in high-risk regions.

Examples of recent global scale research include the Global Rain Forest Mapping Project (GRFM), an international collaborative effort managed by the National Space Development

Agency of Japan, which is currently working towards a high-resolution map of the entire rain forest on four continents from SAR imagery and the JERS-1 satellite (Mayaux et al., 2000). The UN Food and Agriculture Organization's Forest Resources Assessment (FRA) program commissioned a 5-class global forest cover map from satellite data at the USGS EROS Data Centre in 2000 in order to give a global synopsis of forest resources in the world (Zhu, 2003). Another recent project with USGS involvement is a 2000 Land Cover Map of North and Central America by NRCan/CCRS and USGS/EROS Data Centre, produced from SPOT imagery as part of a 22-class global land cover product currently being assembled (Zhu et al., 2004). NASA has also been heavily involved in remote sensing research, including the recent program in which the Moderate Resolution Imaging Spectroradiometer (MODIS) sensor onboard the Earth Observing System (EOS) satellite is being used to develop a 250 meter resolution global land cover change product, to find areas of rapid human-induced land cover change for future higher-resolution research (Defries et al., 2000). Other recent NASA projects using remote sensing for global scale environmental monitoring include the Humid Tropical Landsat Pathfinder project and the Tropical Ecosystem Environment observation by Satellite (TREES) program, both using high-resolution data to assess the current health and extent, and future threats to tropical rain forests (Defries & Townshend, 1999). Finally, no discussion of global scale remote sensing data would be complete without mentioning the nearly 20 year record of global satellite observations of vegetation phenology from NOAA's Advanced Very High Resolution Radiometer (AVHRR) sensor, a 1 km resolution dataset long used for monitoring global drought conditions using NDVI and locating areas of major ecosystem disturbance events (Potter et al., 2003).

On a regional scale, it appears that the majority of current work and research in environmental monitoring by remote sensing satellite is taking place in regions of rapid changes

during the past 5 decades, such as the Amazon Basin and across Africa, and to a lesser extent over China, Southeast Asia and Indonesia, and the American Pacific Northwest. One example of current research in the Amazon Basin include a comparison of change detection techniques using Landsat TM imagery for identifying deforestation and cattle pasture formation in Rondonia, Brazil (Guild et al., 2004). Remote sensing data from many different sensors (ETM+, IKONOS, SPOT-4, SAR) has played a fundamental role in the Large Scale Biosphere Atmosphere (LBA) experiment, an international research program developed to determine how land-use and climate modify biological, chemical, and physical processes in the Amazon Basin (Roberts et al., 2003). A corollary project to the LBA experiment, researchers are seeking to understand the significance of wetlands in the Amazon basin partly by mapping the extent of wetlands for the central Amazon region using L-band synthetic aperture radar (SAR) data from the Japanese Earth Resources Satellite (JERS) (Melack et al., 2003). Lu et al. (2003) are working on an improved classification approach using a linear mixture model (LMM) to classify successional and mature forests in Rondonia, Brazil, using Landsat TM imagery. Souza et al. (2003) are mapping classes of degraded forest in the Eastern Amazon using SPOT 4 imagery, while Braswell et al. (2003) are exploring the relationships between land cover classes derived from Landsat compared to those derived from the lower-resolution MODIS data.

Widespread deforestation, desertification, burning, erosion, and other anthropogenic impacts on the environment make the African landscape a valuable and closely monitored subject of research. Recent remote sensing work in Africa includes efforts to monitor desertification and land degradation over sub-Saharan Africa using vegetation cover and surface moisture data derived from remote sensing data (Symeonakis et al., 2004), and using Landsat ETM+ imagery to identify malaria vector breeding habitats in an irrigated rice growing area in

Mali (Diuk-Wasser et al., 2004), laying the groundwork for future investigation of the relationship between cultivation practices and malaria transmission. Brivio et al. (2003) have shown remote sensing to be the most effective tool in monitoring biomass burning and its effects on natural terrestrial ecosystems in sub-Saharan Africa, using SPOT-VEGETATION and Landsat ETM+ imagery in the Global Burnt Area-2000 (GBA2000) initiative. Nonomura et al. (2003) have used Normalized Difference Vegetation Index (NDVI) data from NOAA's AVHRR sensor to devise a digital vegetation model for eco-climatic analysis and mapping of African land cover types, and NDVI data from AVHRR imagery have been used to monitor phenological cycles in semi-arid lands and ecosystems in northern Africa (Dall'Olmo & Karnieli, 2002). NDVI data from the AVHRR sensor have also been used to assess habitat regimes in Tanzania at multiple spatial and temporal scales (Pelkey et al., 2003). Additionally, in Tanzania, Landsat TM data have been used to study the impact of cattle ranching on large-scale vegetation patterns (Tobler et al., 2003).

China's rapid industrialization is having major impacts on the landscape, presenting numerous opportunities for remote sensing research and applications. Among the many interesting projects recently published include Chen's et al. (2003) use of Landsat TM and SPOT imagery and an IHS-based (Intensity-Hue-Saturation) change detection method to assess the loss of arable land in China as a result of rapid urbanization, and Runnstrom's (2003) use of Landsat and AVHRR imagery to monitor degradation of the dry semiarid ecosystems of north central China. Liu et al. (2003) combined AVHRR imagery with geophysical datasets such as climate and elevation data to derive an improved land cover classification for nine bio-climatic regions in China, and Wang et al. (2002) mapped desert vegetation types in the Tarim River Basin in Xinjiang province using aerial photography and JERS-1/OPS VNIR imagery and analyzed

changes in vegetation distribution and conditions. Seto and Kaufman (2003) integrated economic and demographic data with remote sensing to model the drivers of urban land use change in the Pearl River Delta, and Li et al. (2003) used Landsat ETM+ and NOAA/AVHRR imagery to detect, simulate and analyze the vegetation coverage of typical steppe areas in northern China.

Elsewhere in Asia, economic and population pressures and the environmental degradation caused by extractive industries are causing unprecedented land use/land cover changes. Recent monitoring efforts utilizing remote sensing data include the work of Giri et al. (2003), who used AVHRR imagery to map land cover over continental Southeast Asia and to identify "hot spots" of land cover change, which were then studied in greater detail with higher-resolution Landsat and SPOT imagery. Stibig et al. (2003) used a cloud-free mosaic of SPOT4-Vegetation 10-day composite imagery to successfully classify and map tropical forest cover at the regional level in Southeast Asia; Landsat TM imagery was used to validate the classification results. Yu et al. (2004) used NDVI data derived from NOAA/AVHRR imagery in conjunction with climate record data to study the seasonal vegetation response on the Mongolian grasslands to one of the strongest warming signals in the world over the last 30 years. Yu et al. (2004) also used similar data to study Interannual variations in grassland boundaries in the same region. Finally, Lu (2003) used ERS synthetic aperture radar (SAR) imagery to detect, monitor and map oil spills in the ocean and coastal areas of Southeast Asia.

In Indonesia, another tropical deforestation "hot spot", recent remote sensing applications include mapping of fire scars and burned areas in Kalimantan, using NOAA/AVHRR and Landsat TM imagery (Fuller and Fulk, 2001). In the same area, Siegert and Hoffmann (2000) used high-resolution, multi-temporal ERS-2 SAR imagery to evaluate the 1998 forest fires in

East Kalimantan. Kuntz and Siegert (1999) used multi-temporal ERS SAR imagery and texture analysis techniques to develop a method of continuous monitoring of land use change and deforestation in a tropical rainforest environment in Indonesia. In addition, Indrabudi et al. (1998) used remote sensing data in a holistic look at the spatial patterns of land cover changes and deforestation in an Indonesian watershed, and the driving factors of change such as population, socio-economic aspects, and land policy.

Finally, the Pacific Northwestern United States has seen deforestation of the temperate rain forest on a large scale, and appropriately, remote sensing is playing a role in the assessment and possible mitigation of further damages to these ecosystems. Boyd et al. (2002) compared the use of vegetation indices, regression analysis and neural networks for effectiveness and accuracy in estimating coniferous forest cover across the United States Pacific Northwest. Cohen et al. (2002) analyzed stand displacement disturbance and its effects on forest ecosystem processes over 4.6 million forested hectares in western Oregon, in order to develop a "spatially explicit characterization of clear-cut logging and wildfire" and to understand causes and consequences of forest disturbance. Sabol et al. (2002) have used Landsat TM imagery to identify stages of regrowth in replanted clearcuts in Douglas-fir/western hemlock forests in the Gifford Pinchot National Forest in southern Washington, while Wimberly and Spies (2001) used Landsat TM imagery along with other data to model landscape patterns of understory tree in the Oregon Coast Range. Lefsky et al. (1999) used data from a scanning LIDAR sensor and a novel three dimensional analysis technique to create volumetric characterizations of vegetation structure on 22 plots in Douglas-fir/western hemlock stands in Oregon's Cascade Range. Cohen et al. (1998) used several variations of image differencing of Landsat imagery to determine the most efficient and accurate method for mapping clearcuts in the forests of the Pacific Northwest.

Remote Sensing Research in the Atlanta Region

Several recent remote sensing studies on the Atlanta metropolitan area have examined the rapid unplanned growth pattern in the region. These studies of urban sprawl focus on changes in land cover, and their impact on environmental conditions. Gillies et al. (2003) recently used Landsat TM and MSS imagery to examine change in impervious surface from 1979 to 1997, and to explore the ecological and cumulative water impacts on mussel population in Line Creek watershed south of Atlanta. Lo and Yang (2002) used landuse/land-cover (LULC) change maps and statistics from developed from Landsat imagery for the period 1973 to 1999, along with census data to analyze drivers of LULC changes in Atlanta, revealing a pattern of agriculture and forest being replaced by residential and commercial land uses. Yang (2002) used the same 1973 to 1999 Landsat data to monitor changes in land use and assess urban growth trends along the periphery of the Atlanta metro area, finding a pattern of rapid, sprawling, and land-consuming growth in the suburban counties around Atlanta. The Lo and Yang LULC change studies are a component of Project ATLANTA (Atlanta Land-use Analysis: Temperature and Air-quality), funded by NASA in order to "derive a better scientific understanding of how land cover changes associated with urbanization in the Atlanta area, principally in transforming forest lands to urban land covers through time, has, and will, effect local and regional climate, surface energy flux, and air quality characteristics." The project is ongoing and should prove a highly valuable source of data for urban planners, environmental managers and other decision makers to help them improve the urban climate and environment in the future.

2. Goals of Current Research

This research will compare three commonly employed image algebra techniques, Normalized Difference Vegetation Index (NDVI), Tasseled Cap transformation (TCT), and principal component analysis (PCA), for effectiveness in assessing change in vegetation cover in an urban area. The primary goal of this research is to determine which of the three common remote sensing land cover change detection techniques is most accurate in this study area and for these types of biotic communities (temperate, mid-latitude urban area with a mixed-deciduous forest dominated landscape). It is also hoped that this research will help to demonstrate the tremendous utility of remote sensing data for many applications including assessment of land cover change, natural resource inventory, planning and policymaking, and education and public awareness. Such applications are of particular importance in a large, rapidly growing urban area with a complex pattern of land use and many diverse environments.

Research Questions

The following questions inform this study:

1. Which of the three commonly employed image algebra techniques results in the highest accuracy when used for vegetation and vegetative change detection in the study area?
2. What are some of the concerns, pitfalls and issues to be addressed when performing and assessing the accuracy of change detection using remote sensing data?
3. What are some ways that this type of research could be improved in future studies?
4. What are the changes in vegetation cover that have taken place in Gwinnett County GA during the study period, and why? What are the implications of this study?
5. What are the benefits of change detection using remote sensing data?

6. How useful is change detection using remote sensing data for addressing and improving the understanding of the issues related to urban sprawl?

CHAPTER TWO: DATA AND METHODS

1. Study Area Description: History, Demographics and Physical Characteristics

A Brief History of Gwinnett County, Georgia

Gwinnett County, with an area of 1,133 square kilometers, is located in north central Georgia, United States, approximately 48 kilometers northeast of the City of Atlanta (see Figure 2.1). Gwinnett County was created by the Georgia legislature in 1818 from lands formerly occupied by Native Americans of the Creek and Cherokee tribes. "In 1789 and 1790 the Cherokee Indians ceded to the United States Government all lands north and east of a line running through Kentucky, Tennessee, North and South Carolinas and north Georgia, including portions of Gwinnett." (Flanigan, 1943) White settlements began to occupy the area soon after, including major settlements on the Appalachee River near Hog Mountain and Standing Peachtree, both sites of once thriving Creek villages. Fort Daniel, which brought increasing commerce to Gwinnett, was built near Hog Mountain at the beginning of the War of 1812 to protect the settlements from attacks by the Creek Indians, who had allied themselves with the British against the white settlers. The settlement at Standing Peachtree was the border between Creek and Cherokee territories and an important point of contact between the Indians and the white settlers. A newly created road built along old Indian trails and connecting Fort Daniel and Fort Peachtree at Standing Peachtree was called Peachtree Road, and was the beginning of the region's best-known and most-traveled thoroughfare (Buckhead Civic Association, 2005). The county seat was established in Lawrenceville in 1823 (Flanigan, 1943). Gwinnett flourished as an agricultural area and greatly profited from the institution of slavery, until it was overrun by Union soldiers in 1864 during Sherman's march on Atlanta. Much of Gwinnett's wealth was lost in the Civil War and it took decades for the region to recover. Agriculture remained the primary

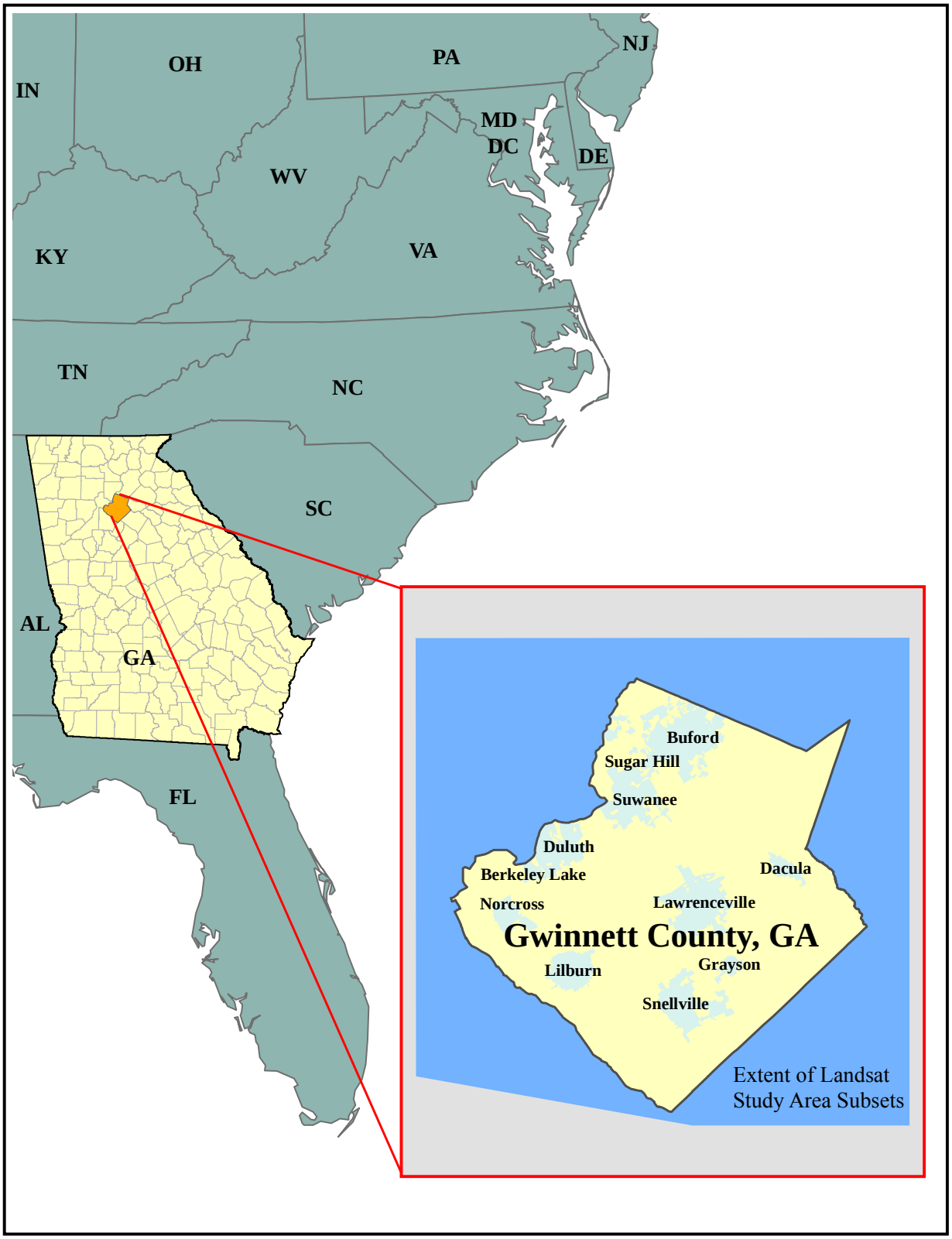

Figure 2.1. Study Area Map. Location of Gwinnett County, GA along with cities and the rectangular extent of the Landsat subset images used in the analysis.

industry in Gwinnett for the remainder of the 19th and the first part of the 20th century, with large plantations having been replaced by small farms. In the mid 1950s thousands of acres of Gwinnett County were flooded behind Buford Dam by Lake Sydney Lanier (Flanigan, 1943; Sabin, 2004). The construction of Interstate 85 through Gwinnett County in the late 1950s, and subsequently I-985 and SR 316 in the early 1960s and early 1970s, respectively (ARC, 2005), opened Gwinnett County up to the automobile-oriented form of residential and commercial development known as urban sprawl, and Gwinnett County soon became a bedroom community for the city of Atlanta. Gwinnett County was a founding member county when the Atlanta Regional Commission, the Regional Development Center (RDC) for the current ten-county planning region, was established in its current form in 1971 (ARC, 2005). Several important communities such as Norcross and Lawrenceville, and to a lesser extent Lilburn, Buford and Suwannee, have developed into the so-called "edge cities" and serve as centers of commercial and residential activities in the area. Gwinnett County has grown from a population of 352,910 in 1900 to today's population of 676,000 and is projected to reach 1.2 million by the year 2025 (ARC, 2005).

Demographics: The Atlanta MSA and Gwinnett County, GA

Gwinnett County is a part of the larger Atlanta Metropolitan Statistical Area (MSA) which in 1990 and 2000 was comprised of twenty counties (see Table 2.1). The MSA has since increased to twenty-eight counties in 2004. Atlanta has been one of the fastest growing cities in the U.S. in the past several decades, with an urbanized area that has grown from 285 km² in 1950 to 985 km² in 1970, and then rapidly expanded to 2095 km² in 1990 and 3106 km² by 2000 (ARC, 2005). The Atlanta MSA had a population of 2,959,950 in 1990 and was ranked thirteenth in the nation. By 2000 the population had grown to 4,112,198, an increase of

Table 2.1. The 1990 and 2000 MSA counties. Counties in bold are under the jurisdiction of the Atlanta Regional Commission Regional Development Center for planning purposes.

County Name	1990 Pop	2000 Pop	% Change 1990-2000	Density 1990 (persons per kilometer^2)	Density 2000 (persons per kilometer^2)
Barrow County	29,721	46,144	55.3	71	110
Bartow County	55,911	76,019	36.0	47	64
Carroll County	71,422	87,268	22.2	55	68
Cherokee County	90,204	141,903	57.3	82	129
Clayton County	182,052	236,517	29.9	492	639
Cobb County	447,745	607,751	35.7	508	690
Coweta County	53,853	89,215	65.7	47	78
DeKalb County	545,837	665,865	22.0	786	959
Douglas County	71,120	92,174	29.6	138	179
Fayette County	62,415	91,263	46.2	122	179
Forsyth County	44,083	98,407	123.2	75	168
Fulton County	648,951	816,006	25.7	474	596
Gwinnett County	352,910	588,448	66.7	315	525
Henry County	58,741	119,341	103.2	70	143
Newton County	41,808	62,001	48.3	58	87
Paulding County	41,611	81,678	96.3	51	101
Pickens County	14,432	22,983	59.3	24	38
Rockdale County	54,091	70,111	29.6	159	207
Spalding County	54,457	58,417	7.3	106	114
Walton County	38,586	60,687	57.3	45	71
TOTALS	**2,959,950**	**4,112,198**	**38.9**	**187**	**259**

1,152,248 persons or 38.9%, and was ranked eleventh in the U.S. (US Census Bureau, 2004). By comparison, the City of Atlanta itself only grew by 22,714 persons (5.8%) from 1990 to 2000 and was ranked 39th in population (US Census Bureau, 2004), an indicator of rapid suburban growth and a relatively weak inner city core. Population density of the MSA as a whole also increased from 187 to 259 persons per km^2. Figure 2.2 shows a map of the twenty counties in the Atlanta MSA and the increase in population density in each by persons per square kilometer.

Gwinnett County had the highest actual population growth in the MSA, increasing by 235,538 persons from 1990-2000. The lowest population growth in the MSA, 3,960 persons

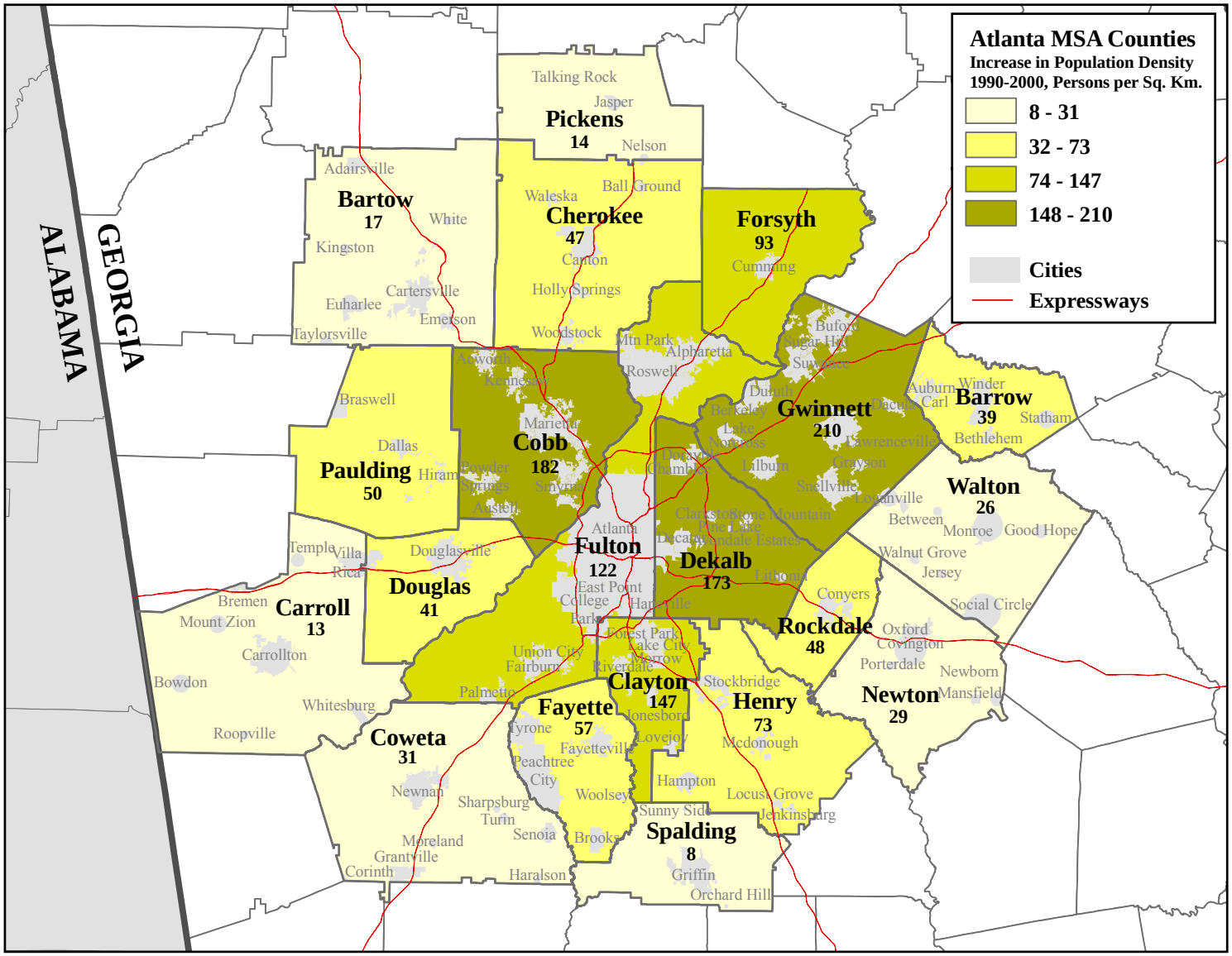

Figure 2.2. Growth in Atlanta MSA Counties. Graduated color map of increase in population density (from Table 2.1) for the 20 counties in the Atlanta Metropolitan Statistical Area, along with cities within the MSA. Actual increase in persons per km² is labeled.

from 1990 to 2000 occurred in Spalding County, a county south of the City of Atlanta and not yet included in the Atlanta Region for planning. The highest growth rate in the MSA occurred in Forsyth County, with a population increase from 1990 to 2000 of a startling 123.2%, the second highest growth rate in the nation (US Census Bureau, 2004). Ironically, Forsyth County belongs to the Georgia Mountain Regional Development Center and not the Atlanta Region, and has historically resisted becoming part of the Atlanta Region. With such enormous growth however, and the fact that a majority of Forsyth residents commute into the Atlanta area for employment, it seems logical for Forsyth to become a part of the Atlanta Region in the near future.

A 2002 report showed Henry, Forsyth and Newton counties, three other metropolitan Atlanta counties, ranked third, fourth and seventh respectively among the 10 fastest-growing counties in the U.S. by percent increase from July 1, 2001, to July 1, 2002 (US Census Bureau, 2003). A more recent report adds Paulding County in northwest Atlanta to the list, giving the Atlanta Region four out of ten of the nation's fastest-growing counties between April 1, 2000, and July 1, 2003 (see Table 2.2). A fifth county, Chattahoochee County in southwest Georgia is also in the top ten, and twenty of the top one hundred fastest growing counties in the U.S. are in Georgia. Each of the top five Georgia counties had a growth rate of at least 20% during the study period (US Census Bureau, 2003). Data such as this illustrates the suitability of Gwinnett County and the Atlanta Region as a study area for urbanization and its many impacts on the landscape, natural resources, and residents.

Gwinnett County was 17th on the list of the fastest growing U.S. counties from 1990-2000 (US Census Bureau, 2000) and 22nd on the list of fastest growing counties in the United States from April 1, 2000 to July 1, 2003. Census data show that population in Gwinnett increased from 72,349 in 1970 to 166,815 in 1980, and then by 186,102 to 352,910 persons in

Table 2.2. Population Estimates for the 10 Fastest Growing U.S. Counties. Data shows population growth from April 1, 2000 to July 1, 2003. Counties in bold are within the Atlanta MSA.

			Population estimates		Change, 2000 to 2003	
Rank	Geographic area		July 1, 2003	April 1, 2000 estimates base	Number	Change
1	Loudoun County	VA	221,746	169,599	52,147	30.7
2	Chattahoochee County	GA	19,333	14,882	4,451	29.9
3	Douglas County	CO	223,471	175,766	47,705	27.1
4	Rockwall County	TX	54,630	43,080	11,550	26.8
5	**Forsyth County**	**GA**	**123,811**	**98,407**	**25,404**	**25.8**
6	**Henry County**	**GA**	**150,003**	**119,341**	**30,662**	**25.7**
7	Flagler County	FL	62,206	49,832	12,374	24.8
8	**Newton County**	**GA**	**76,144**	**62,001**	**14,143**	**22.8**
9	**Paulding County**	**GA**	**100,071**	**81,587**	**18,484**	**22.7**
10	Kendall County	IL	66,565	54,544	12,021	22.0

1990. Gwinnett population continued to explode, increasing by 235,538 persons to 588,448 from 1990 to 2000. This rapid growth is an astonishing 66.7% increase in population during the last decade, compared to 38.9% for the Atlanta MSA and 26.4% growth in the rest of Georgia.

Table 2.3 shows some of the relevant census variables for Gwinnett County from 1990 to 2000, roughly the same time frame as spanned by the imagery used in this study. The table shows a continued trend of rapid growth in several sectors in Gwinnett County population, housing, and employment. In addition to the previously mentioned population increases, there were 4022 new private housing units authorized by building permits in 1990 and 12,372 in 2000, for an impressive 207.6% growth in new housing planned and/or built. Population density increased by 66.7% and the number of housing units increased by 52.4% from 137,608 to 209,682. The commuter information reveals the patterns of the typical auto-oriented suburban sprawl development: the number of new commuters driving alone is nearly four times that of the number of new commuters carpooling, and is 2.5 times the number commuting by any other

Table 2.3. 1990 and 2000 Census data for Gwinnett County

Gwinnett County, Georgia				
Geography Identifier 05000US13135, Geographic Summary Level 50				
VARIABLE	**1990**	**2000**	**CHANGE**	**PERCENT CHANGE**
Total population; Number	352,910	588,448	235,538	66.7
Total housing units; Number	137,608	209,682	72,074	52.4
Housing units authorized by building permits	4,022	12,372	8,350	207.6
Persons per square mile land area	815	1,359	544	66.7
Commuting to work; Workers 16 years and over; Drove alone; Number	169,048	246,884	77,836	46.0
Commuting to work; Workers 16 years and over; In carpools; Number	22,888	43,689	20,801	90.9
Commuting to work; Workers 16 years and over; Using public transportation; Number	1,313	2,632	1,319	100.5
Commuting to work; Workers 16 years and over; Using other means; Number	1,671	2,394	723	43.3
Commuting to work; Workers 16 years and over; Walked or worked at home; Number	6,050	14,198	8,148	134.7
Occupation; Employed persons 16 years and over; Number	203,387	314,471	111,084	54.6
Industry; Employed persons 16 years and over; Agriculture, forestry, and fisheries; Number	2,565	1054	-1,511	-58.9
Industry; Employed persons 16 years and over; Construction; Number	15,642	31,725	16,083	102.8

means than single occupancy vehicle (SOV). The number of new commuters using public transportation is a paltry 1,319, which is merely 1.7% of new commuters driving alone. This pattern of commuting by SOV is the primary reason, along with some of the dirtiest power plants in the nation, that Atlanta has been a chronic violator of national air quality standards and has incurred millions of dollars in penalties and lost federal transportation funding (ARC, 2005). The employment data also reveals a trend away from extractive industries such as agriculture, forestry and fisheries and towards industries such as construction. Growth in managerial, financial, retail, and other white collar jobs among Gwinnett residents is evident of Gwinnett's

continued popularity as a suburban bedroom community for the city of Atlanta and the downtown employment district. Several of the larger Gwinnett cities such as Norcross, Snellville, Duluth, and Lawrenceville are also in the midst of job growth and a transition to becoming more of an employment center than in the past.

The Southern Piedmont Physiographic Province

According to the excellent and well-documented physiographic map of Georgia from Charles Wharton's *The Natural Environments of Georgia* (1977), Gwinnett County is in the Piedmont Province subtype of the Appalachian Highlands. The American Heritage Dictionary of the English Language (2000) defines piedmont as "a*n area of land formed or lying at the foot of a mountain or mountain range"* and Piedmont as "*A plateau region of the eastern United States extending from New York to Alabama between the Appalachian Mountains and the Atlantic coastal plain*". The Southern Piedmont stretches from the Blue Ridge Province and Appalachian Highlands to the Fall Line and the Coastal Plain Province (Wharton, 1977) and covers a large area of the Southeastern United States including portions of Alabama, Georgia, North Carolina, and South Carolina (Figure 2.3). Elevations on the Piedmont are typically 30 m to 100 m but reach approximately 400 m where the Piedmont meets the foothills and the Blue Ridge and Appalachian provinces. The boundary between the Blue Ridge Province and the Piedmont is defined by a sharp change in slope at an altitude of approximately 1,700 feet or 518 m (USGS, 2004). Characterized by rolling hills, irregular plains, occasional table lands, and abundant streams and rivers, the Southern Piedmont contains a wide array of vegetation types (BLM, 2004). Evidence indicates that the Piedmont was historically covered by hardwood forests between 9000 and 5000 years before present (Wharton, 1977), much of which has been replaced with agricultural and urban land uses. The Southern Piedmont has been extensively and

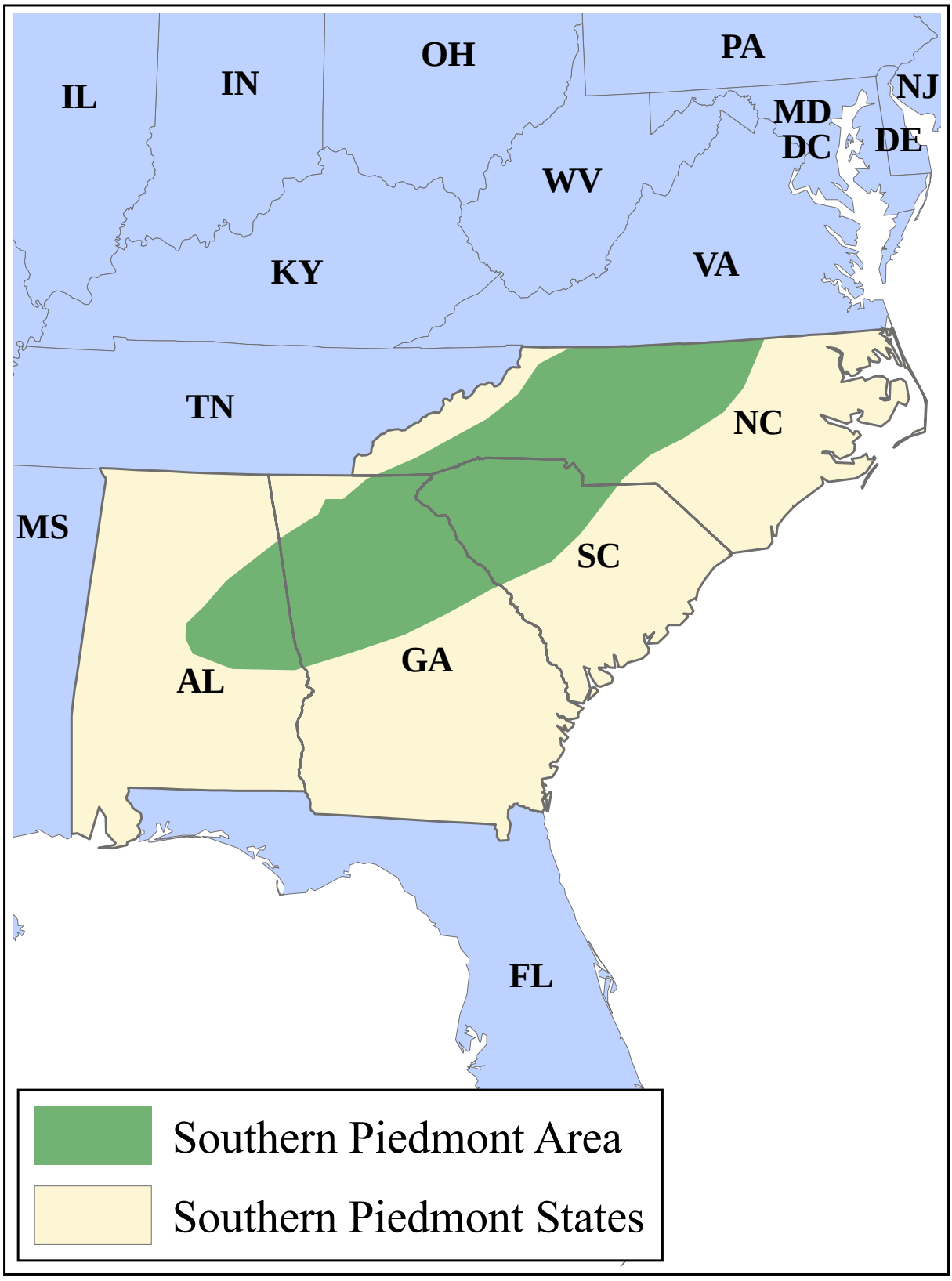

Figure2.3. Approximate extent of the Southern Piedmont physiographic province.

heavily modified by humans, with clearing and burning to create agricultural fields and other openings as the common practice among the Native American population prior to any European contact. After European settlements largely replaced Native American settlements, extensive logging and expansion of agricultural and urban land uses had and continue to have major impacts on the Southern Piedmont. According to Wharton (1977), "By 1825 most of the Piedmont east of the Chattahoochee had been occupied by the Caucasians. By 1935 most or all of the topsoil had been eroded from the Piedmont (due to monoculture cotton farming)….. …Piedmont lands were gradually abandoned, due to economic and social circumstances……this totals 75% abandonment by the 1930s. The land then passed back into secondary forest which (in 1974) Brender estimated to cover 70% of the lower Piedmont, with 55% of this in pine….. ….The secondary forests which grew back on the Piedmont were exploited at least three times: light harvest by small sawmills until 1920, severe harvest during WWII and after, and harvest from pulpwood since the mid 1940s….to find a Piedmont hardwood forest that has never been in agriculture is indeed a prize." Odum (1971) characterized the majority of the Piedmont Province as being in a state of "old field succession", consisting of: 1) fields with crabgrass, horseweed and aster, 2) grass-shrub stage beginning with broom sedge, 3) pine forest (25-100 years old), and 4) oak-hickory climax forest (150 years plus). Broadleaf deciduous hardwood trees are still the dominant type of vegetation on the Southern Piedmont, although in many areas pines have increased in dominance following disturbances (BLM, 2004) and mixed hardwood/pine forests are becoming more prevalent. Virgin forests are increasingly scarce in the Southern Piedmont and exist only in the most inaccessible areas where steep topography made agriculture or timber harvesting impractical (Wharton, 1977). "It is from such remnants that we must obtain most of our information about the natural environments of the Piedmont. The bulk

of the flora is gone, and, unhappily, we cannot as yet determine the impact of man on the fauna which once occupied these extensive hardwood forests" (Wharton, 1977).

Natural Environments and Dominant Tree Species in Gwinnett County

Wharton's physiographic map of Georgia (1977) shows that the area of western and northwestern Gwinnett County from approximately west of I-85 and into Fulton County is known as the Gainesville Ridges subtype of the Piedmont Province. The southern and southwestern portions of the county fall into the Midland subtype of the Piedmont Province. Within the county there are numerous environments and biotic communities, and a wide variety of deciduous hardwood and pine tree species. The Appendix (p. 119) lists the major environment types found within Gwinnett County and the dominant tree species represented there.

Climate

The climate of the Piedmont region in which Atlanta and Gwinnett County lies can best be characterized as a mild, moist or humid Mid-latitude climate, known as a "Cfa" classification in the dated but still popular Köppen System for climate classification. Under Köppen's method, the "C" indicates the major category of "mild mid-latitude", the second letter "f" stands for the German word *feucht* or "moist," and the third letter "a" indicates that the average temperature of the warmest month is above 72°F (22°C) (Lutgens & Tarbuck, 1995). The Köppen Cfa climate is characterized by hot and humid summers with primarily convective precipitation and thunderstorms, and mild winters with winter precipitation resulting from passing mid-latitude cyclonic systems. Under normal conditions there are no pronounced wet/dry periods and moderate rainfall year-round. A lack of natural topographic barriers in the Atlanta region results in little to no orographic precipitation.

Climatological data for the Gwinnett County study area were examined in more detail for the years studied, to determine if conditions were roughly similar in 1991 and 2000. Severe anomalies in climate between the two study years could impact the research by introducing additional variables that may affect vegetation cover and interpretation of change from remotely sensed data. In particular, it is important to look at annual and seasonal precipitation and temperature as well as the Palmer Drought Severity Index (PDSI) readings. Three climate stations in and around Gwinnett County were compared for 1991 and 2000 (Table 2.4). Table 2.4 shows that while 1991 and 2000 average summer temperatures were virtually identical, some definite inequities in precipitation exist between 1991 and 2000. On average for these three stations, the year 2000 was drier, with 41.5 cm (28.4%) less annual rainfall and 3.0 cm (22%) less summer precipitation. Summer is defined here as June through September.

Table 2.4. Climate station data for Gwinnett County and surrounding area

Station Name	**Norcross 4 N**	**Cumming**	**Winder 1 SSE**	**Station Average**
Station No.	096407-2	092408-2	099466-2	
Long./Lat.	-84.2, 34.0	-84.133, 34.2	-83.716, 33.983	
Elevation (meters)	290	402	293	328
1991 Ann. Precip (cm)	157.35	145.01	135.26	145.87
2000 Ann. Precip (cm)	106.35	108.74	98.07	104.39
1991 Summer Precip (cm)	15.57	12.94	12.87	13.79
2000 Summer Precip (cm)	11.28	11.70	9.29	10.75
1991 Avg. Summer Temp. (ºC)	NA	NA	24.06	24.06
2000 Avg. Summer Temp. (ºC)	NA	NA	23.94	23.94

The Palmer Drought Severity Index (PDSI), developed by Wayne Palmer in 1965, uses temperature and rainfall data to calculate dryness and is a useful measure for comparison of climatic conditions over time and space (NOAA, 2005). The PDSI "represents the severity of dry and wet spells over the U.S. based on monthly temperature and precipitation data as well as the soil-water holding capacity at that location" (Dai et al., 1998). The PDSI values for the study

period show additional evidence of a disparity between 1991 and 2000. Table 2.5 shows a comparison of the PDSI values for Georgia climate division 2 by hydrologic year (October-September) between 1991 and 2000. Records indicate that while 1991 annual and summer values are slightly above average indicating a relative abundance of rainfall and absence of drought, 2000 values are significantly below average (more than one standard deviation below) and indicate the condition of a moderate drought. In fact, the values for the two study years are approximately two standard deviations apart. According to the University of Georgia College of Agricultural and Environmental Sciences (2000), in September 2000 the drought was twenty nine months old. In arid climates, such a difference would be of serious concern to a vegetation change detection study. However, in the relatively lush and heavily vegetated Southeastern United States, fluctuations in the drought index of plus or minus one standard deviation would not preclude the occurrence of adequate rainfall for healthy vegetation growth. Put in another way, while 2000 was definitely drier, in a climate such as Atlanta's the drought index would have to be significantly more severe (i.e., a PDSI value < -3.0) to have an impact on vegetation growth of a magnitude as to make the study years incompatible and the results of the research suspect (Dai et al., 1998).

Table 2.5. PDSI values for Georgia climate region 2

Annual		**Summer**	
Annual Mean	-0.093	Summer Mean	0.003
Annual SD	1.589	Summer SD	1.946
-1 std dev	-1.682	-1 std dev	-1.943
+1 std dev	1.495	+1 std dev	1.949
1991 Value	1.398	1991 Value	1.675
2000 Value	-1.893	2000 Value	-2.248

2. Remote Sensing Data Used in This Study

Landsat Data: A Brief History

The Landsat satellite data collection program began with the launch of the first Landsat satellite (then named the ERTS-1) in 1972. ERTS-1 "represented the first unmanned satellite specifically designed to acquire data about earth resources on a systematic, repetitive, medium resolution, multispectral basis" (Lillesand & Kiefer, 2000, p.377). This first satellite was equipped with Return Beam Vidicon (RBV) and Multispectral Scanner (MSS) sensors that captured seven bands at 80m pixel resolution. Subsequent sensors improved in spatial and radiometric resolution, accuracy of measurement, and elimination of problems. The current study uses Landsat 5 TM and Landsat 7 ETM+ imagery, which both contain six bands of data at a pixel resolution of 30 meters and a lower resolution thermal IR band (see Table 2.6).

Table 2.6. Landsat 5 TM and Landsat 7 ETM+ spectral and spatial resolution. Bands 1-5 and 7 have 30 m pixel resolution for both sensors, bands 6 and 8 have resolution as indicated.

Sensor	**Spectral Sensitivity**							
Band (spatial resolution)	**Band 1**	**Band 2**	**Band 3**	**Band 4**	**Band 5**	**Band 6 (60-120 m)**	**Band 7**	**Band 8 (15 m)**
TM	0.45-0.52	0.52-0.60	0.63-0.69	0.76-0.90	1.55-1.75	10.4-12.5 (120 m)	2.08-2.35	NA
ETM+	0.45-0.52	0.52-0.60	0.63-0.69	0.76-0.90	1.55-1.75	10.4-12.5 (60 m)	2.08-2.35	0.50-0.90

While Landsat 7 ETM+ has some enhanced capabilities over the TM imagery, such as the addition of a 15 m resolution panchromatic band and an improvement in the spatial resolution of the thermal band from TM's 120 m to 60 m resolution (Lillesand & Kiefer, 2000, p.379), it is readily comparable to the Landsat 5 images. In fact perhaps the greatest asset of Landsat data

and the primary reason for its popularity is that it has the longest record of satellite remote sensing imagery available. The images collected since the inception of the program in 1972 form an invaluable library of data and images that have greatly furthered research in many fields. One important characteristic of Landsat imagery is the sun-synchronous orbit of the sensor-carrying satellite. Orbits are calculated so that Landsat sensors pass over a given area at a constant time, approximately 9:42 AM local sun time; in the case of Landsat 5 TM and 7 ETM+ sensors, this pass occurs every sixteen days over the exact location on Earth. This sun-synchronous orbit is advantageous because it "ensures repeatable sun illumination conditions…(which) are desirable when mosaicking adjacent tracks of imagery and comparing annual changes in land cover" (Lillesand & Kiefer, 2000, p. 383). Additional reasons for the widespread use of the Landsat data in earth-surface studies are its useful range of wavelengths sensed, consistent scale and look angle geometry (Jensen, 1986), moderately high resolution, ready availability, and ease of distribution. Recently de-privatized and returned to the care of the USGS, Landsat data is now widely accessible for reasonable costs compared to other imagery. In addition, most or all of the major imagery processing software products have routines for processing Landsat data, making it very accessible and easy to work with. Landsat imagery is becoming the accepted standard for land cover and vegetation change analysis, and is found in many universities, government agencies, and private research firms across the country and worldwide.

Landsat Imagery Used in This Research

Two scenes of Landsat Thematic Mapper imagery covering northern metropolitan Atlanta (Path 19, Row 36) were used for this project (see Figure 2.4). The images chosen were a Landsat 5 TM image from 9/28/1991 and a Landsat 7 ETM+ image from 9/28/2000. The 1991

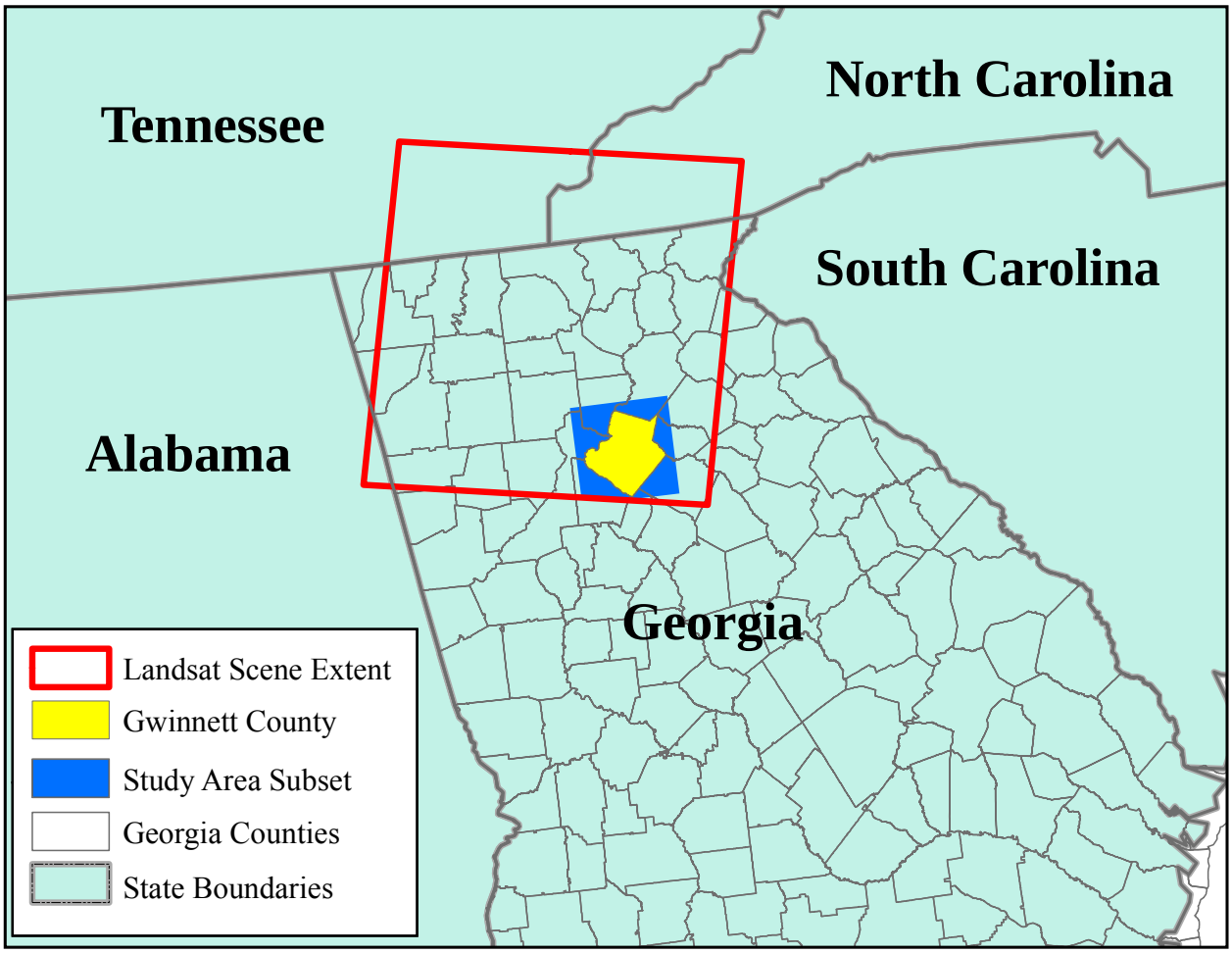

Figure 2.4. Extent of original Landsat scenes. Extent of 1991 and 2000 scenes (Path 19, Row 36) along with study area subset image area and Gwinnett County boundary.

and 2000 images are 95% and 97% cloud free respectively. Although images from the ETM+ sensor have several advances over images from the TM sensor, they are identical in spectral and spatial sensitivity within the six bands used in this study (see Table 2.6) and are therefore readily comparable for purposes of image differencing. The low resolution (120 m) thermal IR band is not used in any of the processing for this research, only the 30 m bands 1-5 and 7 are used. Use of anniversary or near-anniversary images such as these whenever possible is important in change detection in order to minimize any extraneous variations in sun angle, phenologic state,

and soil moisture conditions (Minnesota DNR, 1999). Both images are from early autumn but before leaf-off and still exhibit full vegetation canopy.

The two Landsat TM scenes were provided by the Georgia Institute of Technology Center for GIS in ERDAS Imagine .IMG format and a UTM Zone 17, GRS80 projection. However, due to the fact that the 24 GB of aerial photography and other reference data used for the project were only available in a State Plane (feet) NAD83 FIPS Zone 1002 Georgia West projection, it was necessary to reproject the Landsat images to match the reference data prior to any other image processing procedures. The images were reprojected using a rigorous transformation and nearest neighbor resampling method in order to preserve the original pixel reflectance values. Both original images have been previously Orthorectified by USGS to remove distortion of area, angle, distance, and direction due to variations in terrain and elevation.

Reference Images and Collateral Data

Several sets of high resolution aerial photography were used as collateral data for georectification, picking pseudo-invariant features for radiometric normalization, and ground-truthing purposes. The 1993 USGS panchromatic Digital Orthorectified Quarter Quadrangles (DOQQs) are single band grayscale photos with a spatial resolution of 1 m. The 1999 Color Infrared (CIR) DOQQs are three-color photos containing data in the green, red, and near-infrared wavelengths and also have a spatial resolution of 1 m. This particular set of CIR DOQQs has been histogram matched, color balanced, and mosaicked in ERDAS Imagine to produce a relatively seamless tile covering the study area. A third set of reference photos consists of both 1999 and 2001 true color (blue, green, & red wavelengths) aerial photography from Aerials Express, Inc. (formerly Digi-Air, Inc.), which have a resolution of approximately 1 m as well. All aerial photography was provided courtesy of the GIS Division of the Atlanta Regional

Commission in MrSID format. The majority of these aerial photographs were taken early in their respective years and represent 'leaf-off' conditions in which distinctions in the type and condition of land cover can be more easily determined without interference from dense or overhanging vegetation canopy. Additional reference data including shapefiles of Gwinnett County and the surrounding region were also obtained from the Atlanta Regional Commission's Atlanta Region Information Systems (ARIS) CD Volume 1B published in 2002.

A USGS National Elevation Dataset (NED) was used to check the elevation of points used in radiometric normalization to ensure uniform elevation among the selection set. NED is an improved Digital Elevation Model (DEM) product available on a national level from USGS. Grid cell resolution is 30 meters and elevation Z values are in units of meters.

3. Summary of Image Processing Methods Used in This Study

Digital Change Detection

Digital change detection using remote sensing imagery involves comparison of two or more images from different dates in order to detect inter-annual (or inter-seasonal in some cases) changes in some variable or feature. The process of change detection is to analyze the spatial, spectral and temporal characteristics of remote sensing data in order to derive statistics that will indicate the presence or absence of land-use or other types of changes. The "fundamental assumption of digital change detection is that there exists a difference in the spectral response of a pixel on two dates if the land-use changes from one type of land cover to another" (Jensen, 1986, p.235). Negative change (i.e., deforestation, degradation, etc.), positive change (i.e., regrowth, regeneration, etc.), and no change can be monitored. There are many change detection techniques currently in use including pre-classification or spectral-value-based techniques such

as image algebra (differencing, ratioing, image regression, principal components analysis, Tasseled Cap transformation), multi-date composites, write function memory insertion, and change vector analysis. Post-classification change detection on multi-date imagery can be performed as well (Morisette, 1997). Image algebra techniques are perhaps the most commonly employed techniques for change detection using Landsat TM imagery for the reasons discussed above, and three such methods will be explored in detail in this paper. There are two crucial preprocessing requirements for digital change detection using multi-temporal images, image registration and radiometric normalization (Coppin & Bauer, 1996). These two steps will be discussed in detail later in this chapter.

Image Differencing

Image differencing simply involves the subtraction of the digital pixel values of an image from one date from the corresponding pixel values for a different date. This method is favored by many for its accuracy, simplicity of computation, and ease of interpretation (Hayes & Sader, 2001; Minnesota DNR, 1999). The resulting difference in pixel values is an indication of positive or negative change, or lack of change in land cover type or other variable studied. Statistical thresholds to indicate presence or absence of change in a given pixel, band or component are an important element in producing an accurate and meaningful change detection product, and will be discussed further in the section on choosing a change threshold. Image differencing can be performed using raw pixel values, or using new pixel values resulting from any number of image algebra transformations. The three image algebra functions being compared in this research, performed prior to image differencing, are detailed in the following sections.

Normalized Difference Vegetation Index (NDVI)

NDVI (Normalized Difference Vegetation Index) is an image enhancement based on the difference between the near-infrared and red wavelengths (Landsat TM bands 4 and 3, respectively).

The equation for NDVI is:

$$\frac{\text{Near infrared minus red}}{\text{Near infrared plus red}} \quad \text{OR} \quad \frac{\text{Band 4} - \text{Band 3}}{\text{Band 4} + \text{Band 3}} \qquad \text{(Jensen, 1996)}$$

Due to the spectral reflectance peak in the near-infrared range seen in healthy vegetation, NDVI is useful in identifying and assessing the health and vigor of vegetation, as well as estimating biomass (Hayes & Sader, 2001). Differencing of NDVI images has been successfully used for land cover change detection. Hayes and Sader (2001) used NDVI image differencing to detect change in Guatemala's remote Maya Biosphere Reserve. A study of 75 change detection techniques and variations conducted as part of the North American Landscape Characterization (NALC) project in Washington, D.C., found NDVI image differencing to outperform nearly all of the other techniques tested (Yuan & Elvidge, 1998). Lyon et al. (1998) determined that NDVI differencing performed better than seven other vegetation indices and was least effected by topographic factors in a change detection experiment in Chiapas, Mexico. Finally, Fung and Siu (2000) found that NDVI was more effective than simple image differencing or PCA in identifying subtle changes in urban green space in Hong Kong. Areas of continuous decrease in NDVI values revealed urban expansion, while areas of continuous increase scattered around old urban districts indicated improved landscaping; in this study NDVI "provided valuable information for the assessment of environmental quality for planning and management of the environment."

Principal Components Analysis (PCA)

Principal components analysis (PCA) is another commonly used transformation of image data prior to change detection by image differencing. A method of data compression, PCA allows redundant data to be compacted into fewer components or bands, which are orthogonal or uncorrelated to each other (Smith & Brown, 1999). PCA as applied to Landsat TM imagery is an image-specific transformation, with transformation matrix values derived from the unique pixel values found in each particular image. Principal components analysis results in a new image with the same number of bands as the original input image, with the first three components in most cases corresponding to the variables of brightness, wetness, and greenness in the image, and typically representing 95% of the information in all bands of the original image. The resulting image may be more interpretable than the raw images (Wilson, 1997). In addition, PCA can account for exogenous differences between images, making preprocessing of multi-date images less critical when using this method (Collins & Woodcock, 1996). In an assessment of several linear change detection techniques applied to forest canopy changes, PCA outperformed the Gramm-Schmidt orthogonalization process and performed similarly to a multitemporal Kauth-Thomas (K-T) transformation (Collins & Woodcock, 1996). However, Hayes and Sader (2001) found PCA to be inferior to NDVI image differencing and RGB-NDVI change detection in monitoring clearing of tropical forests in Guatemala. Collins and Woodcock (1996) also found that "while multi-date PCA can be effective, it represents…the weakest tie to physical interpretation of the results."

Tasseled Cap Transformation

The third transformation examined is Tasseled Cap transformation (TCT), developed by R.J. Kauth and G.S. Thomas for Landsat MSS imagery (Kauth & Thomas, 1976), and later

adapted for Landsat TM imagery by E.P. Crist and R.C. Cicone (Crist & Cicone, 1984; Crist & Kauth, 1986). Like PCA, Tasseled Cap transformation is a data reduction transformation that compresses scene spectral data into a few bands associated with physical scene characteristics (Crist & Cicone, 1984). In TCT, the original image is put through a linear transformation based on the digital numbers of each individual band. The coefficients of the linear equations were developed through analysis of many images and are sensor/platform-specific. Like PCA, a Tasseled Cap transformation results in a new image with the same number of bands as the original image, with the most important components from a change detection standpoint again being the first three components relating to values of brightness, greenness, and wetness. These three components correspond closely to the actual physical characteristics of the scene and represent approximately 95% of image data (Crist & Kauth, 1986; Crist & Cicone, 1984). A fourth component, representing haze, is used in ERDAS Imagine to perform haze reduction of Landsat TM imagery. TCT allows for efficient extraction of complex data and the derivation of meaningful spectral features, which are easier to handle and interpret than the raw data; for this reason it has become one of the most accepted methods of image transformation for change detection in the remote sensing community (Crist & Kauth, 1986). Differing from PCA, which is image-specific, TCT is sensor/platform-specific, with transformation matrix values developed specific to the Landsat MSS, TM and now ETM+ sensors. This allows consistent performance from the application of TCT to virtually any image from a given sensor. In addition, Crist and Kauth (1986) stated that "While this concept has been used primarily in agricultural or vegetation applications, there is good reason to expect that it could be similarly employed in geologic or urban land-use applications." Collins and Woodcock (1996) found change in Kauth-Thomas wetness to be the single most reliable indicator of changes in forest canopy. They found

an advantage over PCA in that change information was consistently found in a well-defined set of components, making tasseled-cap able to identify change as well as PCA but in a more understandable, consistent manner. Ridd and Liu determined, in a comparison of four algorithms for change detection, that "among the Tasseled Cap transformations, the greenness function was sensitive (above 90%) to changes in categories 3, 5, and 6, where substantial changes in green vegetation are involved…" (Ridd & Liu, 1998).

Recently a group from the USGS Eros Data Center updated the TCT matrix to reflect the subtle but important differences present in the ETM+ sensor on the Landsat 7 satellite. Prior transformation matrices had been optimized for MSS and TM sensors; deriving a transformation for the ETM+ sensor facilitates comparison of Landsat 7 images to data from previous sensors (Huang et al., 2002).

4. Image Processing Steps

All image processing was performed using ERDAS Imagine v8.6 software.

Subsetting

Because the spatial extent of the two Landsat images is far greater than the study area and the aerial photography available for geometric registration, the images were first subset to a smaller area using a bounding rectangle around Gwinnett County. Once the subset images were geometrically registered to each other (see below), it is these co-registered subsets that are used for all subsequent image processing and analysis. Subsetting was done by using the AOI tools in the Imagine viewer to draw an "area of interest" (AOI) rectangle around a shapefile boundary of Gwinnett County (again all data are in State Plane (feet) NAD83 Georgia West projection). This AOI layer was then saved to a file, and was then loaded into the Subset Image dialog box

under the Data Prep menu and used to create a subset of the input image. Four corners were used in this case and all other parameters were left at default settings. The new subset output images retain the projection information and all the original pixel data values as the original source image. The subset images are included in the CD-ROM attached with this work.

Geometric Correction of Landsat Imagery and Photography

In any change detection study, the importance of accurate registration between images being compared cannot be overstated. Jensen (1996) notes that "accurate spatial registration of at least two images is essential for digital change detection" (Jensen, 1996, p.235). Image registration is the "translation and rotation alignment process by which two images of like geometries and of the same set of objects are positioned coincident with respect to one another so that corresponding elements of the same ground area appear in the same place on the registered images" (Haralick et al., 1973). While the Landsat images used in this research have been orthorectified to remove distortion due to topographic variation, it is also important that the image pair be well registered to each other and to the aerial photography used for ground truthing and accuracy assessment.

Misalignment of pixels can result in a dramatic reduction in accuracy of the change detection product. This was explored by Dai and Khorram (1998), who systematically investigated and quantitatively evaluated the effects of misregistration on the accuracy of remotely sensed change detection results, realizing that in order to use remotely sensed data responsibly for change detection studies, it is important to know the quality of the data used and to quantify the degree of error present. They stated that "the majority of current change detection techniques depend critically on the accuracy of geometric registration of two images since change analysis is generally performed on a pixel-by-pixel basis" (Dai & Khorram, 1998).

Lack of accurate registration between images will result in spurious changes being indicated, resulting in errors of both commission (when a pixel is committed to an incorrect class) and omission (when a pixel is incorrectly classified into another category, therefore being omitted from its correct class) (NOAA, 2005). It has also been noted that studies of spatially heterogeneous landscapes tend to suffer increased effects of misregistration on the accuracy of change detection products (Stow, 1998). This observation is especially relevant in urban and urban-fringe areas such as Gwinnett County and Atlanta.

For this study, the 2000 Landsat 7 ETM+ image was registered to the 1999 USGS CIR DOQQs, and then the 1991 Landsat 5 TM image was registered to the 2000 image. By registering to the DOQQs there is an established standard of quality (the USGS) set as the baseline for spatial referencing, and the 1993 and 1999 DOQQs are already registered to each other. The one meter resolution true color photography from Aerials Express is also adequately registered to the DOQQs for ground truthing purposes. The critical element is the registering of the two Landsat images to each other. Ideally one could achieve a perfect pixel-to-pixel match, but this is extremely difficult if not impossible. Registration error is measured in root mean squared error, or RMSE. RMSE is an indication of the degree of misregistration, and is expressed in pixels, or units of ground resolution, based on a set of ground control points (GCPs). It is calculated as:

$$RMSE = \mathrm{sqrt}\{\Sigma[(x_i - X_i)^2 + (y_i - Y_i)^2]/n\};$$

where x_i and y_i are predicted coordinates of the GCPs using the polynomial transformation functions, and X_i and Y_i are the reference coordinates of the same points. General practice indicates that when registering images an RMSE of 0.5 pixels or less is desired. With 30 meter Landsat data, this amounts to an acceptable shift in pixel location of 15 meters – a very small

error over an area as large as a county or region. Dai and Khorram (1998) took it even further, finding that "On average, less than 0.1934 pixel of registration accuracy should be achieved to detect 90% of the true changes, which means that a registration accuracy of less than one-fifth of a pixel is required to achieve a change detection error of less than 10%." Interestingly, they also conclude that band 4, the near-IR band so important to many of the vegetation indices is the most sensitive of the six non-thermal Landsat bands to the effects of misregistration. The implications of this finding for vegetation change detection studies are potentially serious and will possibly yield some new techniques to improve accuracy in response.

Image registration was performed in ERDAS Imagine using the Image Geometric Correction tools under the Data Prep menu in the image viewer. The 2000 Landsat image and 1999 CIR DOQQ were viewed side by side in separate viewers. Using the GCP (ground control point) tool, corresponding pixels were chosen from each image to the best of the author's ability. The differing resolutions (1 m photography and 30 m imagery) present challenges of photo-interpretation. The best sites for GCPs are permanent features with a clearly defined boundary and an easily recognizable spectral signature. Examples are road intersections, bridges, and the corners of buildings. Great care must be taken in the selection of GCPs to pick features that have not changed shape or position in the time between images.

Each pair of GCPs (beyond 3 pair) results in the calculation of a RMSE value using that particular set of GCPs. The effects of a single GCP on the RMSE can sometimes be unpredictable and it may be necessary to delete a certain GCP in order to achieve an RMSE of 0.5 pixels or below. The minimum number of GCPs required for registration is 3; however, in the interest of increased accuracy and representativeness of the GCPs the goal is at least ten GCPs and an RMSE below 0.5 pixels and below 0.2 pixels if at all possible. GCPs must be

stored in a file for later use if necessary. Once a sufficient number of GCPs have been chosen and the RMSE is satisfactory, a new image is created by resampling of the input image. Resampling will populate the pixels in the new image with the digital numbers from the original image and so align the images of different dates to each other, and resampling using the 'Nearest Neighbor' technique with a rigorous transformation best preserves the pixel reflectance values from the original image (Lillesand & Kiefer, 2000).

Radiometric normalization of Landsat data

The importance of radiometric correction and normalization among multiple images of the same area as a pre-processing step in change detection and other applications has been shown repeatedly (Hall et al., 1991; Heo & Fitzhugh, 2000; Yang & Lo, 2000; Song et al., 2001; Du et al., 2002; Jantzen, 2004). Radiometric correction or normalization can be defined as a process intended to "remove radiometric differences between multi-temporal images that are due to non-surface factors" in pursuit of a common radiometric response, required for quantitative analysis (Heo & Fitzhugh, 2000). In fact, the goal is that "all rectified images should appear as if they were acquired with the same sensor, while observing through the atmospheric and illumination conditions of the reference image" (Hall et al., 1991), so that changes in pixel values will reflect actual changes on the surface. Through a number of normalization techniques the user can dramatically reduce the effects of differences in scene illumination, atmospheric conditions, viewing geometry, and instrument response characteristics (Lillesand & Kiefer, 2000, p. 477). The result is a reduction of error and a more accurate, reliable image analysis product, an "improvement in visual image quality and statistical robustness" (Yang & Lo, 2000). According to Heo & Fitzhugh (2000), "Accurate normalization is essential for image processing procedures that use multi-date imagery, such as change detection."

There are two types of radiometric normalization or correction, absolute and relative. The principal objective of absolute radiometric normalization is the retrieval of surface energy properties such as spectral reflectance, albedo, or surface temperature (Jensen, 1996). Absolute normalization requires additional data on sensor calibration recorded at the time of imaging, as well as data on atmospheric conditions, satellite ephemeris data, and ground targets of known reflectance. Such data can be very difficult to obtain and is not available for many archived images. Absolute normalization is not necessary for all image analysis procedures, but is mandatory when two or more images are in different radiometric scales (Song et al., 2001). Atmospheric correction, a component of absolute normalization, uses historical data on atmospheric conditions at the time of imaging to minimize differences between images, including relative amounts of scattering and absorption, which are primary sources of error in extracting useful information from the images (Jensen, 1996).

Relative radiometric normalization also consists of correcting differences between multi-temporal images due to non-surface factors (Heo & Fitzhugh, 2000), but the images are corrected relative to each other and are not necessarily tied to absolute ground measurements. Relative normalization does not require atmospheric correction, ephemeris data or data on sensor calibration to perform, but does correct for the effects of solar angle, scattering and absorption, and sensor performance. While in many ways much simpler to perform than absolute radiometric correction, it is nevertheless very effective and sufficient for certain types of analyses including change detection (Song et al., 2001), and a properly normalized pair of images will yield more accurate and useful results from a change detection procedure. There are many methods of relative normalization currently used in research, including use of pseudo-

invariant features (PIFs), radiometric control sets, image regression, no-change set determined from scattergrams, and histogram matching (Yang & Lo, 2000).

Relative radiometric normalization was performed on the two Landsat image subsets using a band-by-band linear regression procedure. Linear regression involves the selection of pseudo-invariant ground features (PIFs) common to each image, and establishing a regression relationship between corresponding pixel values that can be used to "explain" and correct the radiometric differences between images. According to Heo & Fitzhugh (2000) "linear regression using temporally invariant targets is a widely accepted method for normalization." The generally accepted criteria for choosing the pseudo-invariant features as described in Heo and Fitzhugh (2000) are:

- Approximately equal elevation resulting in similar atmospheric thickness over each point
- Minimal amounts of vegetation present, to minimize the effects of spectral changes over time
- Location in relatively flat areas to minimize the effects of changes in sun angle between images (not as important with anniversary date images)
- Consistent appearance and spectral characteristics over time
- A wide range of brightness values (BVs) for a reliable regression model

Examples of appropriate PIFs include building rooftops, paved areas, road intersections, beaches and deep water (Heo & Fitzhugh, 2000). The inherent subjectivity in the choice of PIFs introduces error, and therefore the screening and elimination of outliers becomes important. Outliers are eliminated on a band-by-band basis, with each band potentially having a unique sample of data points. Band-by-band regression was shown to be a more successful method than

regression on an integrated image (Heo & Fitzhugh, 2000). Once the final set of PIF points is determined, the pixel values for each spectral band are input into Excel, SAS, SPSS, or other statistical software and a linear regression equation for each band is computed describing the relationship between the two images. The regression equations are used to create a new image for each band by 'predicting' pixel values across the new image from the input image pixel values, and a new multi-band image is created by layer stacking the bands together. The result is a visually improved and statistically more robust image pair (Yang & Lo, 2000), which should result in improved accuracy, credibility, and reproducibility in the change detection analysis.

For this study 25 sample PIF radiometric control target points were chosen from each Landsat image and converted to a shapefile in ESRI's ArcView 3.2 software. In keeping with the criteria outlined above, the targets chosen consisted of road and highway intersections, concrete and asphalt parking lots, rooftops of commercial buildings, rock outcrops and areas of bare soil near quarries, and areas of deep water. Care was taken to pick points that had remained unchanged according to the best available high resolution aerial photography (1993 black and white and 1999 CIR DOQQs, 1999 and 2001 Aerials Express true color). Care was also taken not to choose targets containing vegetation, based on reference to the Landsat imagery and aerial photography. The USGS National Elevation Dataset (an improved Digital Elevation Model product) was used to determine the elevation of the control points to assure compatibility. Table 2.7 shows the X,Y location (in State Plane feet), surface type, and elevation of the radiometric control targets used in this study.

The radiometric control target points were then brought into the Imagine viewer with the Landsat imagery, and using the Inquire Cursor pixel values for Landsat bands 1 -5 and 7 were identified and recorded into an Excel spreadsheet (again, the lower resolution Band 6 thermal

Table 2.7. Radiometric control targets. Twenty five targets used for relative radiometric correction of Landsat images. Highlighted records are the outliers which were ultimately removed.

ID	X Coordinate	Y Coordinate	Suface Type	Elevation (m)
1	2342396.32784	1525449.37490	deep water	326
2	2303082.28363	1382974.52575	granite outcrop (Stn Mtn)	392
3	2307129.80130	1384827.26271	deep water	254
4	2381593.35162	1411934.36843	quarry	258
5	2329357.41915	1515913.62833	deep water	326
6	2267037.43670	1417147.33484	interstate (285)	294
7	2335603.82742	1499158.50235	bare soil	335
8	2290749.37174	1450277.33361	deep water	297
9	2296594.70485	1449129.03067	building roof	326
10	2350130.06638	1526592.99419	deep water	326
11	2286827.92458	1400611.78996	building roof	325
12	2281451.40596	1423756.37698	asphalt pkg lot	314
13	2280461.19238	1427457.91162	building roof	315
14	2267209.52483	1418114.12781	dark rooftop	297
15	2269765.21661	1415836.53590	graded dirt hillside	276
16	2304794.37137	1384215.39784	granite outcrop (Stn Mtn)	336
17	2328686.77899	1364992.38733	granite outcrop	345
18	2329435.41250	1365651.39570	granite outcrop	263
19	2325890.81631	1364182.20062	bare soil (quarry)	246
20	2299889.82071	1429693.21445	bare soil (quarry)	239
21	2273762.28497	1434366.57400	asphalt (hwy)	303
22	2308618.56238	1440036.62497	asphalt (mall pkg lot)	294
23	2308317.60129	1440939.50826	building roof	298
24	2259763.88646	1421527.43898	building roof	307
25	2262526.46324	1420789.34594	asphalt (hwy)	320

values were not used in this analysis). Once in Excel, a linear regression equation was computed using the Slope and Intercept functions, and scatterplots were generated for each complete image and each individual band in both images. In this case the 9/28/2000 image was used as the reference image (known Y values) and the 9/28/1991 image (known X values) was radiometrically corrected relative to the 2000 image.

The new radiometrically corrected 9-28-91 subset image was generated using the equation Y= MX + B where Y are the radiometrically corrected pixel values in the new 1991 subset image, M is the slope of the best fit line from the linear regression, X are the input pixel values from the original 1991 subset image, and B is the Y-intercept from the regression line. In order to accomplish this the original 1991 subset image was first divided into six individual bands in Imagine. These individual original bands are then put into the Spatial Modeler of Imagine, having an input image type of Float and Interpolation set for Nearest Neighbor. A Function is added using the coefficients from the linear regression equation, and an output is created as an Unsigned 8-bit continuous image containing the new radiometrically corrected pixel values resulting from the function equation. This process is repeated for all six individual bands of the original 1991 subset image, and the resulting six new bands are then layer-stacked into a new multi-band image. This new radiometrically corrected image for 9-28-91 is used for all subsequent analysis and will hereafter simply be referred to as the 9-28-91 or 1991 study area subset image.

Image Transformation Using NDVI, PCA and Tasseled Cap

Digital change detection is performed on the registered, radiometrically normalized subset images using image algebra. Three different transformation techniques are compared in this study, using image differencing to detect changes to vegetation cover during the study period. The three transformations, NDVI, PCA and Tasseled Cap, discussed earlier in this paper, are available in the ERDAS Imagine Spectral Enhancement submenu of the Interpreter menu. For all three methods, the 1991 and 2000 Landsat subset images are input and a new image pair is generated. NDVI for the TM sensor is chosen from an Indices submenu, while Principal Components Analysis and Tasseled Cap are available directly from the Spectral Enhancement

menu. Default values are used for Data Type and Output Options (Float single for NDVI and PCA, Signed 16 bit for TCT). For PCA, the eigen matrix and eigenvalues are written to file for later examination, and six components are chosen.

It should be noted that ERDAS Imagine Spectral Enhancement module contains the coefficients for the Tasseled Cap transformation of Landsat MSS, TM 4 and TM5 imagery, but not the coefficients for Landsat 7 ETM+ imagery as it is the most recent sensor type in use. Huang et al. (2002) have developed Tasseled Cap coefficients for the Landsat 7 ETM+ sensor using top of atmosphere at-satellite reflectance values, but these were not used in this study for the 2000 image as the image data represents digital number values and not top of atmosphere at-satellite reflectance. It is possible to convert the image data to at-satellite reflectance through application of statistical equations factoring in sensor gains, solar angle, atmospheric depth, and other information collected at time of imaging. However, such information is not easily obtained and the relative radiometric calibration of the images along with the image transformations makes this conversion largely unnecessary for this study. The Landsat 5 TM and Landsat 7 ETM+ sensors are identical in spatial and spectral resolution for the image bands involved in this analysis, therefore the Landsat 5 TM Tasseled Cap coefficients found in the ERDAS Imagine Spectral Enhancement module are applied to both the 9-28-91 and 9-28-2000 images. As the images are anniversary date the solar angle is the same for both images, and any slight differences in atmospheric depth and sensor performance have been minimized by careful relative radiometric calibration between the two images. Table 2.8 shows the coefficients matrix used in the Tasseled Cap transformation of both images. For example, the DNs of the TCT Brightness band are produced as the linear function of the Landsat image bands 1-5 and 7 based on the coefficients in the first row of Table 2.8.

Table 2.8. Tasseled Cap coefficient matrix for TM 5 images from ERDAS Imagine.

	Landsat Image Band					
Index	**1**	**2**	**3**	**4**	**5**	**7**
Brightness	0.2909	0.2493	0.4806	0.5568	0.4438	0.1706
Greenness	-0.2728	-0.2174	-0.5508	0.7221	0.0733	-0.1648
Wetness	0.1446	0.1761	0.3322	0.3396	-0.6210	-0.4186
Haze	0.8461	-0.0731	-0.4640	-0.0032	-0.0492	0.0119
Fifth	0.0549	-0.0232	0.0339	-0.1937	0.4162	-0.7823
Sixth	0.1186	-0.8069	0.4094	0.0571	-0.0228	-0.0220

Image Differencing

After each image is enhanced or transformed using NDVI, principal components analysis, or Tasseled Cap, image differencing (also known as image subtraction) was used to create a continuous change image from each transformed image pair. Subtracting the 1991 pixel values from the 2000 pixel values, the pixel values in the resulting change image indicate the amount, if any, of positive or negative change in the appropriate index value or component. The NDVI change image indicates changes in reflectance of red and infrared radiation resulting from changes to health, density and extent of vegetation cover. The PCA and Tasseled Cap change images indicate changes in the second or "greenness" component, also indicating change in the extent or status of vegetation cover. The image differencing was performed using the Change Detection function in ERDAS Imagine, found in the Utilities submenu of the Interpreter menu. Each differencing operation in Imagine results in two images, a single-band continuous data 'Image Difference' image, and a classified 'Highlight Change' image using five classes: Decreased, Some Decrease, Unchanged, Some Increase, and Increased, based on percentage or value thresholds. However, in this study an alternative thresholding method was used to create the 'Highlight Change' images, which will be discussed in detail in the next section.

Choosing a Change Threshold

In change detection using remote sensing data, thresholds are used to define what is and what is not a meaningful change from the continuous change images produced by image differencing. There is little literature available concerning selecting appropriate thresholds, and indeed "Threshold selection is generally the most subjective, and often problematic, step in detecting change with remotely sensed imagery, and is often determined qualitatively by the analyst" (Wilson et al., 2004). This study is no different in that regard. However, all attempts have been made to determine the appropriate change threshold that is sensitive to real changes in land cover and vegetation while reducing the appearance of "false changes". In this study, thresholds were based on z-scores for each change image variable, so that levels of change could be standardized and compared between image transformation methods irrespective of the range of values in the change images themselves. This method is based on the fact that "pixels of no brightness value change are distributed around the mean and pixels of change are found in the tails of the distribution." (Jensen, 1996, p. 241). A z-score change image was generated in the Spatial Modeler from each of the three original change images based on the range of pixel values and using the formula z = (x - mean)/sd, where x is a pixel value, mean is the mean pixel value for all pixels in the image, and sd is the standard deviation.

From these new z-score images multiple 'Highlight Change' images were generated for the following z-value thresholds: plus or minus 1.0, 1.25, 1.5, 1.75, 2.0, and 3.0. This was again carried out in the Spatial Modeler using a conditional expression in the following format:

CONDITIONAL {($n2_ndvi_change_z <= -1.5) 1 , (($n2_ndvi_change_z >-1.5) && ($n2_ndvi_change_z <1.5)) 2, ($n2_ndvi_change_z >=1.5) 3}.

By applying this conditional expression the z-score images were recoded into thematic change images containing three classes: Decreased (1), Unchanged (2), and Increased (3). The resulting thematic change images were color coded to facilitate interpretation (Decrease = red, Unchanged = tan, Increased = green) and then carefully examined in relation to the original Landsat image subsets and the high resolution aerial photographs to choose the best possible threshold.

Ground Truthing and Accuracy Assessment

Ground truthing and accuracy assessment involve careful comparison of the thematic change images with high resolution aerial photography to determine on a pixel by pixel basis whether a given change detection methodology has accurately classified areas of decreased, increased, or unchanged vegetation cover. The aerial photographs, in this case 1993 black and white and 1999 color infrared USGS DOQQs and 1999 and 2000 true color orthophotos from Aerials Express, serve as a proxy dataset in place of actual field verification of data points. As evaluating every pixel in a change image is not practical or necessary, a set of check points randomly generated over the study area serves as a statistical sample by which the entire thematic change image was evaluated.

In this study, 300 accuracy assessment check points were randomly placed across the study area using ERDAS Imagine's Accuracy Assessment utility, which is found under the Classifier menu. A highlight change image must be selected first before the points are placed, and in this case the NDVI thematic image was used as the basis for generating the points to be checked for all three thematic change images; there was no particular reason for choosing NDVI over the other methods, and choosing one over the other does not impact the results one way or another. There are several distribution parameter options in ERDAS Imagine for the placement of random points across the study area, all of which require picking the classes to be included in

the distribution; in this case all three change classes (Decreased, Unchanged and Increased) were selected. The Random option generates a set of truly random points with no rules as to their distribution. The Stratified Random option places points randomly within each class, with the number placed in each class based upon that class's proportional representation in the change image. Using this method, due to the overwhelming majority of pixels in the thematic change image falling into the Unchanged class, of the 300 random points in an experimental trial, 266 were in the Unchanged class, 25 in the Decreased class, and 9 in the Increased class. As the focus of this study is primarily to assess the accuracy of the three different image transformations in detecting deforestation and urbanization, this distribution was not acceptable. Therefore, the third distribution option, Equalized Random, was chosen and 100 points were randomly placed within each of the three classes ensuring good representation of each class in the final results.

The accuracy assessment of the random check points was performed in ESRI's ArcGIS/ArcMap 9.0 software as this platform offers several tools that facilitate the accuracy assessment task. In order to do this, the X, Y coordinates (in State Plane feet) of the random points from ERDAS Imagine were exported first to a .dat file, then opened in WordPad and saved as a Rich Text Document, which was then opened in Excel and cleaned up, and finally saved as a .dbf file. This .dbf file was then brought into ArcMap and used to create an event theme shapefile of the 300 checkpoints from the X, Y coordinates, and fields were added to contain the image classification results and ground truth data codes. A project interface was set up containing the check point shapefile, the three thematic change images based on the z-score change images, the Landsat images themselves, and the various multi-date sets of high resolution aerial photographs. Each point was then visited in turn, and the class assigned by each method as well as the actual ground truth data was determined using the Identify tool and recorded in the

attribute table of the shapefile. Figures 2.5 and 2.6 show the distribution of the 300 check points over the study area and the ArcMap project interface with the data layers used in the accuracy assessment. Figures 2.7-2.12 show examples of the Landsat subsets and the various aerial photograph datasets used in the assessment, using the newly constructed Mall of Georgia as an example. It should be noted that due to the fact that the earliest available aerial photograph is from 1993, two years after the 1991 image was taken, for those points where the 1993 photo shows built up or cleared land it is necessary to refer to the 1991 Landsat itself to see if the build up and de-vegetation occurred between 1991 and 1993. Similarly, as the later Landsat image is from 2000, if an area is unchanged in the 1999 photos, it is necessary to also check the 2001 photos to make sure that the land cover did not change between 1999 and 2001. If the area is unchanged in 1999 but built up in the 2001 photos it is necessary to refer to the 2000 Landsat image itself as there is no other way of knowing exactly when the change occurred relative to the Landsat scene capture.

Results of the ground truthing of the 300 sample points were recorded in an Excel spreadsheet and then a pivot table was used to create a classification error matrix and compute several types of accuracy statistics. Overall accuracy is be obtained by dividing the total number of correctly classified pixels by the total number of reference pixels. Producer's accuracy measures errors of omission and indicates how well the ground truthing pixels of a given class (Decreased, Unchanged, and Increased) are classified. Producer's accuracy is determined by dividing the number of correctly classified reference pixels in each class by the number of reference pixels actually in that class based on ground truth data. User's accuracy, obtained by dividing the number of correctly classified reference pixels in each class by the total number of reference pixels assigned to that class, measures errors of commission and indicates the

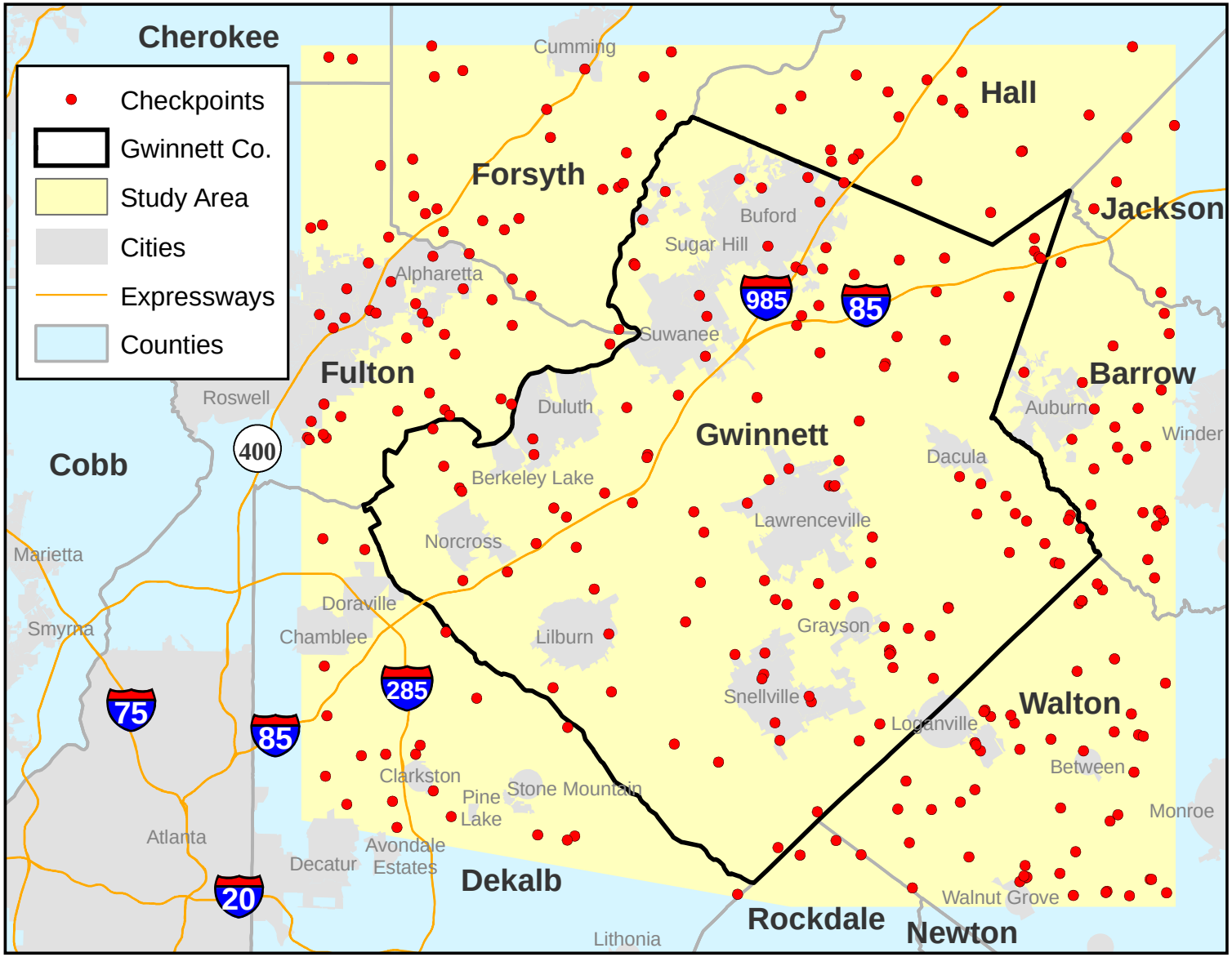

Figure 2.5. The distribution of the 300 random check points used in the accuracy assessment. Also shown are the study area subset extent and the Gwinnett County boundary.

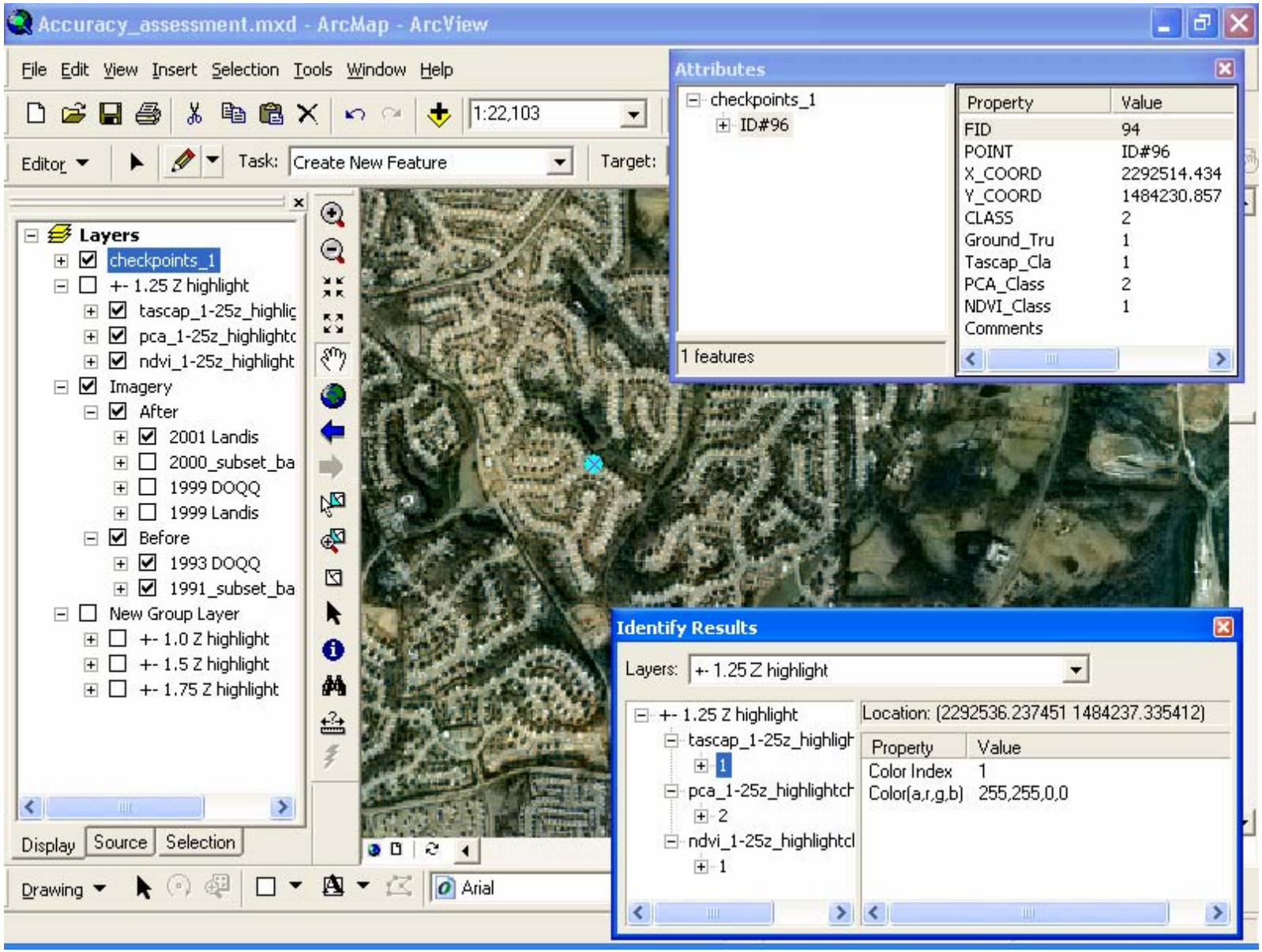

Figure 2.6. The ArcMap interface and datasets used in accuracy assessment.

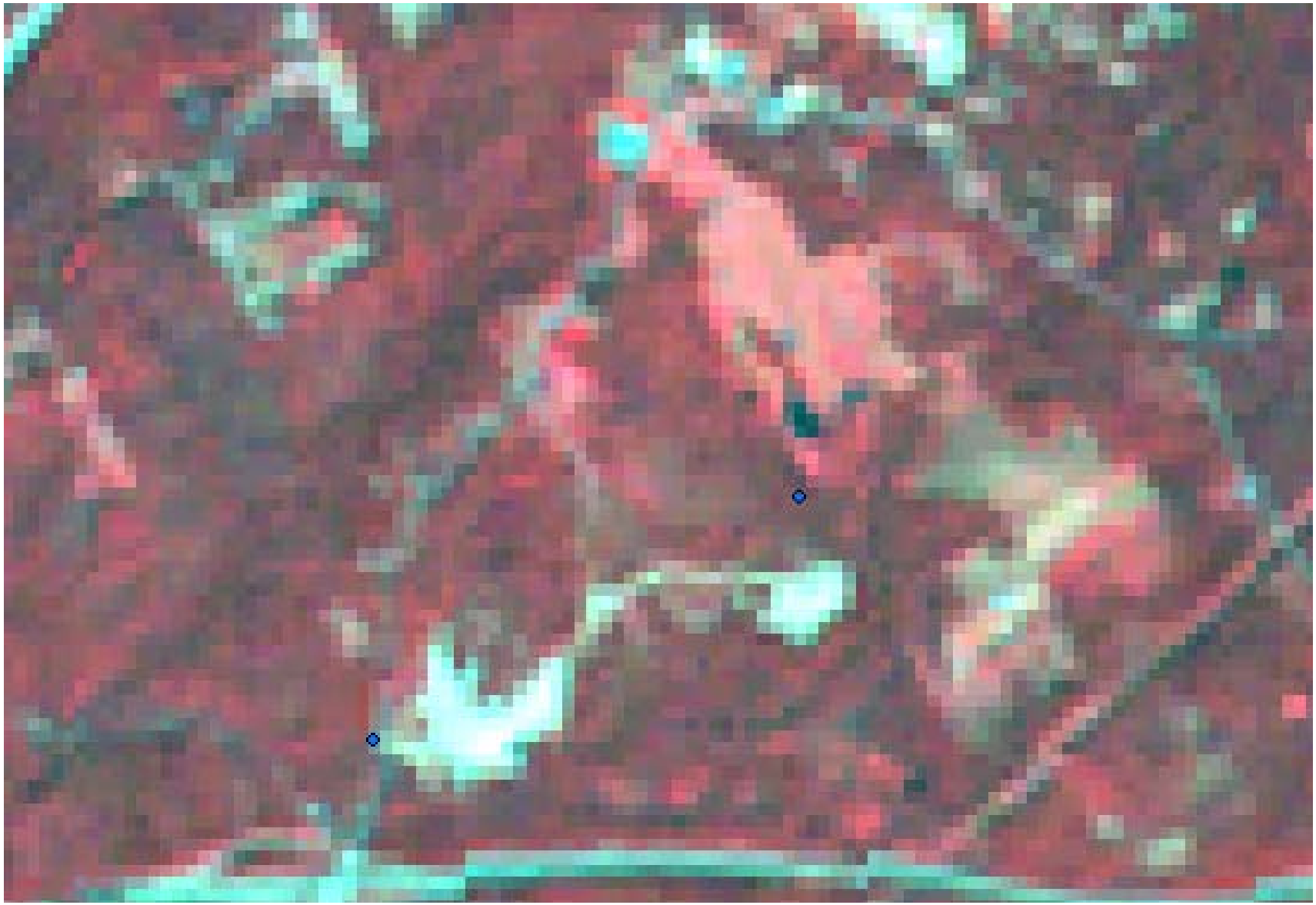

Figure 2.7. 1991 Landsat image. Example showing the future site of the Mall of Georgia.

Figure 2.8. 1993 panchromatic DOQQ. Example showing future site of the Mall of Georgia.

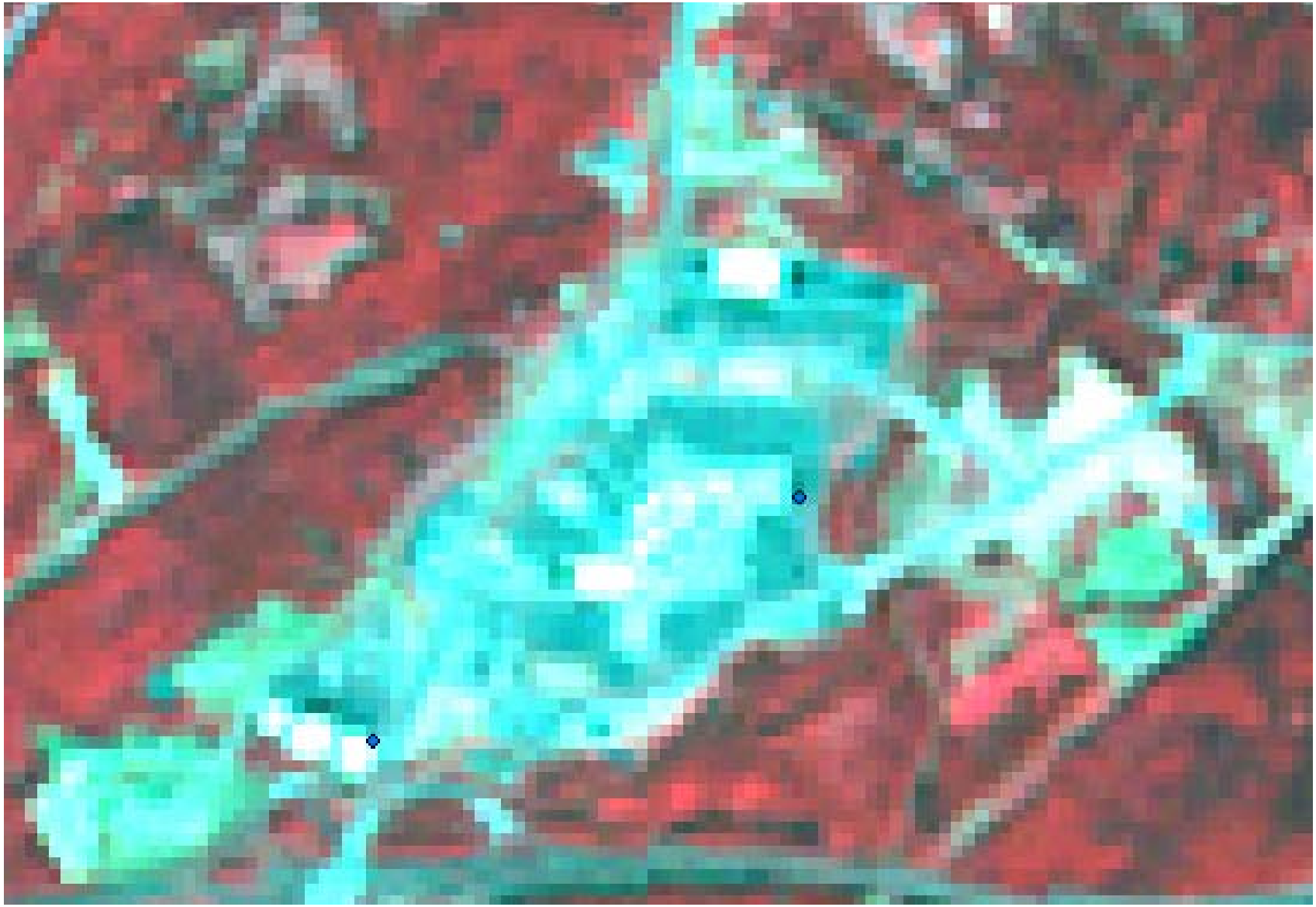

Figure 2.9. 2000 Landsat image. Example showing loss of vegetation and increased urbanized area resulting from the construction of the Mall of Georgia.

Figure 2.10. 1999 color infrared DOQQ. Example showing the Mall of Georgia during construction.

Figure 2.11. 1999 Aerials Express orthophotos. Example showing the Mall of Georgia during construction.

Figure 2.12. 2001 Aerials Express orthophotos. Example showing the finished Mall of Georgia.

probability (as a percentage) that a pixel placed in a given class actually represents that class on the ground (Lillesand and Kiefer, 2000, p. 570; NOAA, 2005). The goal for this study is to determine which of the three image algebra transformations produce the least error and the greatest accuracy in a change detection product, with the accepted standard being an overall accuracy of classification of greater than 80%. Results of accuracy assessments provide quantitative evaluations on the effectiveness of the three methods examined in this study.

Kappa Coefficient (KHAT statistic)

The Kappa Coefficient (Cohen, 1960) or KHAT is a discrete multivariate statistic used to evaluate the results of an error matrix. It is a measure of the difference between the performance of a given classification, and a classification based on purely random pixel assignments. KHAT "serves as an indicator of the extent to which the percentage correct values of an error matrix are due to 'true' agreement versus 'chance' agreement (Lillesand and Kiefer, 2000). Unlike the User's, Producer's, and overall accuracy statistics, KHAT "incorporates the off diagonal observations of the rows and columns as well as the diagonal to give a more robust assessment of accuracy than overall accuracy measures" (NOAA, 2005). KHAT generally ranges from 0 to 1, with 0 being no better than a chance classification and 1 being an ideal 'true' agreement between the classified pixels and the reference data (Lillesand and Kiefer, 2000). The Kappa coefficient is computed using the following formula:

$$\text{KHAT} = \frac{N * \sum_{i=1}^{r} x_{ii} - \sum_{i=1}^{r} (x_{i+} * x_{+i})}{N^2 - \sum_{i=1}^{r} (x_{i+} * x_{+i})}$$

where

r = number of rows in the error matrix;

x_{ii} = the number of observations in row *i* and column *i* (on the major diagonal);

x_{i+} = total of observations in row *i* (shown as the marginal total to right of matrix);

x_{+I} = total of observations in column *i* (shown as marginal total at bottom of matrix);

N = total number of observations included in the matrix (Lillesand and Kiefer, 2000).

The Kappa Coefficient was calculated for all error matrices resulted from the accuracy assessment of the change detection, in order to better evaluate the strength and statistical soundness of the assessment for each method's results.

Summary of Vegetation Changes in Gwinnett County 1991-2000

A summary of change results within Gwinnett County during the study period was done for each method using the ± 1.25 z value thematic change images. First, the thematic change images for the study area were subset using an AOI created from the Gwinnett County boundary. From these new Gwinnett County subset highlight change images, the number of pixels in each of the three change classes was recorded from the Raster Attributes dialog in the ERDAS Imagine viewer. These pixel numbers were then converted into hectares using the following formula:

((number of pixels in a given class) * 900) / 10,000,

where 900 is the area of each pixel in square meters, and 10,000 is the number of square meters in one hectare.

Next, using the ± 1.25 z thematic change image(s) resulted from the transformation and differencing method(s) determined to be the most accurate, an estimated area of change during the study period for different types of original vegetation surfaces is computed, based on the

range of NDVI values in the 1991 Landsat study area subset image. The 1991 NDVI-transformed study area image was recoded in Spatial Modeler into a thematic image with four classes based on the following conditional statement:

CONDITIONAL { ($n2_1991_ndvi_masked <= -0.2) 1 , (($n2_1991_ndvi_masked >-0.2) && ($n2_1991_ndvi_masked <=0)) 2, (($n2_1991_ndvi_masked >0) && ($n2_1991_ndvi_masked <=0.25)) 3, ($n2_1991_ndvi_masked >0.25) 4}.

This produced a thematic image with four classes of NDVI values ranging from -0.69 (the minimum NDVI value in this dataset) to -0.2, greater than -0.2 to 0.0, greater than 0.0 to 0.25, and greater than 0.25 to 0.64 (the maximum NDVI value in this dataset). These ranges were chosen based on the examination of NDVI values for several hundred pixels to roughly correspond to different land cover types. It was found that the majority of forested pixels in the 1991 image have an NDVI between 0.0 and 0.25, while most of the agricultural areas have an NDVI value between 0.25 and 0.64. This is not a clearly defined separation, as areas of particularly dense or healthy forest have NDVI values greater than 0.25, and areas of sparse or unhealthy grass or crops can have NDVI values of less than 0.25. However, for the purposes of this analysis it is a sufficiently accurate generalization. Similarly, it was found that areas of bare soil or very sparse vegetation generally have NDVI values between -0.2 and 0.0, while areas of concrete, asphalt and other urban land cover types generally have an NDVI value of less than -0.2. Again this is not true in every case but serves the intended purpose here. It should be noted that water areas have the lowest NDVI values as water is a good absorber of near-infrared radiation.

This four-class thematic NDVI image was then masked into separate images using the Mask utility under the Interpreter menu in Imagine. The pixels in the Decreased and Increased

classes from the Gwinnett County subset highlight change image(s) were used as the mask to produce thematic images containing the recoded NDVI ranges for only the Decreased and Increased pixels. The count of pixels in each change class by NDVI value range were then recorded from the Raster Attribute dialog in the Imagine viewer into an Excel spreadsheet, and converted to area in hectares using the formula above.

CHAPTER THREE: RESULTS AND DISCUSSION

Geometric Rectification Results

For this study, the 2000 ETM+ Landsat image study area subset was rectified to the 1999 USGS DOQQs using 12 ground control points with a resulting Root Mean Squared Error of 0.4945 (48.675 State Plane feet/98.4252 ft. pixel resolution) with a first order polynomial transformation, and a new image was generated using Nearest Neighbor resampling, again to preserve original pixel reflectance values. The 1991 TM 5 Landsat image study area subset was then geometrically rectified to the 2000 ETM+ image subset using 14 ground control points evenly distributed over the study area with a resulting RMSE of 0.232 (22.8421 State Plane feet/98.4252 ft. pixel resolution) with a second order polynomial transformation, and again a new geometrically corrected 1991 subset image of the study area was generated using Nearest Neighbor resampling. Table 3.1 shows the X, Y location (in State Plane feet) of input and reference GCPs, residual error, RMSE and contribution to the total RMSE for the fourteen GCPS used to rectify the Landsat image subsets to each other.

Table 3.1. GCPs used for rectification of 1991 to 2000 Landsat subset images.

GCP	X Input	Y Input	X Ref.	Y Ref.	X Res.	Y Res.	RMSE	Cont.
GCP 1	2369030.25	1449333.57	2369084.06	1449381.13	-11.30	-11.09	15.83	0.69
GCP 2	2252771.89	1469363.68	2252756.94	1469237.46	-5.90	17.69	18.65	0.82
GCP 3	2294669.71	1512494.43	2294660.30	1512387.37	4.11	-28.70	29.00	1.27
GCP 4	2403856.37	1490530.68	2403991.01	1490612.30	3.42	-15.83	16.19	0.71
GCP 5	2270891.65	1388166.02	2270885.73	1388116.49	5.37	-18.08	18.86	0.83
GCP 6	2415387.38	1384929.56	2415540.90	1385007.37	10.86	-9.11	14.18	0.62
GCP 7	2300944.47	1391028.19	2300952.72	1391030.70	14.89	-5.08	15.73	0.69
GCP 8	2383549.64	1407262.17	2383644.16	1407341.30	10.29	3.96	11.03	0.48
GCP 9	2362062.89	1506065.55	2362096.77	1506157.05	-19.12	43.57	47.58	2.08
GCP 10	2268418.67	1415711.76	2268399.76	1415666.38	-9.59	17.44	19.91	0.87
GCP 11	2323121.12	1446625.96	2323122.42	1446624.87	-9.14	-3.92	9.94	0.44
GCP 12	2308055.88	1422313.95	2308052.38	1422306.48	-2.98	-2.02	3.60	0.16
GCP 13	2379453.52	1376755.92	2379501.78	1376854.39	-22.24	19.14	29.34	1.28
GCP 14	2334462.52	1484179.22	2334513.56	1484178.52	31.33	-7.96	32.33	1.42

Results of Relative Radiometric Correction

Visual analysis of the scatterplots was used to determine the existence of three outliers, two of which were rooftops of commercial buildings and the third being an area of bare soil near a quarry. In this case, the same three outliers were found in the scatterplot for each image band. Removal of these outliers resulted in a significantly improved linear relationship between the two images based on the remaining twenty two radiometric control targets, although the range of brightness values was slightly reduced. Figures 3.1A – 3.1G show the scatterplots from the twenty five radiometric control targets for the entire images and each of the six bands used in the analysis. Figures 3.2A – 3.2G show the scatterplots with the three outliers removed; the remaining twenty two control targets were used for the relative radiometric correction linear regression equations. R-square values, resulting linear regression equations and trend lines are also shown on each plot.

Table 3.2 shows the R-square values for the entire six-band image and for each band both with and without the outliers removed, and the resulting linear regression equation used to generate the new, radiometrically corrected Landsat study area subset for 9-28-91 from the twenty two targets ultimately used.

Table 3.2. Summary of linear regression from radiometric control targets.

Image Band	R^2 with All Targets	R^2 with 3 Outliers Removed	Final Equation
All 6 Bands	0.5864	0.9067	y = 1.0144x + 61.92
Band 1	0.3985	0.8885	y = 0.767x + 15.891
Band 2	0.4295	0.9029	y = 1.4069x + 14.862
Band 3	0.5652	0.897	y = 1.236x + 10.975
Band 4	0.6253	0.9016	y = 0.7652x + 6.1927
Band 5	0.7413	0.9023	y = 0.8843x + 9.5655
Band 6	0.6948	0.9099	y = 1.2213x + 11.038

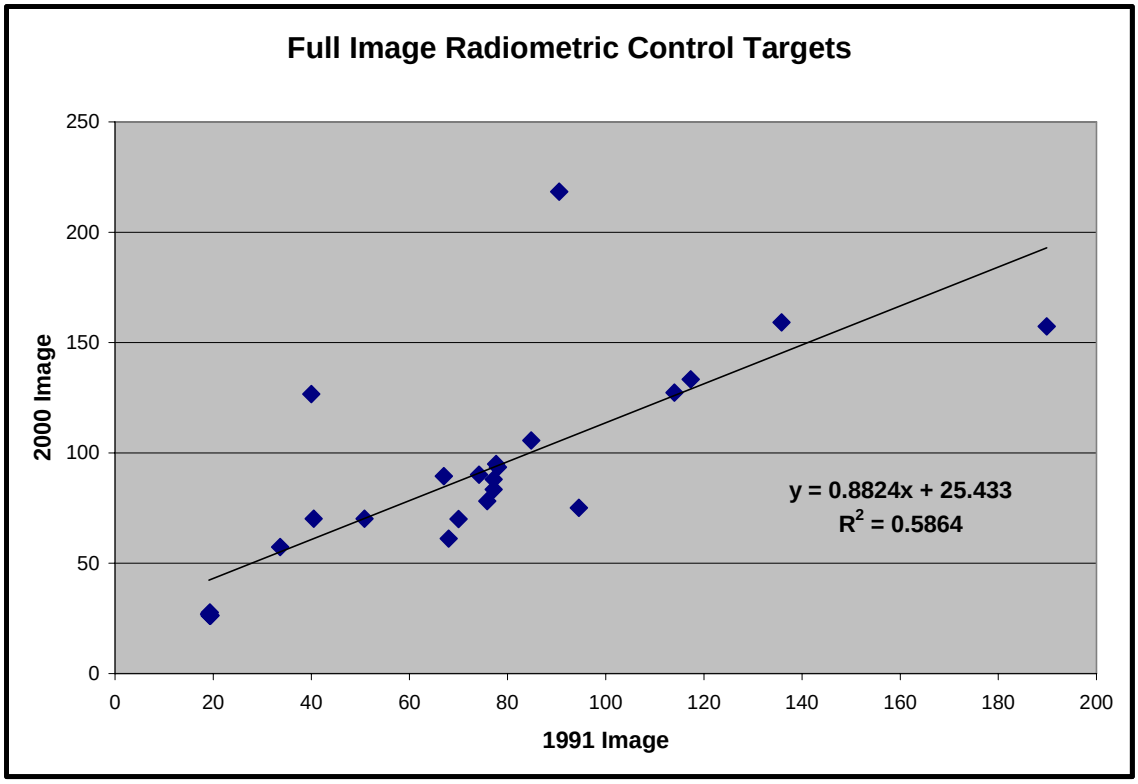

Figure 3.1A. Scatterplot of twenty five radiometric control targets for all six image bands combined.

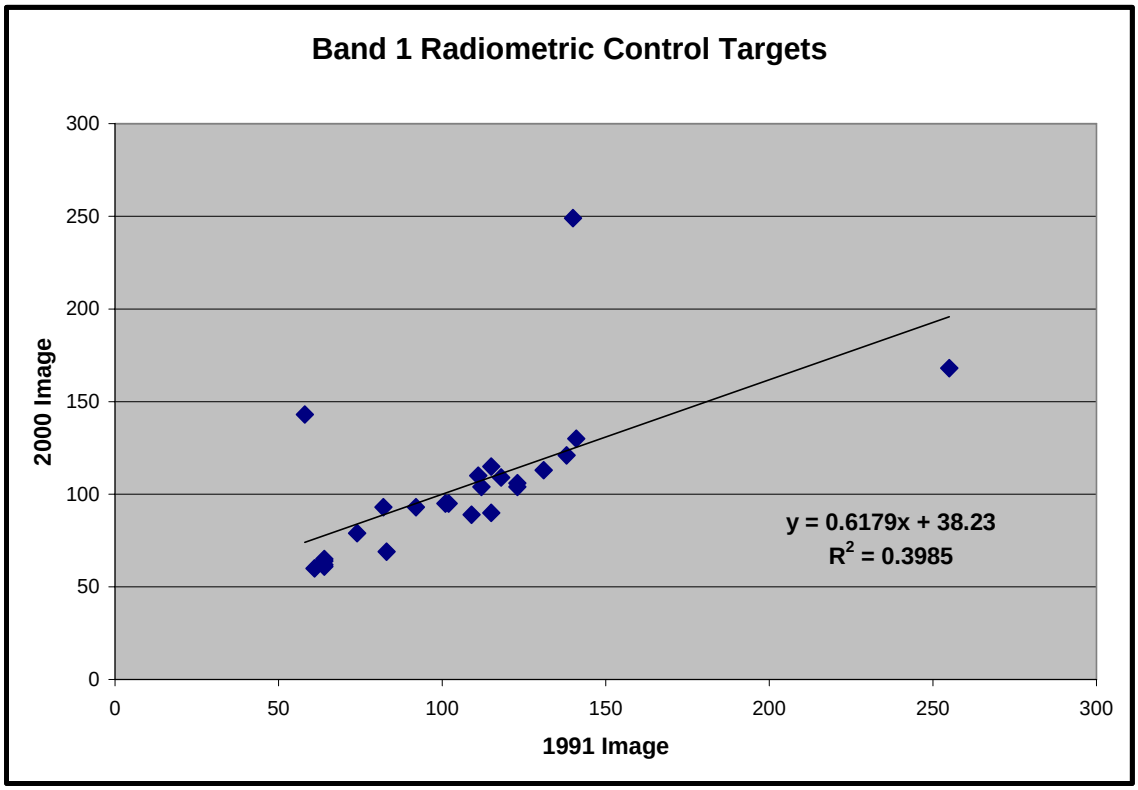

Figure 3.1B. Scatterplot of twenty five radiometric control targets for image band one.

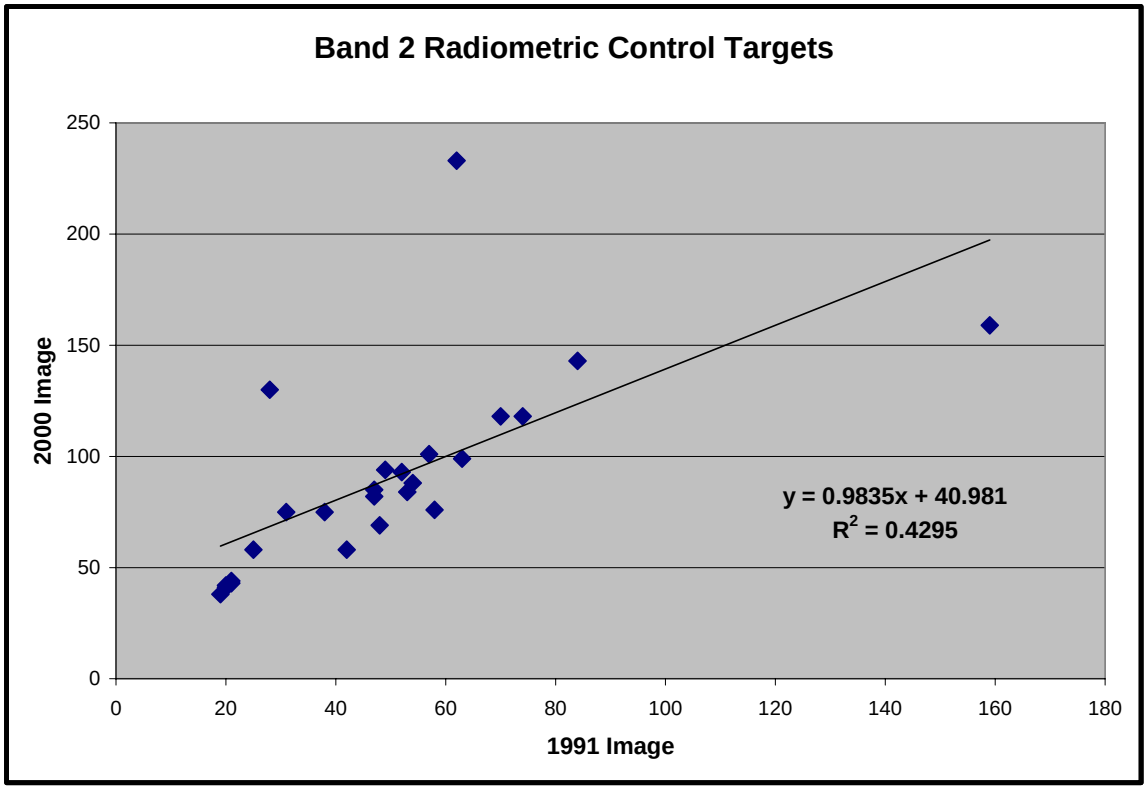

Figure 3.1C. Scatterplot of twenty five radiometric control targets for image band two.

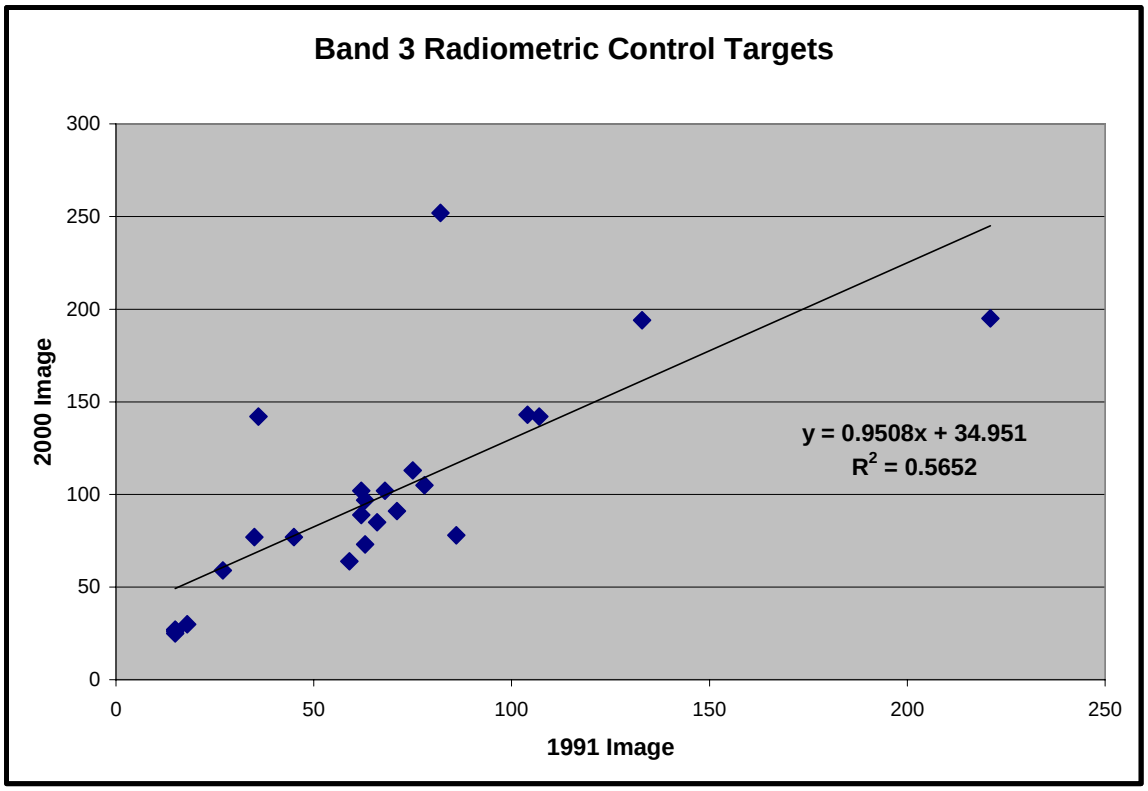

Figure 3.1D. Scatterplot of twenty five radiometric control targets for image band three.

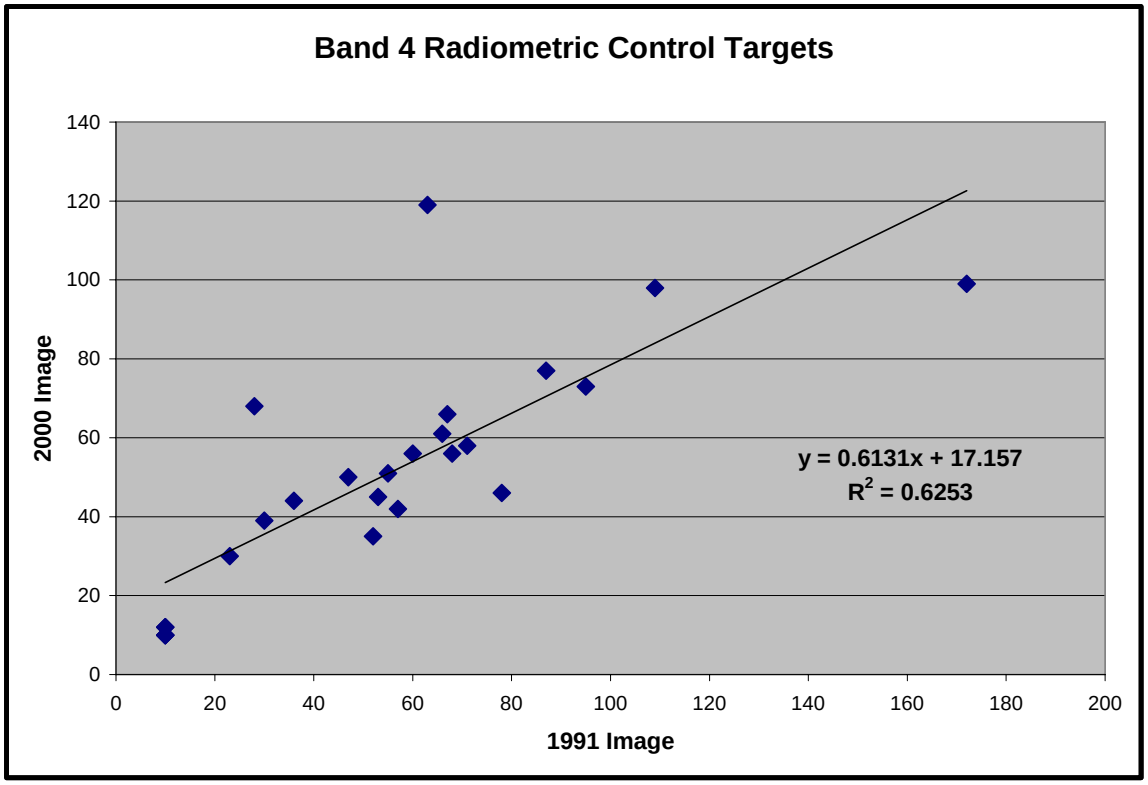

Figure 3.1E. Scatterplot of twenty five radiometric control targets for image band four.

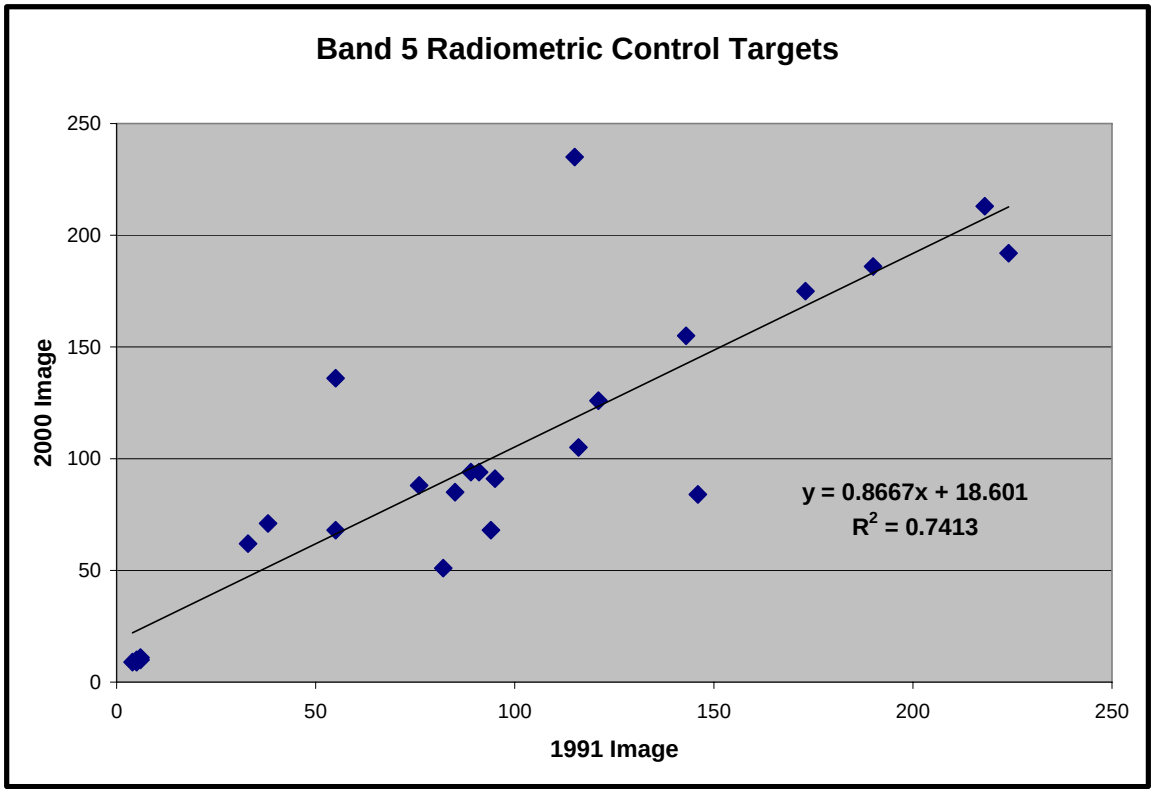

Figure 3.1F. Scatterplot of twenty five radiometric control targets for image band five.

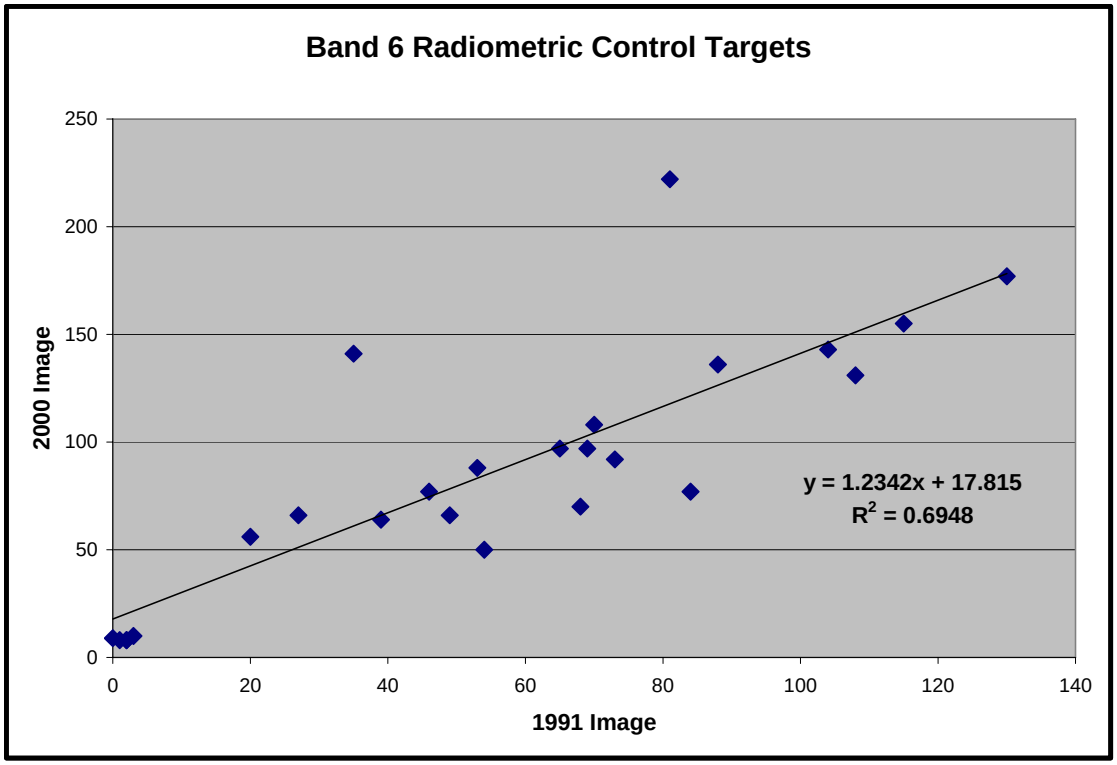

Figure 3.1G. Scatterplot of twenty five radiometric control targets for image band six.

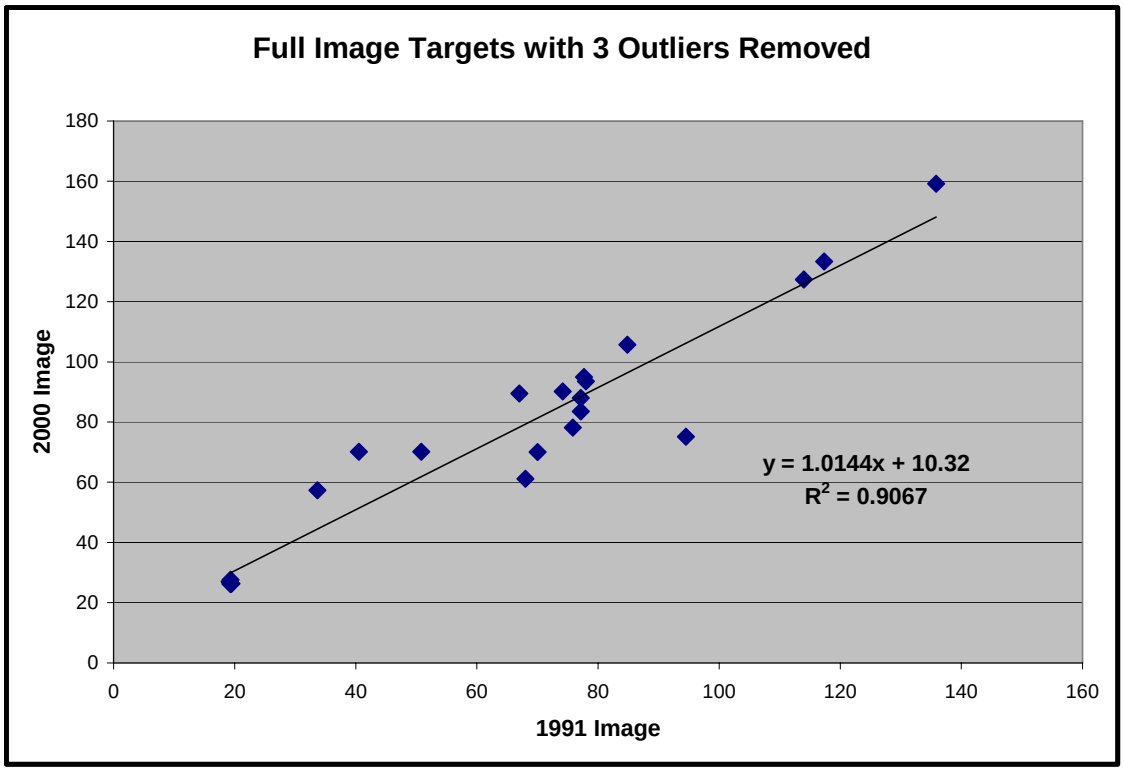

Figure 3.2A. Scatterplot of twenty two radiometric control targets for all six image bands combined.

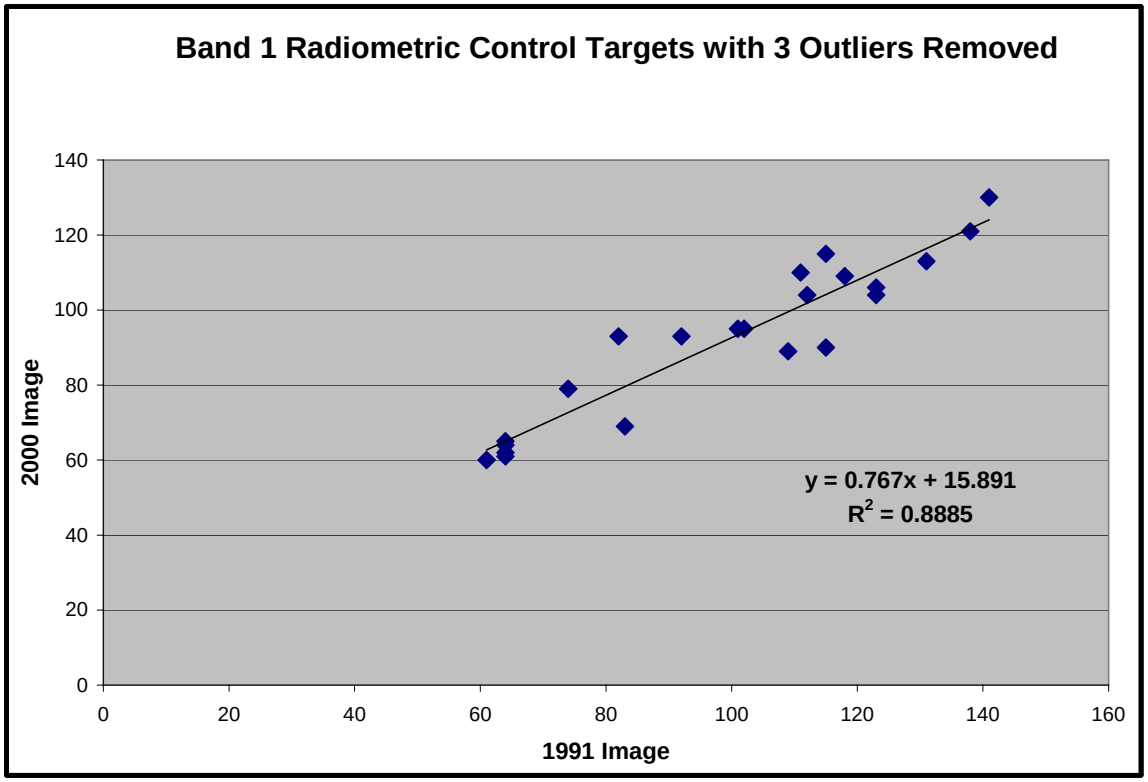

Figure 3.2B. Scatterplot of twenty two radiometric control targets for image band one.

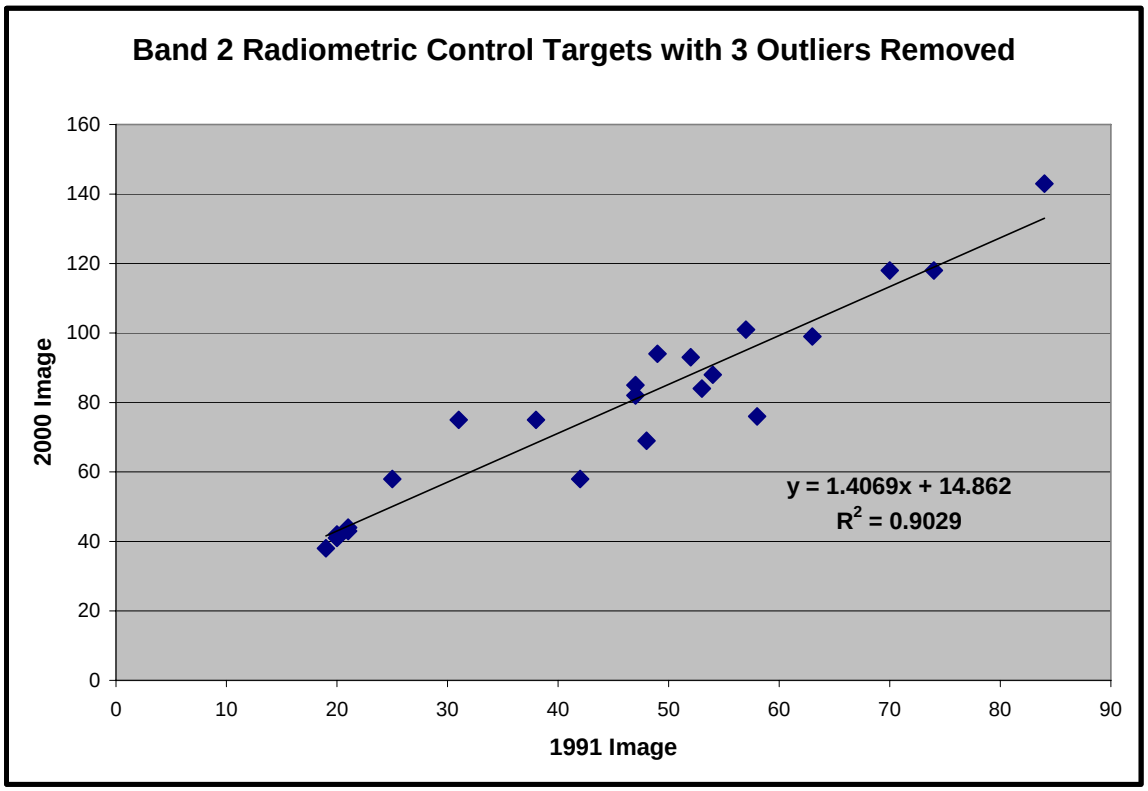

Figure 3.2C. Scatterplot of twenty two radiometric control targets for image band two.

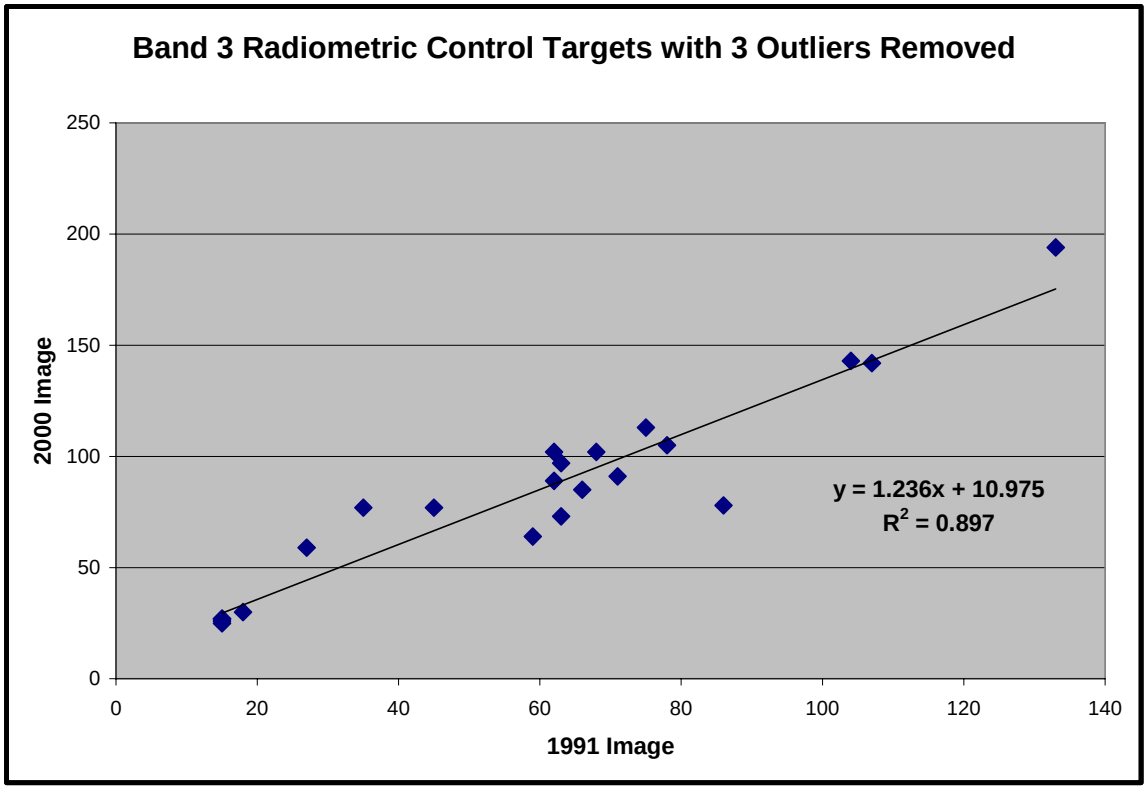

Figure 3.2D. Scatterplot of twenty two radiometric control targets for image band three.

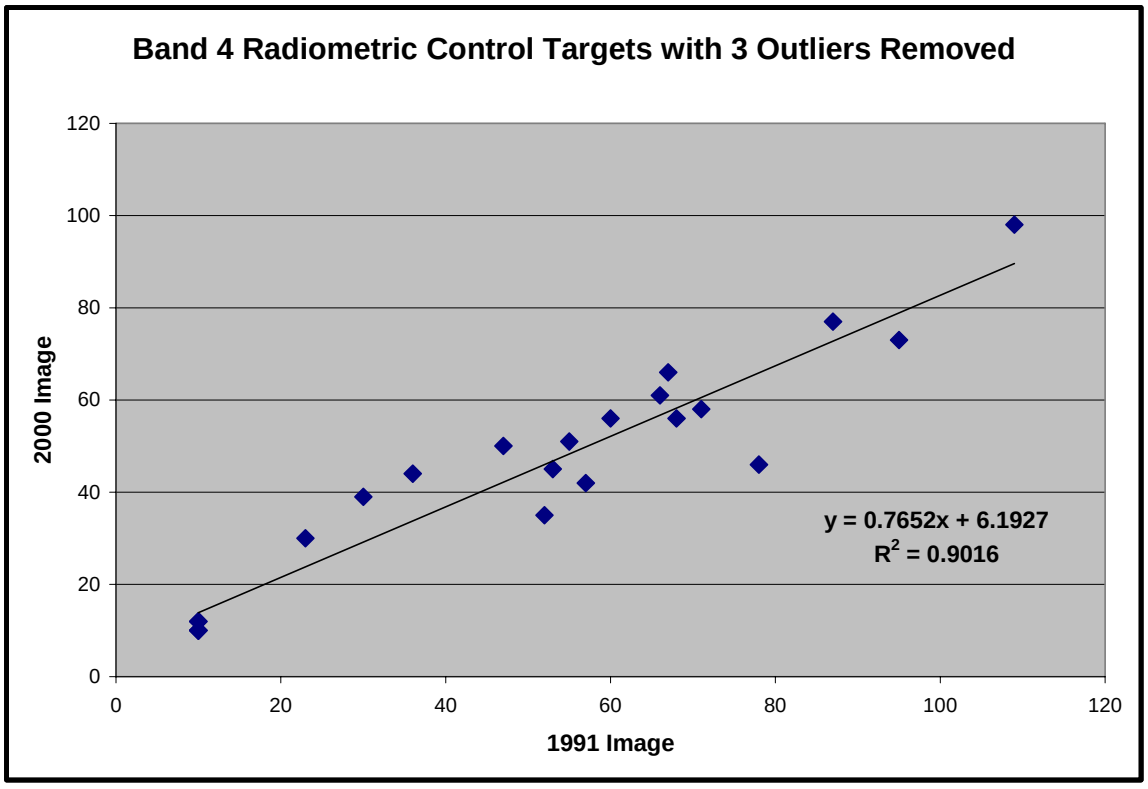

Figure 3.2E. Scatterplot of twenty two radiometric control targets for image band four.

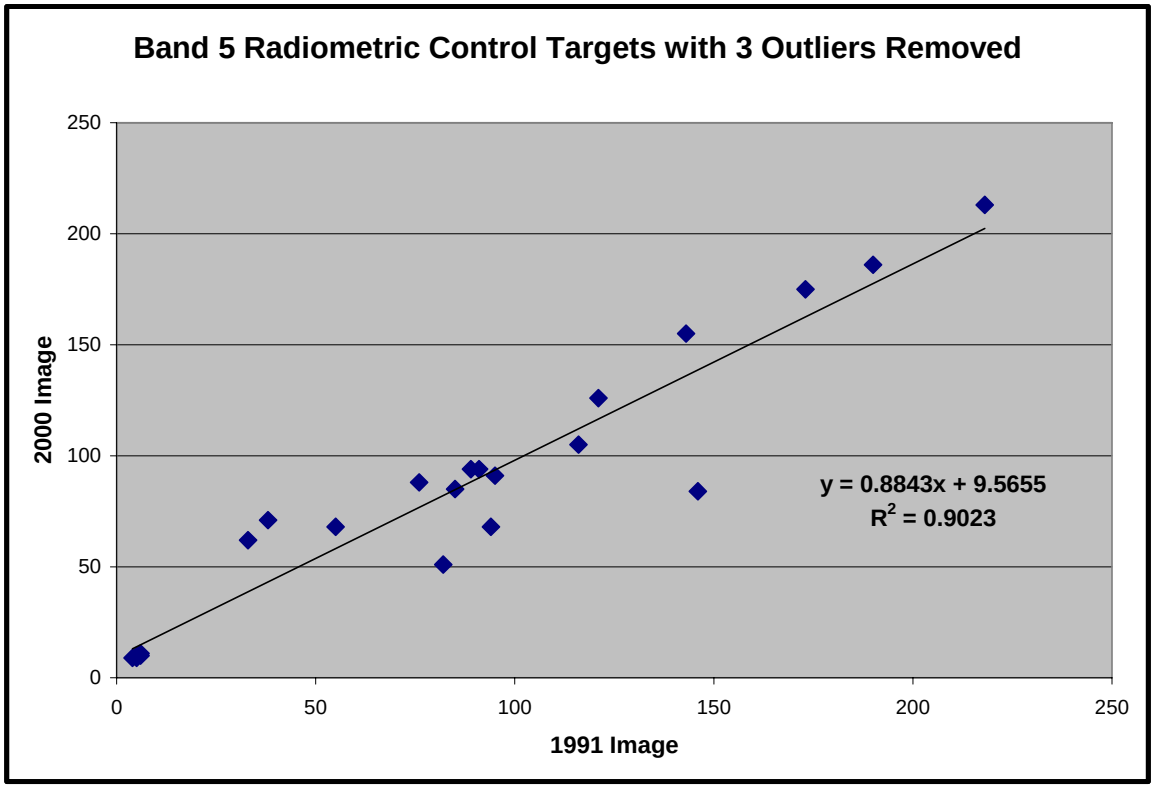

Figure 3.2F. Scatterplot of twenty two radiometric control targets for image band five.

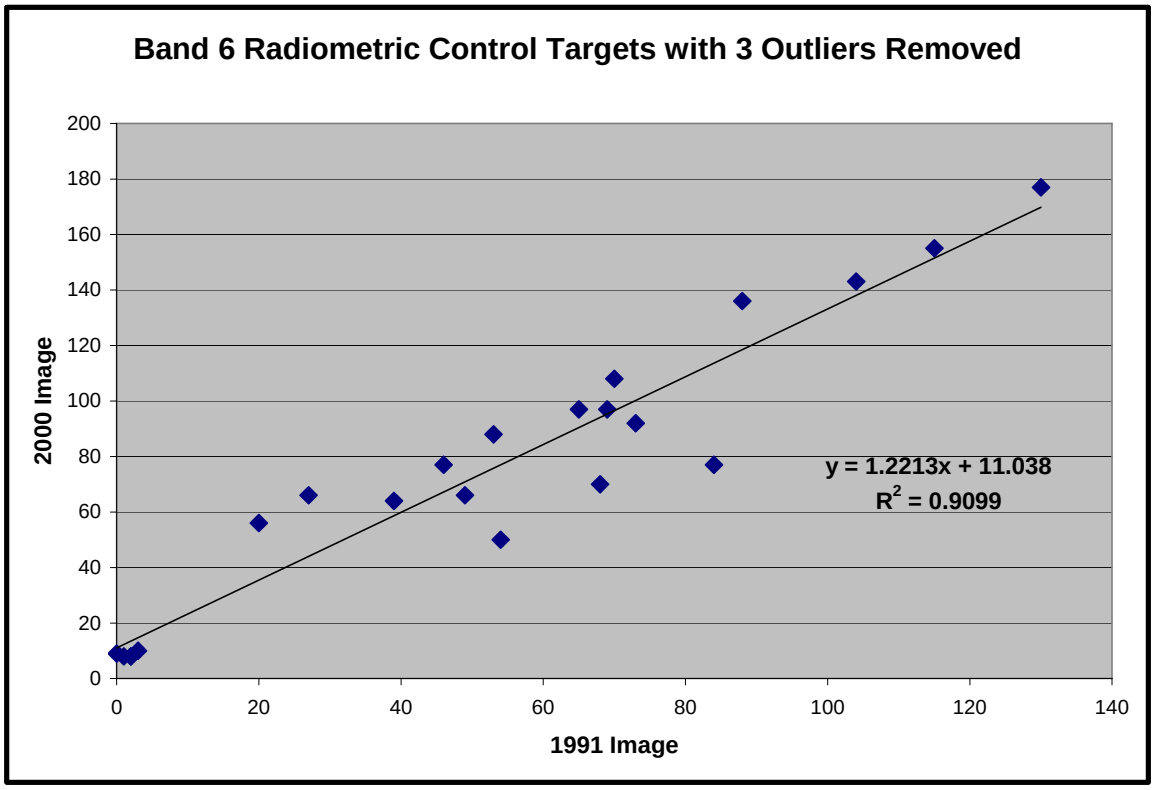

Figure 3.2G. Scatterplot of twenty two radiometric control targets for image band six.

Figure 3.3 shows the geometrically rectified, radiometrically corrected study area subset image pair ready for change detection analysis, along with the location and distribution of the ground control points used in geometric rectification, the location of the radiometric control targets, and the outline of Gwinnett County, GA, the focus of this analysis.

Image Algebra Results: Image Transformations and Differencing

The result of the NDVI transformation is a single band image with index values in each pixel. The result of the PCA transformation is a multi-band image containing six components, the second of which from this particular image pair represents "greenness". Similarly, the Tasseled Cap transformation results in a multi-band image with six components, the second of which always represents "greenness" in the image. Interestingly, following the PCA transformation, in the 9-28-2000 image the second component was reversed as compared to the 9-28-1991 image, and therefore an additional second component image was generated in the Spatial Modeler by multiplying the 2000 second component values by -1.0. Figures 3.4 through 3.7 show the results of each image transformation prior to image differencing.

Image differencing results in a single band image showing decrease, no change, or increase in the appropriate pixel value (NDVI index value or greenness component). Again, the 1991 image pixel values are subtracted from the 2000 image pixel values resulting in the change image. Both PCA and Tasseled Cap transformation methods use the band two greenness component in the differencing. Figures 3.8 through 3.10 show the single band change images produced from image differencing of the three types of transformed image pairs.

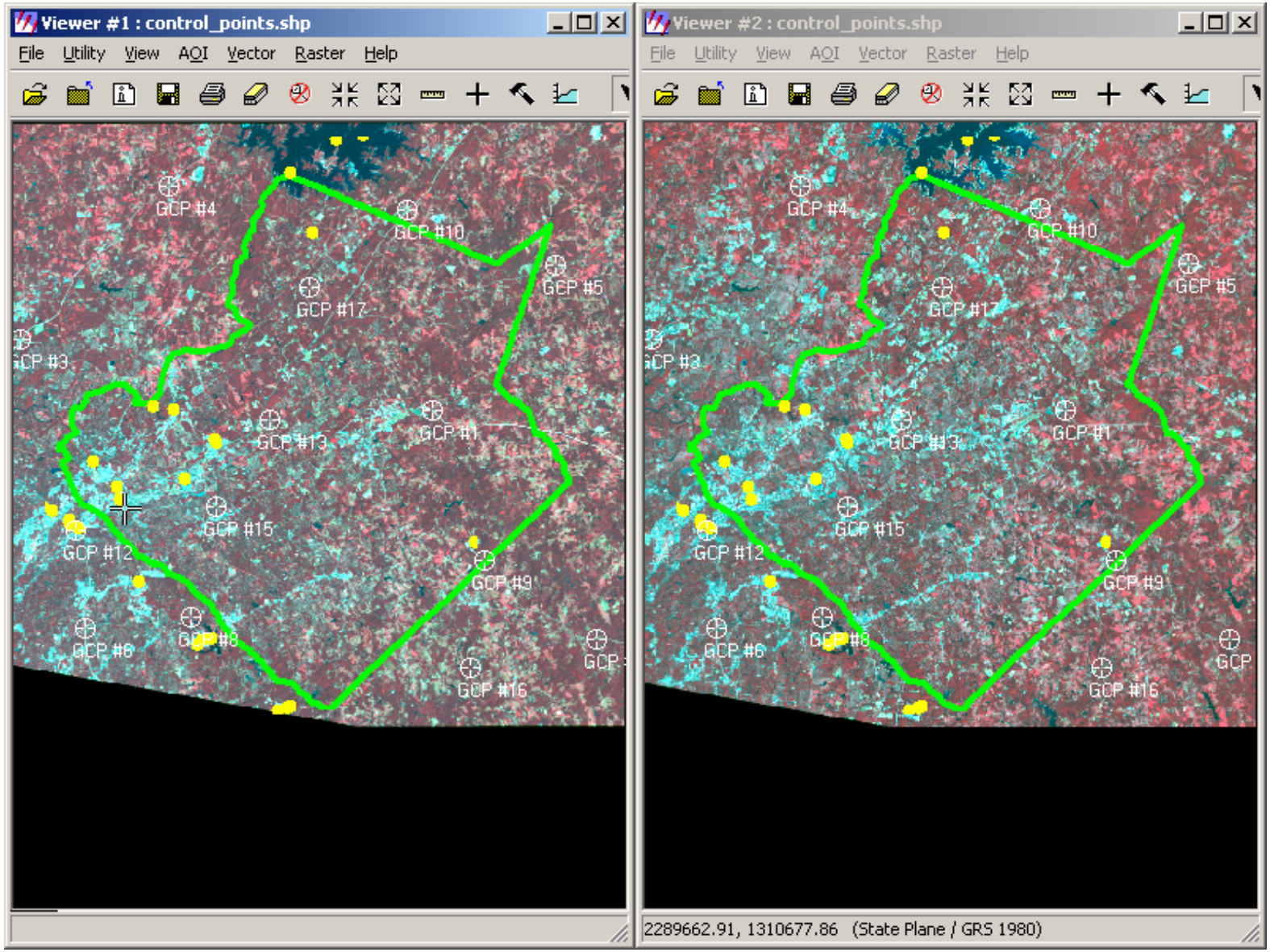

Figure 3.3. 9-28-91 and 9-28-2000 Landsat subsets ready for analysis. Also shown are the locations of the 14 GCPs used in geometric correction and the twenty two pseudo-invariant feature targets used in the relative radiometric normalization.

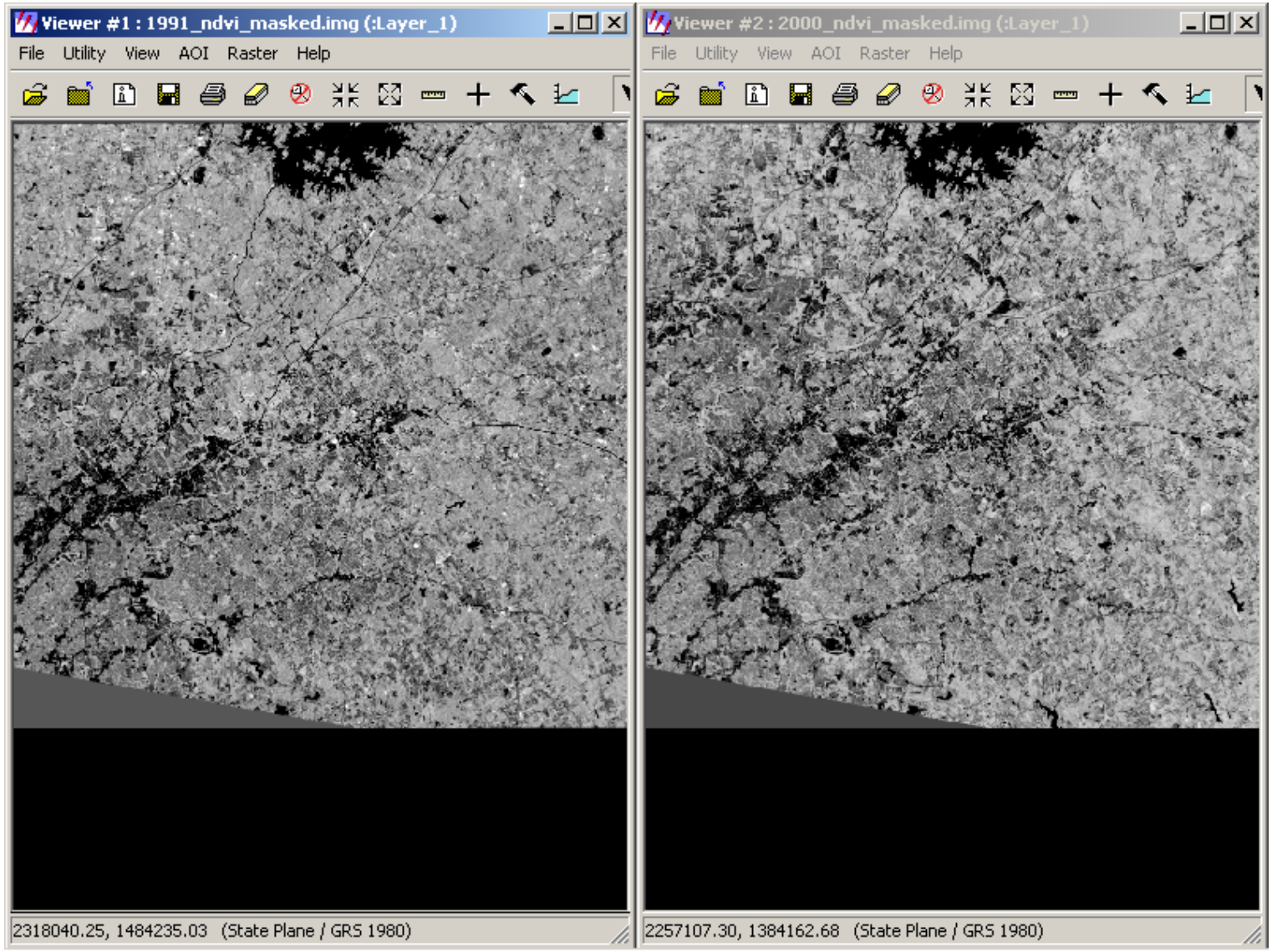

Figure 3.4. NDVI transformed images prior to differencing. Light colored pixels represent high NDVI values indicating dense, healthy vegetation cover, while dark colored pixels represent sparse vegetation or absence of vegetation such as bare dirt, asphalt, urban areas, etc.

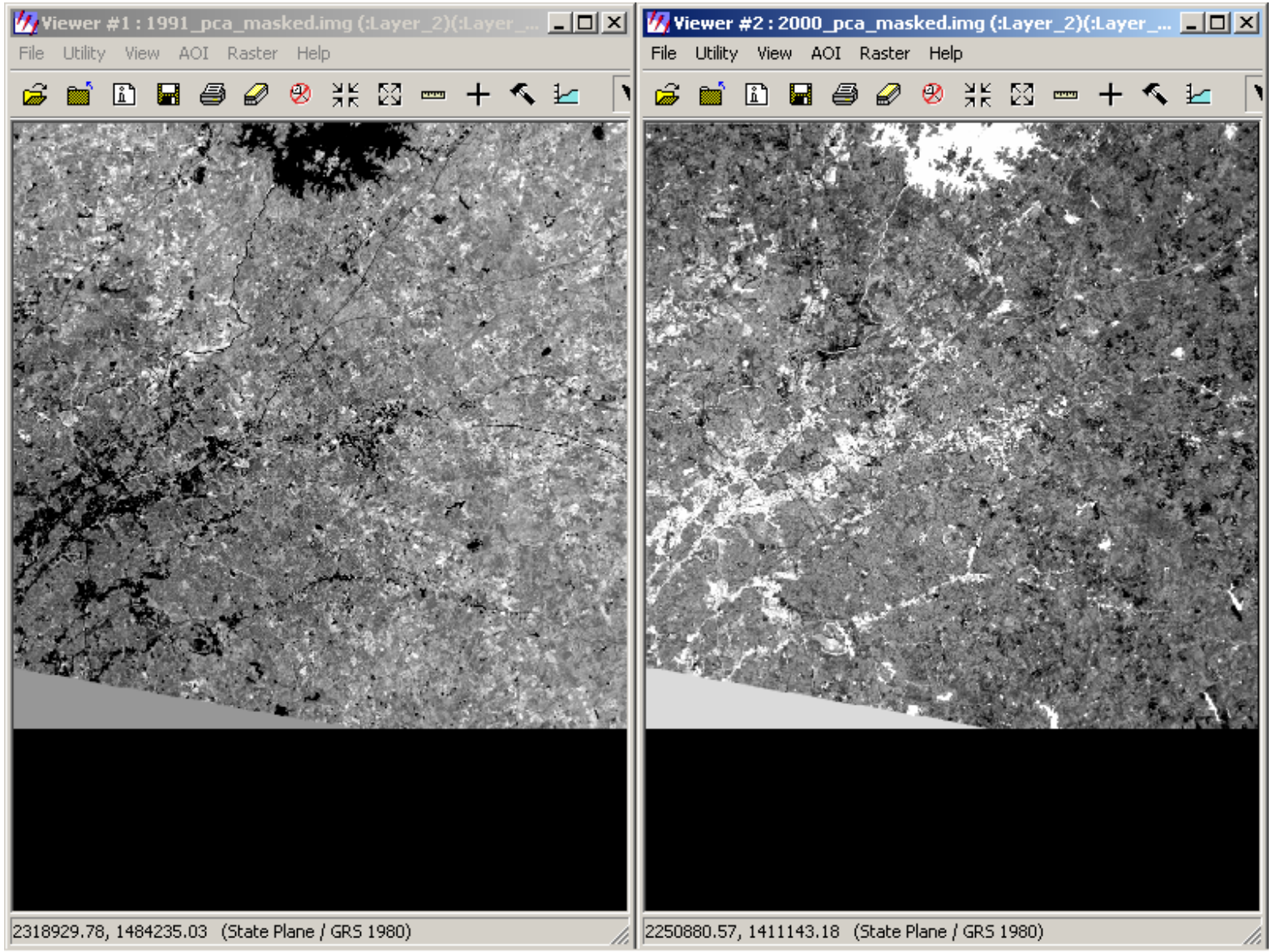

Figure 3.5. Second "greenness" component from PCA prior to image differencing and reversal of 2000 component. Note how the images are opposite each other, particularly in urban deep water areas where there is an absence of vegetation cover.

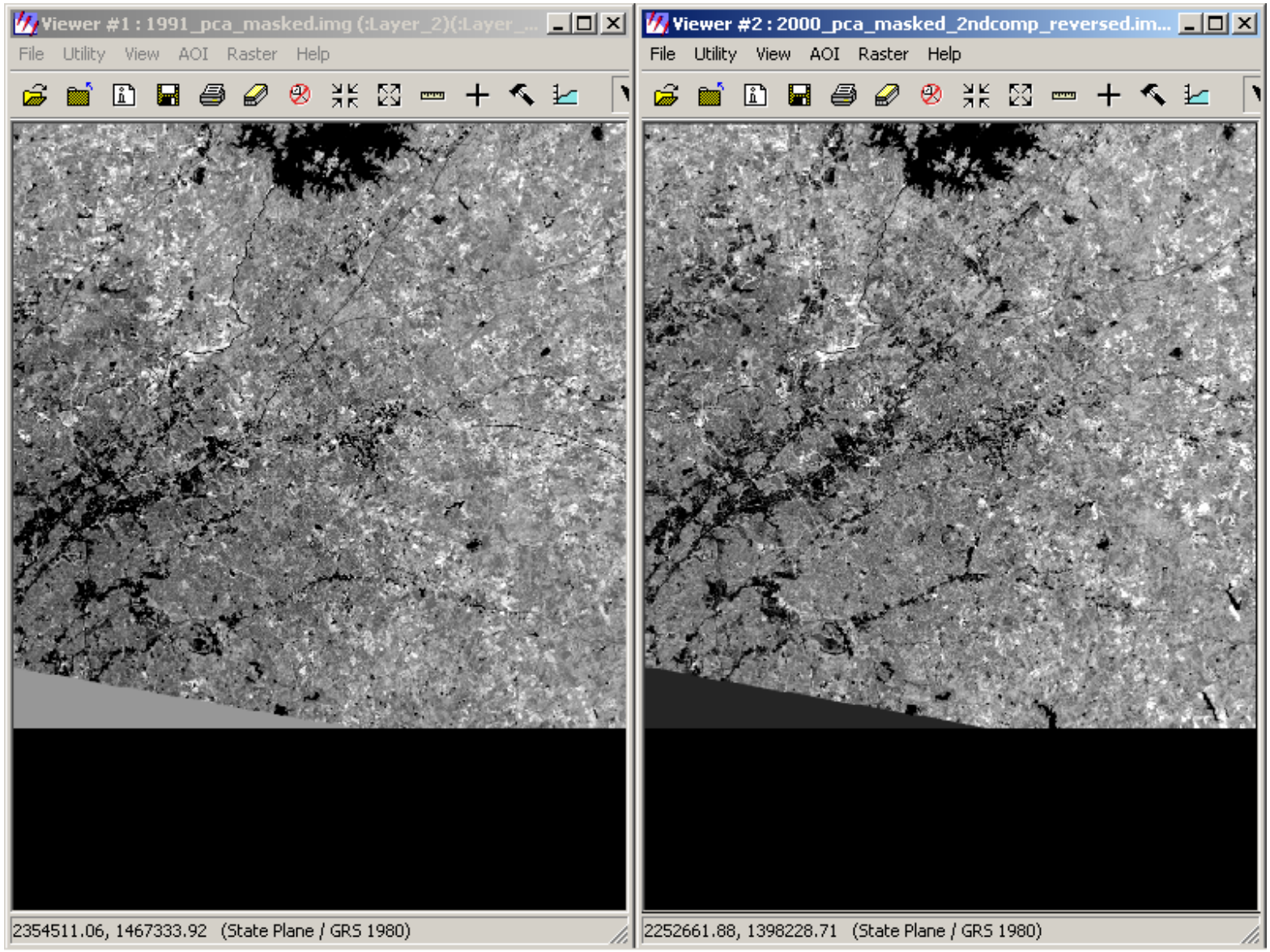

Figure 3.6. Second "greenness" component from PCA after reversal of values in 2000 image. Light colored pixels represent high levels of "greenness" or vegetation cover while dark colored pixels indicate an absence of vegetation.

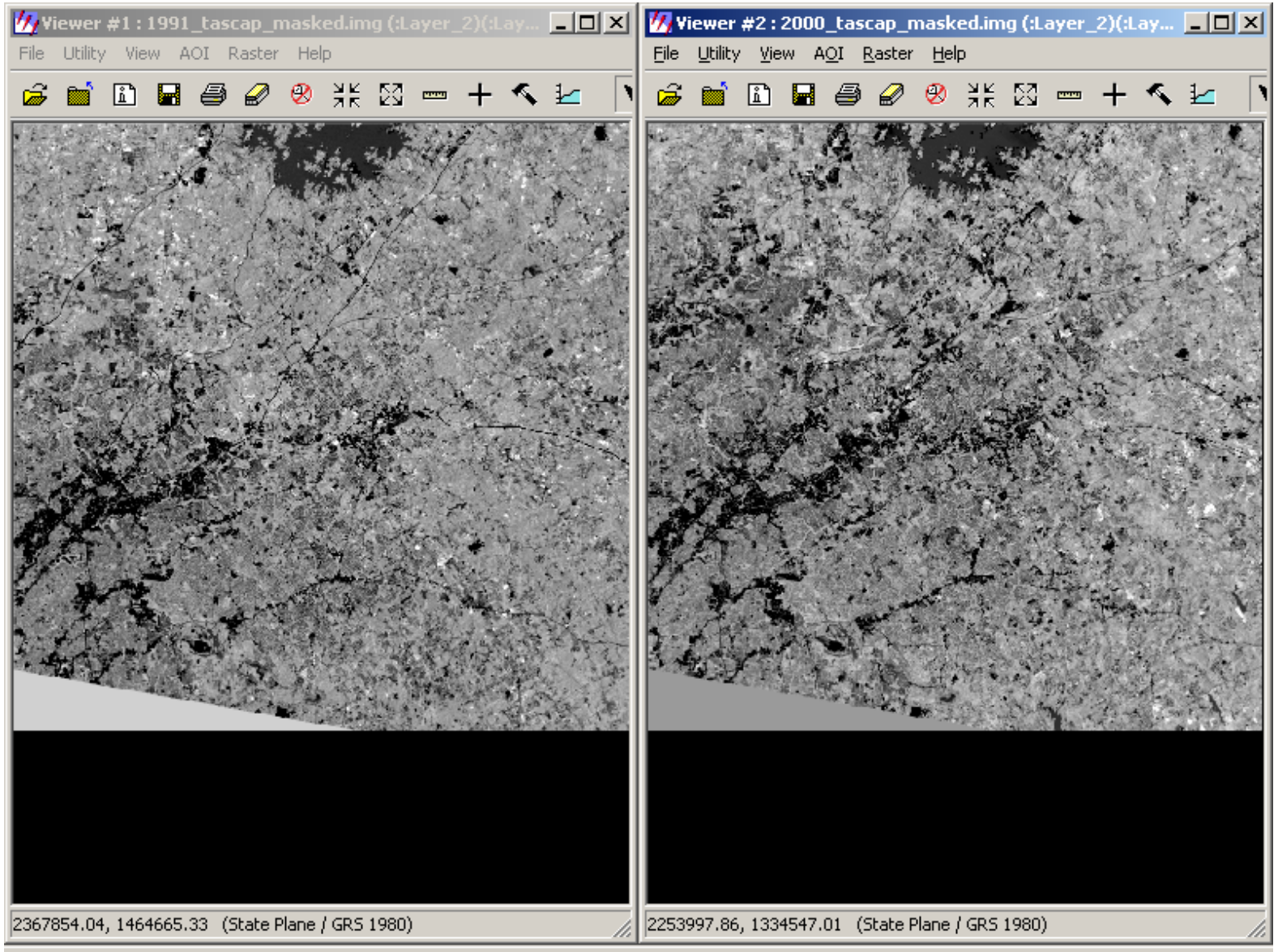

Figure 3.7. Second "greenness" component from the Tasseled Cap transformation prior to image differencing. Light colored pixels represent high levels of "greenness" or vegetation cover while dark colored pixels indicate an absence of vegetation.

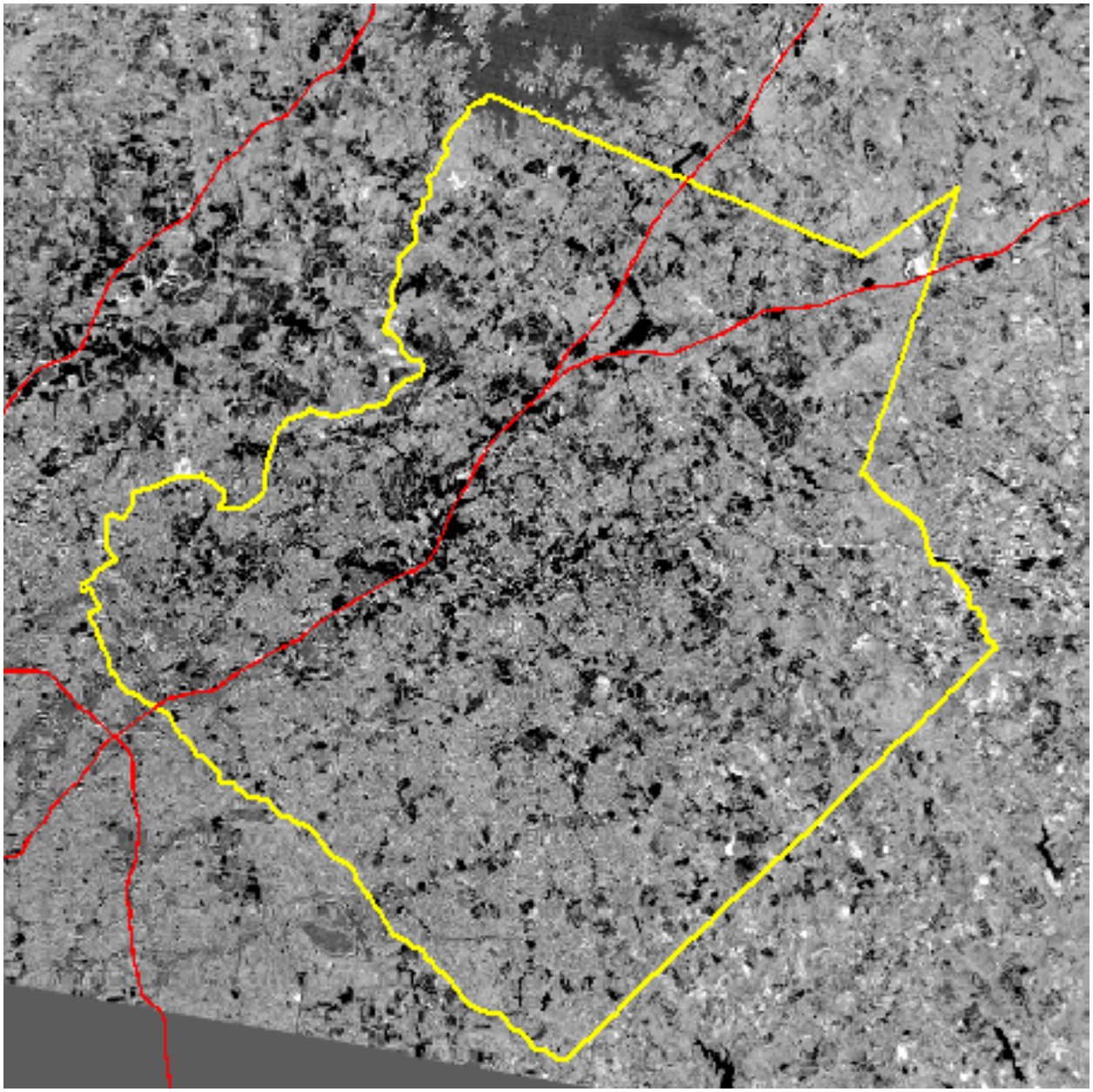

Figure 3.8. NDVI change image. Dark colored pixels indicate a reduction in vegetative reflectance, while light colored pixels indicate an increase. The Gwinnett County boundary and interstates are included for reference. The large dark area in the fork of I-85 and I-985 is the footprint of the Mall of Georgia.

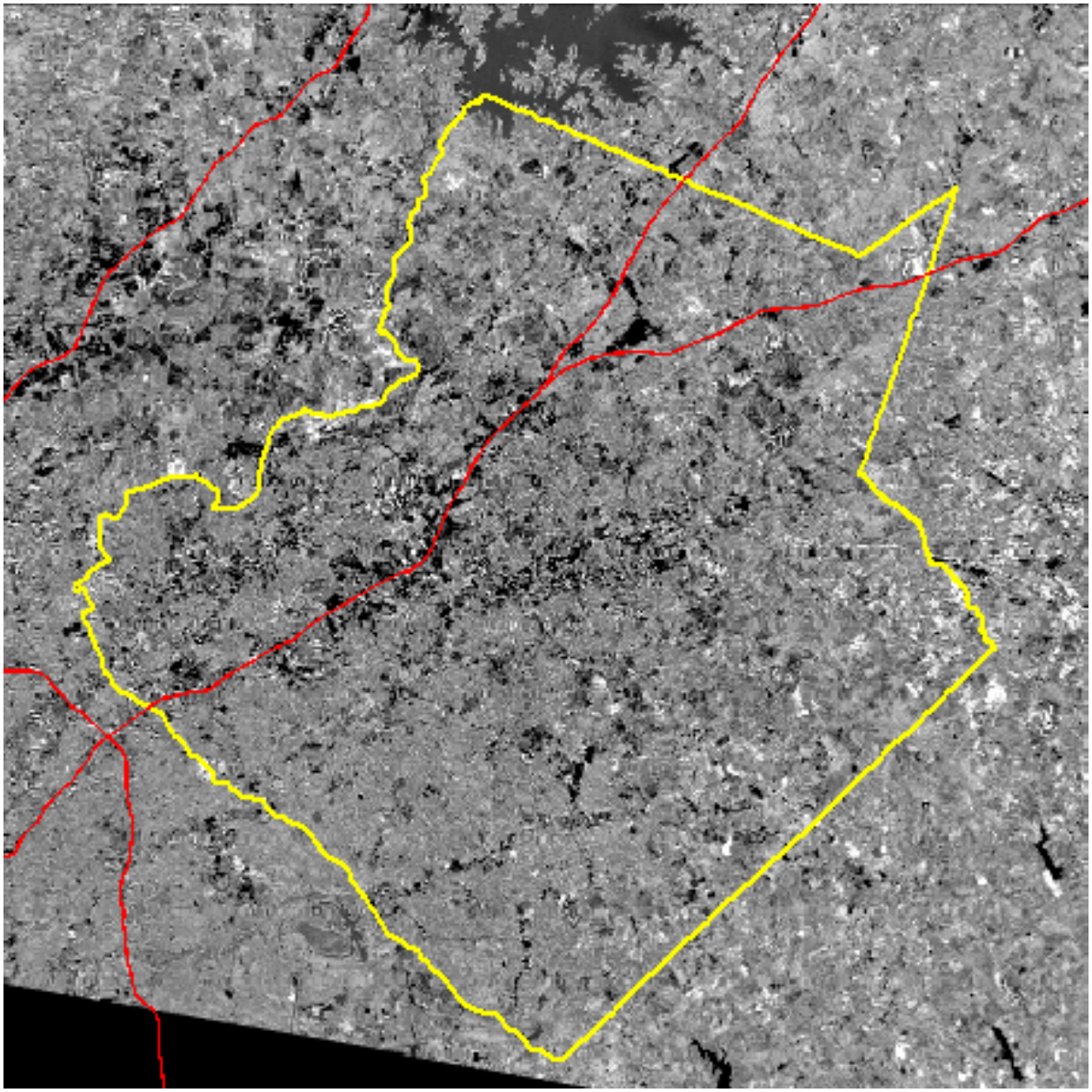

Figure 3.9. PCA change image. Dark colored pixels indicate a reduction in the second or "greenness" component, while light colored pixels indicate an increase. The Gwinnett County boundary and interstates are included for reference. The large dark area in the fork of I-85 and I-985 is the footprint of the Mall of Georgia.

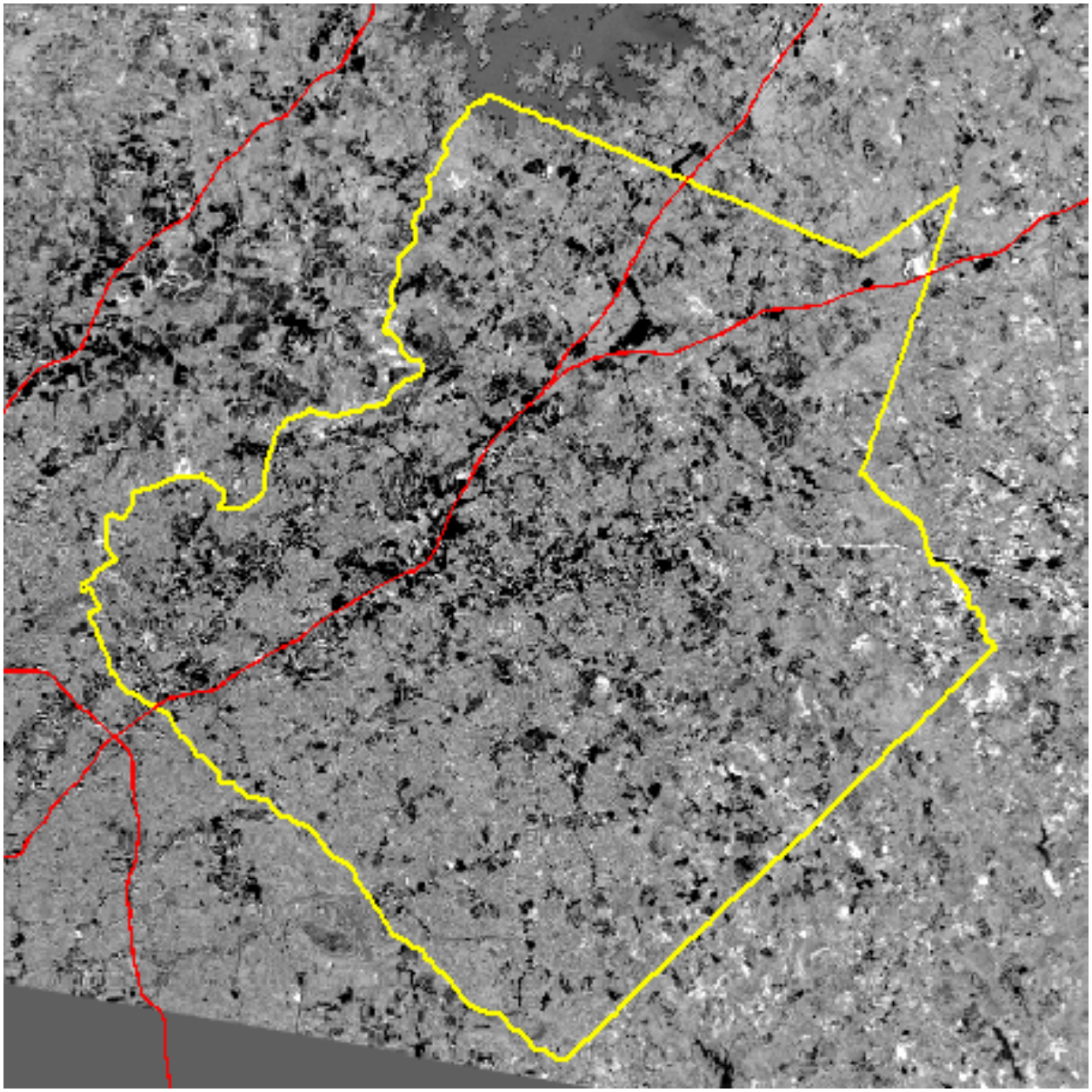

Figure 3.10. Tasseled Cap change image. Dark colored pixels indicate a reduction in the second or "greenness" component, while light colored pixels indicate an increase. The Gwinnett County boundary and interstates are included for reference. The large dark area in the fork of I-85 and I-985 is the footprint of the Mall of Georgia.

Change Thresholding Results

As stated earlier, pixel values from the three change images were standardized using z-scores for comparison of results. Table 3.3 shows the statistics and formulas used to generate a z-score image from each change image.

Table 3.3. Statistics and equations used to generate z-score change images.

Method	Mean Pixel Value	Standard Deviation	Equation
NDVI	0.095	0.168	(x - 0.095) / 0.168
PCA	30.606	13.710	(x - 30.606) / 13710
Tasseled Cap	8.552	17.445	(x - 8.552) / 17.445

Based on interpretation of ground truth data compared to results for different thresholds, it was decided that the +- 1.25 z-value threshold is the most accurate, clearly defining areas of distinct positive and negative change while minimizing false change and "noise". Figures 3.11 through 3.13 show the plus or minus 1.25 z-score thematic highlight change images that were ultimately derived from each transformed image pair.

Figures 3.14 through 3.16 show close-ups of these ± 1.25z threshold highlight change images focusing on the construction site of the Mall of Georgia in Gwinnett County. The image extent is the same as the examples of the various high resolution aerial photograph datasets used in accuracy assessment shown in Figures 2.7 through 2.12. These images clearly indicate the loss of vegetation cover resulting from the clearing of the site and construction.

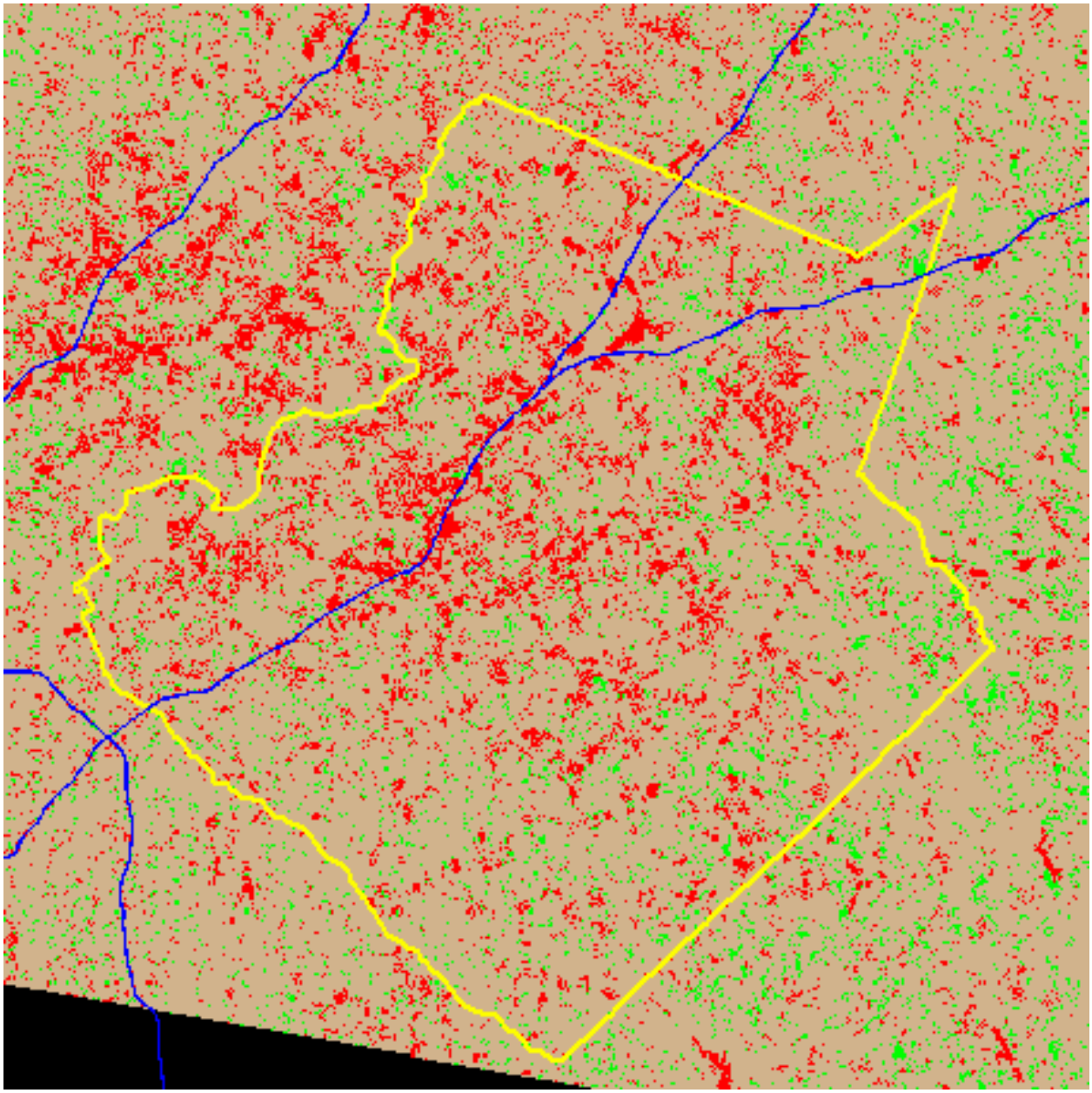

Figure 3.11. NDVI highlight change image with ± 1.25z threshold. Red pixels indicate areas of significant vegetation loss, green areas indicate increase, and tan areas indicate no change. The Gwinnett County boundary and interstates are included for reference. The large red area in the fork of I-85 and I-985 is the footprint of the Mall of Georgia.

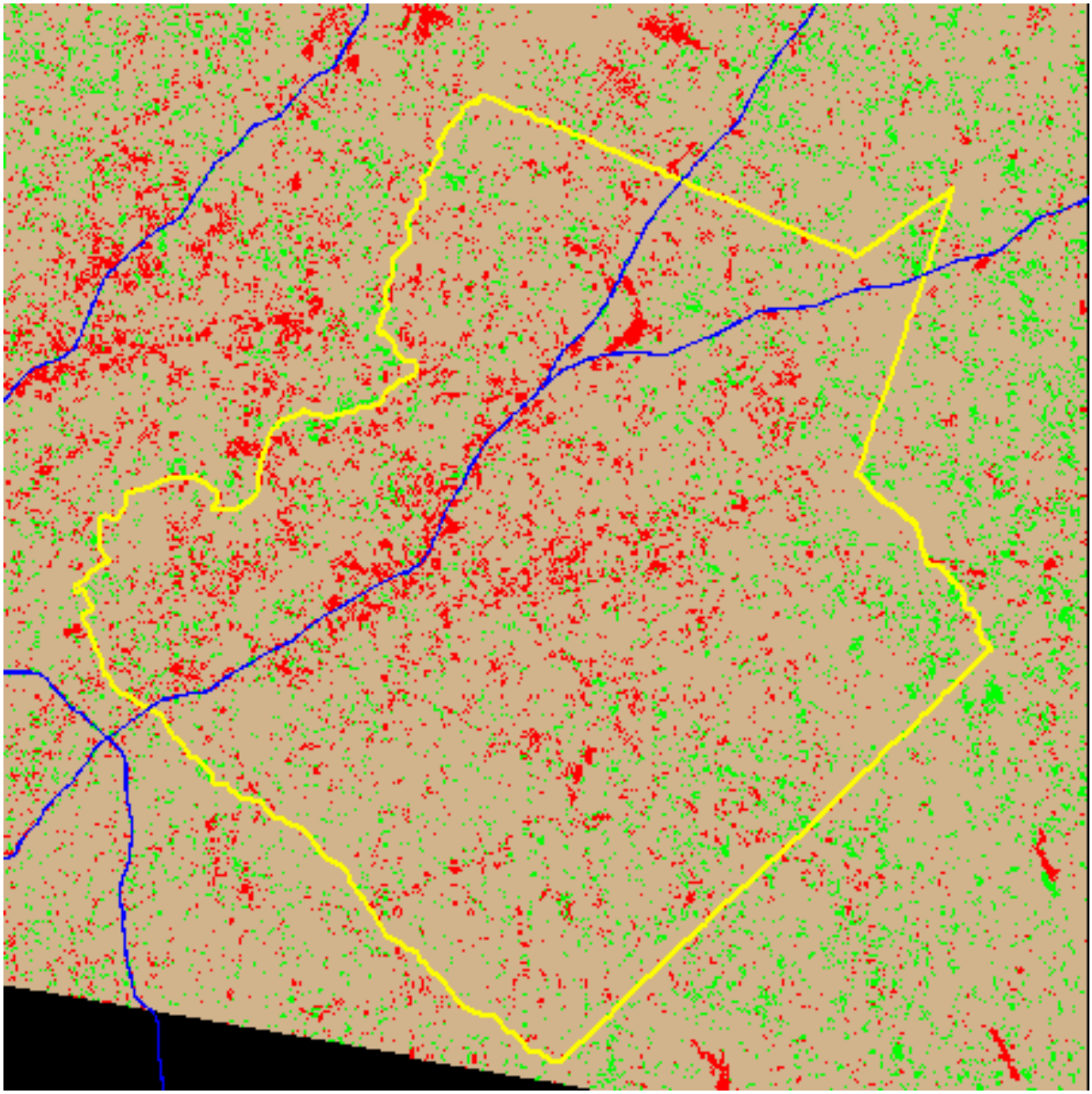

Figure 3.12. PCA highlight change image with ± 1.25z threshold. Red pixels indicate areas of significant vegetation loss, green areas indicate increase, and tan areas indicate no change. The Gwinnett County boundary and interstates are included for reference. The large red area in the fork of I-85 and I-985 is the footprint of the Mall of Georgia.

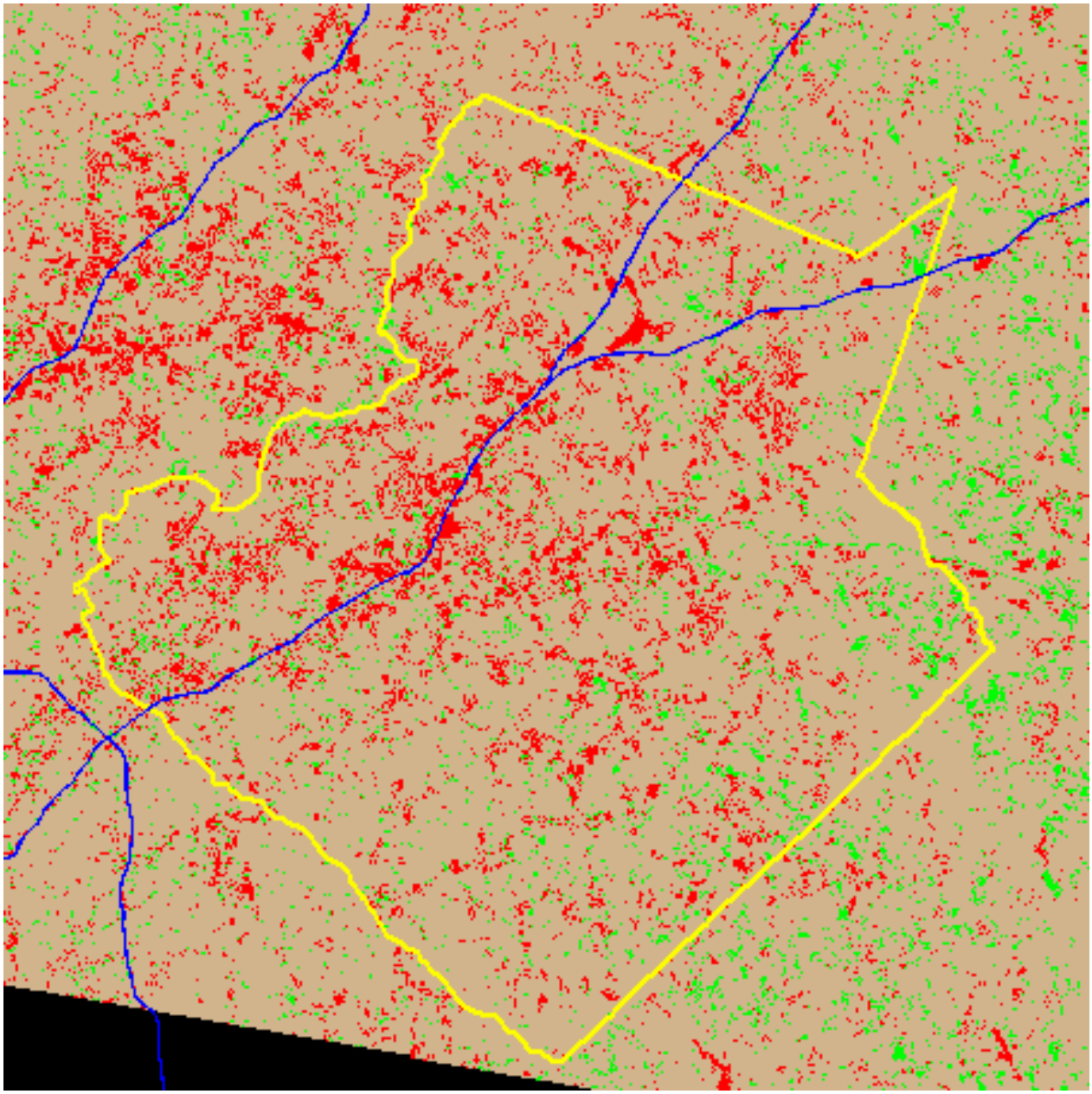

Figure 3.13. Tasseled Cap highlight change image with ± 1.25z threshold. Red pixels indicate areas of significant vegetation loss, green areas indicate increase, and tan areas indicate no change. The Gwinnett County boundary and interstates are included for reference. The large red area in the fork of I-85 and I-985 is the footprint of the Mall of Georgia.

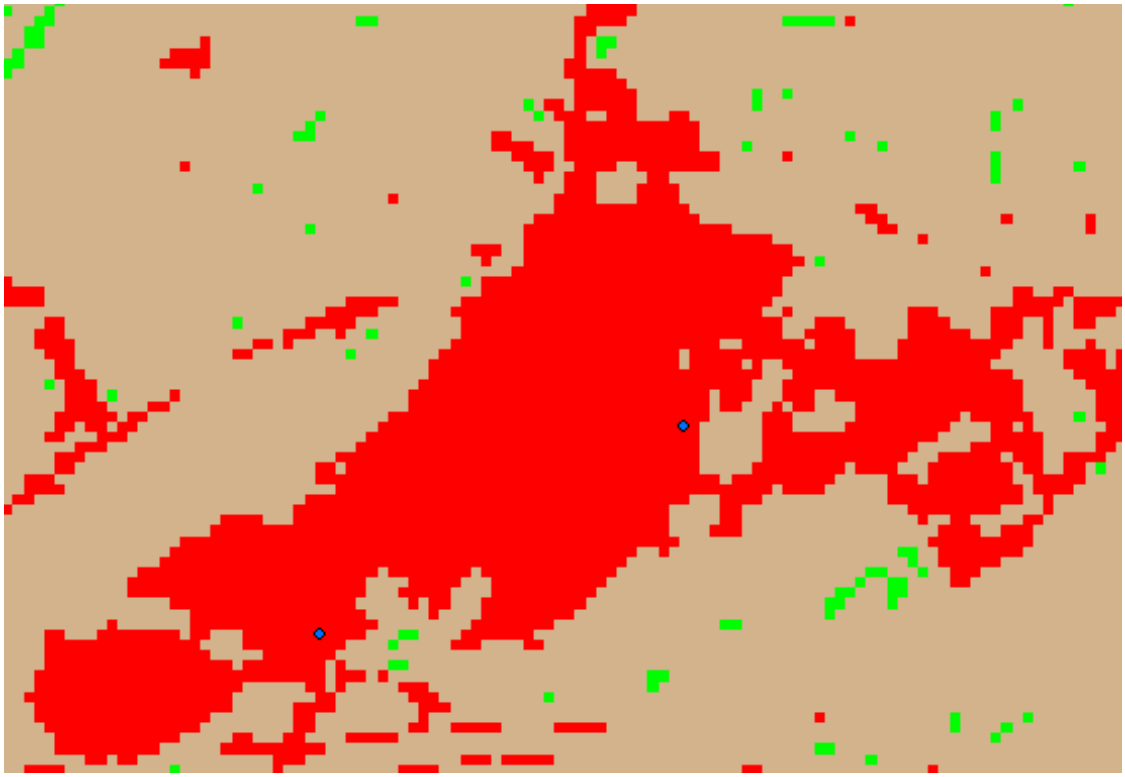

Figure 3.14. NDVI thematic change image close-up. Red pixels indicate loss of vegetation on the Mall of Georgia construction site from 1991 to 2000.

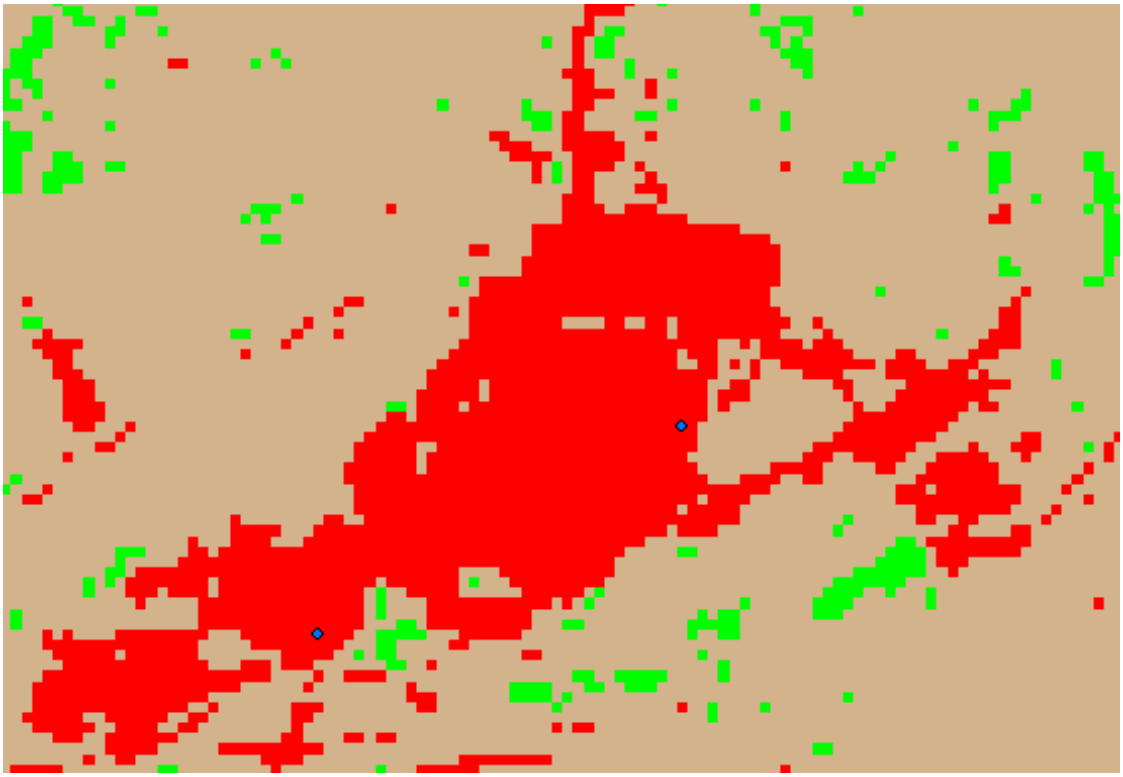

Figure 3.15. PCA thematic change image close-up. Red pixels indicate loss of vegetation on the Mall of Georgia construction site from 1991 to 2000.

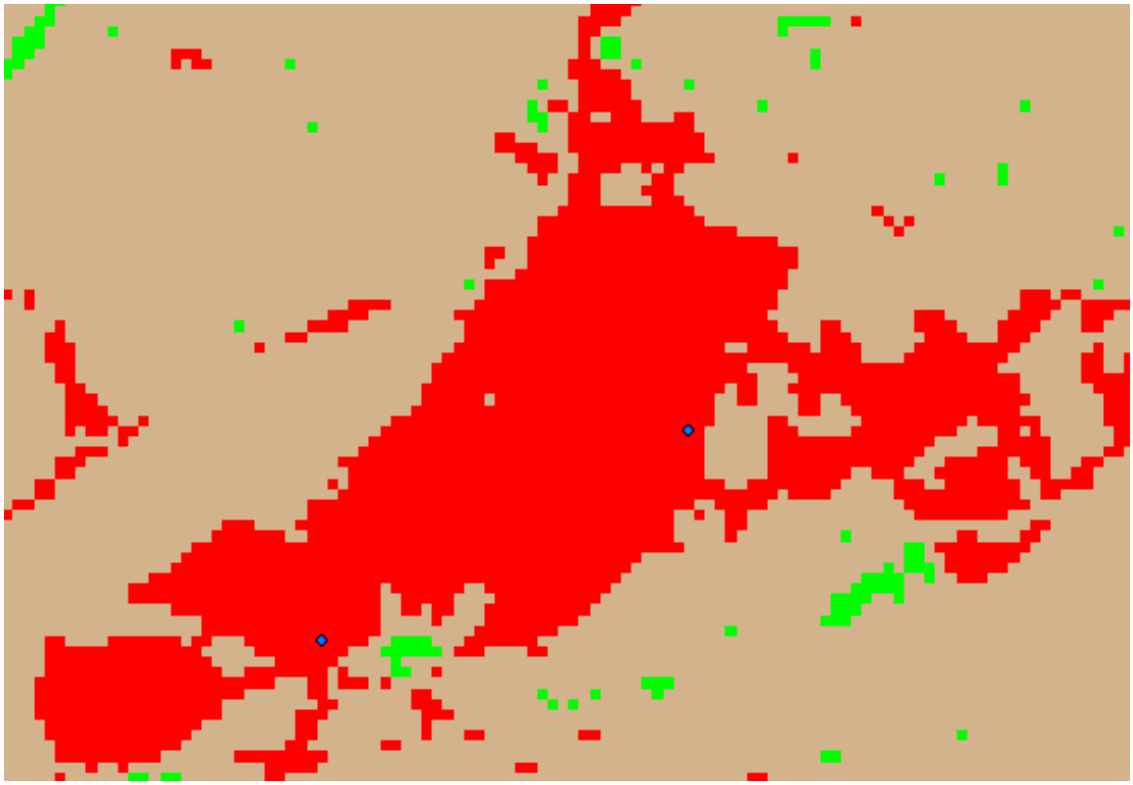

Figure 3.16. Tasseled Cap thematic change image close-up. Red pixels indicate loss of vegetation on the Mall of Georgia construction site from 1991 to 2000.

Results of Accuracy Assessment

Tables 3.4 – 3.6 show the pivot tables and calculated accuracies for all 300 check points.

Table 3.4. Error matrix and accuracies for change detection using NDVI differencing.

Count of NDVI Class	**Ground Truth**				
NDVI Class	**Decreased**	**Increased**	**Unchanged**	**Grand Total**	
Decreased	99	0	5	104	
Increased	0	13	82	95	
Unchanged	7	0	94	101	
Grand Total	106	13	181	300	
Producer's Accuracy		**User's Accuracy**		**Overall Accuracy**	**68.67%**
Decreased	93.40%	**Decreased**	95.19%		
Increased	100.00%	**Increased**	13.68%		
Unchanged	51.93%	**Unchanged**	93.07%		

Table 3.5. Error matrix and accuracies for change detection using PCA differencing.

Count of PCA Class	Ground Truth				
PCA Class	**Decreased**	**Increased**	**Unchanged**	**Grand Total**	
Decreased	82	0	5	87	
Increased	1	11	80	92	
Unchanged	23	2	96	121	
Grand Total	106	13	181	300	
Producer's Accuracy		**User's Accuracy**			
Decreased	78.10%	**Decreased**	94.25%	**Overall Accuracy**	**63.00%**
Increased	84.62%	**Increased**	11.96%		
Unchanged	53.04%	**Unchanged**	79.34%		

Table 3.6. Error matrix and accuracies for change detection using Tasseled Cap differencing.

Count of Tasseled Cap Class	Ground Truth				
Tasseled Cap Class	**Decreased**	**Increased**	**Unchanged**	**Grand Total**	
Decreased	98	0	2	100	
Increased	1	13	85	99	
Unchanged	7	0	94	101	
Grand Total	106	13	181	300	
Producer's Accuracy		**User's Accuracy**			
Decreased	92.45%	**Decreased**	98.00%	**Overall Accuracy**	**68.33%**
Increased	100.00%	**Increased**	13.13%		
Unchanged	51.93%	**Unchanged**	93.07%		

Several things are apparent from these tables. NDVI differencing performed the best of the three methods with a 68.67% overall accuracy, Tasseled Cap was the second best with 68.33% overall accuracy, and PCA performed the worst with 63.00% overall accuracy. However, the overall accuracy for all three methods was lower than anticipated and none of the methods meet the generally accepted accuracy standard of 80% overall accuracy.

All accuracy percentages for the Decreased class were very high, indicating that these three methods all perform quite well in detecting removal of vegetation surface and subsequent urbanization. However, a closer examination of the User's and Producer's accuracies for the Unchanged and Increased classes reveals that the Producer's accuracy for the Unchanged classes was quite low, and the User's accuracy for the Increased classes was extremely low, both of which are bringing the overall accuracy down. The reasons for this are fairly simple, yet not easily explained. During the accuracy assessment it was noted that many agricultural areas, open space areas, golf courses, and other grassy areas such as athletic fields showed a strong increase in vegetation cover from 1991 to 2000 as indicated by a higher reflectance in the near-infrared Band 4 of the Landsat imagery. However, the high resolution aerial photographs used in the ground truthing did not indicate a change in the status of these areas with regards to land cover or land use types. Some check points showed clear increases in vegetation due to a change in land cover status such as regrowth of cleared forest, draining and reclamation of a reservoir, and conversion of forested land to agricultural land or golf courses. However, the vast majority of the check points showing an increase in vegetative reflectance from 1991 to 2000 were in areas that appear for all intents and purposes to be unchanged. The first thought is that there may be a possible climatic explanation, but in fact analysis of rainfall patterns and drought indices (see previous section on site description) show that 1991 was actually a wetter year than 2000, which is the opposite of what these results might indicate. Another possible explanation is related to differences in sensor sensitivity to infrared radiation, with an improvement in the 2000 image over the 1991. However, the careful relative radiometric calibration of the 1991 image to the 2000 image should have removed this factor, and indeed an examination of unchanged forested areas adjacent to the agricultural and open space areas in question shows very similar reflectance

in the forested areas between the two images. One can only assume that there is another cause for this phenomenon, whether it is a better or later growing season in 2000, different crops or ground covers being grown, increased use of irrigation in the drier year (2000 was in the middle of a fairly severe drought in the study region), or some other explanation. This situation is further complicated by the fact that the earlier aerial photos used for ground truthing are monochromatic black and white, making it very difficult to interpret increases in vegetation cover from the photographs, much more so than interpreting instances of decrease or no change. When relying only on the reflectance signatures of the Landsat data for insight, one can safely say that in many of these agricultural and open space areas the 1991 image shows areas of bare soil (greenish pixels) where the 2000 image shows healthy vegetation (bright pink/reddish pixels). Again, however, from the high resolution aerial photography it is equally clear that the fundamental landuse and land cover type of these areas did not change. Unfortunately, whatever the explanation, this is introducing a significant amount of error in these areas, and since the goal of this research is to determine the best method for detecting deforestation and urban growth in urban areas rather than changes in phenological state of agricultural lands or crop health, the accuracy assessment should evaluate these methods both with and without many of these agricultural areas included in the assessment. While this may seem to the reader to be manipulation of the data in order to achieve better results and higher accuracies, it is important to remember that the number of test pixels showing increased vegetation in the study area is quite small (3% or 9/300) relative to the number of pixels showing decrease (8.3% or 25/300) and no change (88.6% or 266/300). However, due to the Equalized random distribution of 100 check points over each of the three classes, these areas of increase are disproportionately represented in the overall accuracy percentages. Also, due to the known occurrence of rapid urbanization in the

study area during the study period, it is important to note that the condition of increased vegetation cover is in reality uncommon, and in terms of landuse, insignificant relative to the amount of vegetation removal. If nothing else, it is interesting to look at the results both with and without these areas, and include only those test pixels which showed either increase or decrease in vegetation cover due to changes in land use types, rather than vegetative changes in phenological characteristics within a static landuse. Tables 3.7 – 3.9 show these results with the 77 test pixels in agricultural areas, open spaces, golf courses, and athletic fields showing no change in landuse removed, leaving a new sample of 223 accuracy assessment checkpoints.

Table 3.7. Error matrix and accuracies for NDVI differencing with 77 agricultural and open space check points removed.

Count of NDVI CLASS	**GROUND TRUTH**				
NDVI CLASS	**Decreased**	**Increased**	**Unchanged**	**Grand Total**	
Decreased	99	0	5	104	
Increased	0	**11**	10	21	
Unchanged	6	0	92	98	
Grand Total	105	**11**	107	223	

Producer's Accuracy		**User's Accuracy**			
Decreased	94.29%	**Decreased**	95.19%	**Overall Accuracy**	**90.58%**
Increased	100.00%	**Increased**	52.38%		
Unchanged	85.98%	**Unchanged**	93.88%		

Table 3.8. Error matrix and accuracies for PCA differencing with 77 agricultural and open space check points removed.

Count of PCA CLASS	**GROUND TRUTH**				
PCA CLASS	**Decreased**	**Increased**	**Unchanged**	**Grand Total**	
Decreased	82	0	5	87	
Increased	0	10	12	22	
Unchanged	23	1	90	114	
Grand Total	105	11	107	223	

Producer's Accuracy		**User's Accuracy**			
Decreased	78.10%	**Decreased**	94.25%	**Overall Accuracy**	**81.61%**
Increased	90.91%	**Increased**	45.45%		
Unchanged	84.11%	**Unchanged**	78.95%		

Table 3.9. Error matrix and accuracies for TCT differencing with 77 agricultural and open space check points removed.

Count of TASCAP CLASS	GROUND TRUTH				
TASCAP CLASS	**Decreased**	**Increased**	**Unchanged**	**Grand Total**	
Decreased	98	0	2	100	
Increased	0	11	11	22	
Unchanged	7	0	94	101	
Grand Total	105	11	107	223	

Producer's Accuracy		User's Accuracy			
Decreased	93.33%	**Decreased**	98.00%	**Overall Accuracy**	**91.03%**
Increased	100.00%	**Increased**	50.00%		
Unchanged	87.85%	**Unchanged**	93.07%		

Examination of this second set of results shows significant improvement in overall accuracy as well as Producer's accuracy for the Unchanged classes and User's accuracy for the Increased classes for all three methods. With this new dataset TCT differencing performed best overall with 91.03% accuracy, followed by NDVI with 90.58% accuracy and PCA with 81.61% accuracy. With the removal of the problematic agricultural and open space checkpoints PCA just slightly exceeds the generally accepted 80% overall accuracy level.

While the overall accuracy of TCT and NDVI is quite good with this new sample, it is troubling that it was necessary to remove the problematic checkpoints and worthy of further research to find out the cause of that phenomenon. It was speculated that perhaps a stricter threshold for significant change, say plus or minus 1.5, 1.75 or even 2.0 z values would reduce the apparent error in the agricultural classes. To verify this idea, 102 new random checkpoints (34 in each of the three change classes) were generated and assessed for thematic change images with a threshold of ± 2.0 z values. Figures 3.17 through 3.19 show the thematic change images for each method using the ± 2.0 z change threshold.

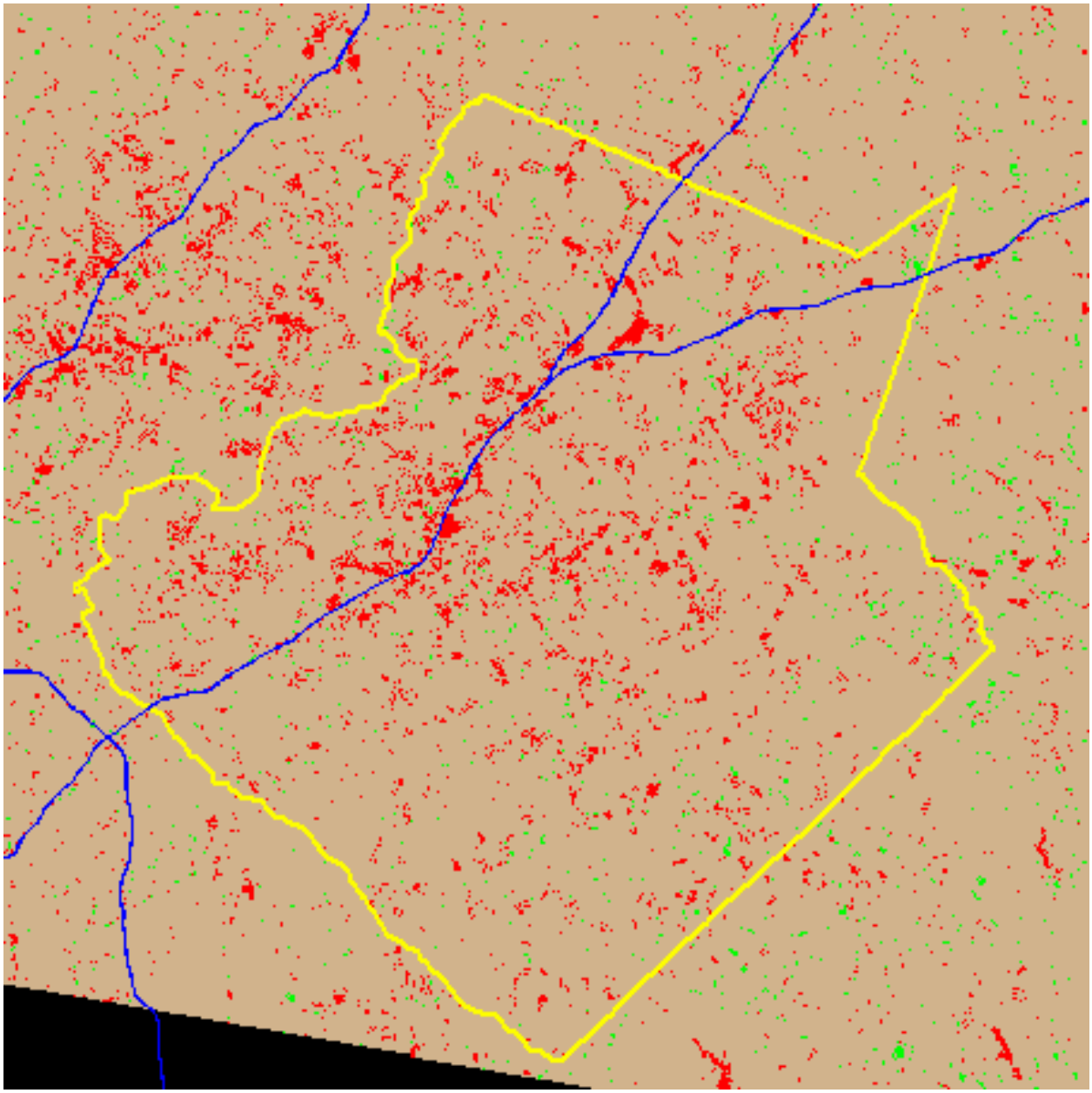

Figure 3.17. NDVI highlight change image with ± 2.0z threshold. Red pixels indicate areas of significant vegetation loss, green areas indicate increase, and tan areas indicate no change. The Gwinnett County boundary and interstates are included for reference. The large red area in the fork of I-85 and I-985 is the footprint of the Mall of Georgia.

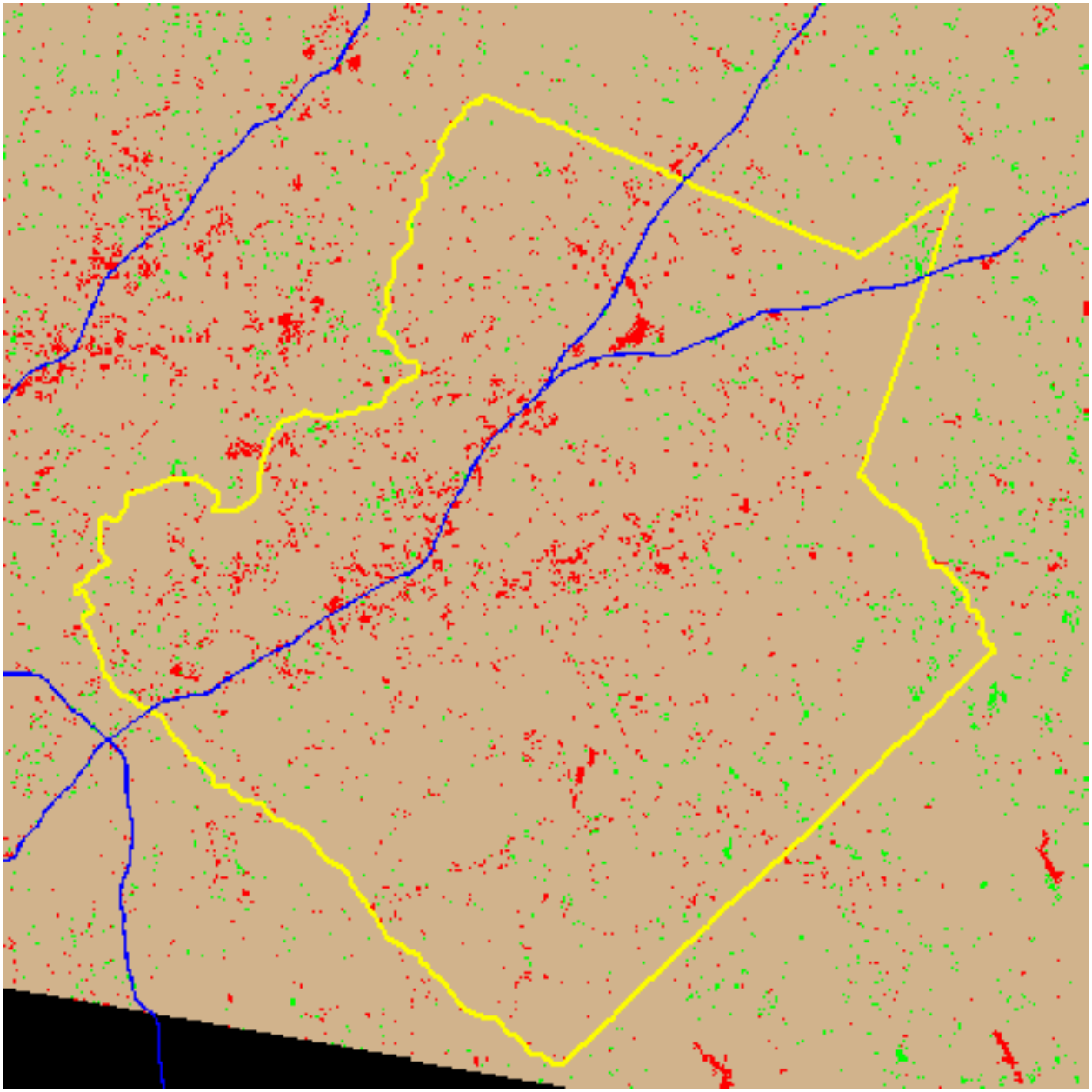

Figure 3.18. PCA highlight change image with ± 2.0z threshold. Red pixels indicate areas of significant vegetation loss, green areas indicate increase, and tan areas indicate no change. The Gwinnett County boundary and interstates are included for reference. The large red area in the fork of I-85 and I-985 is the footprint of the Mall of Georgia.

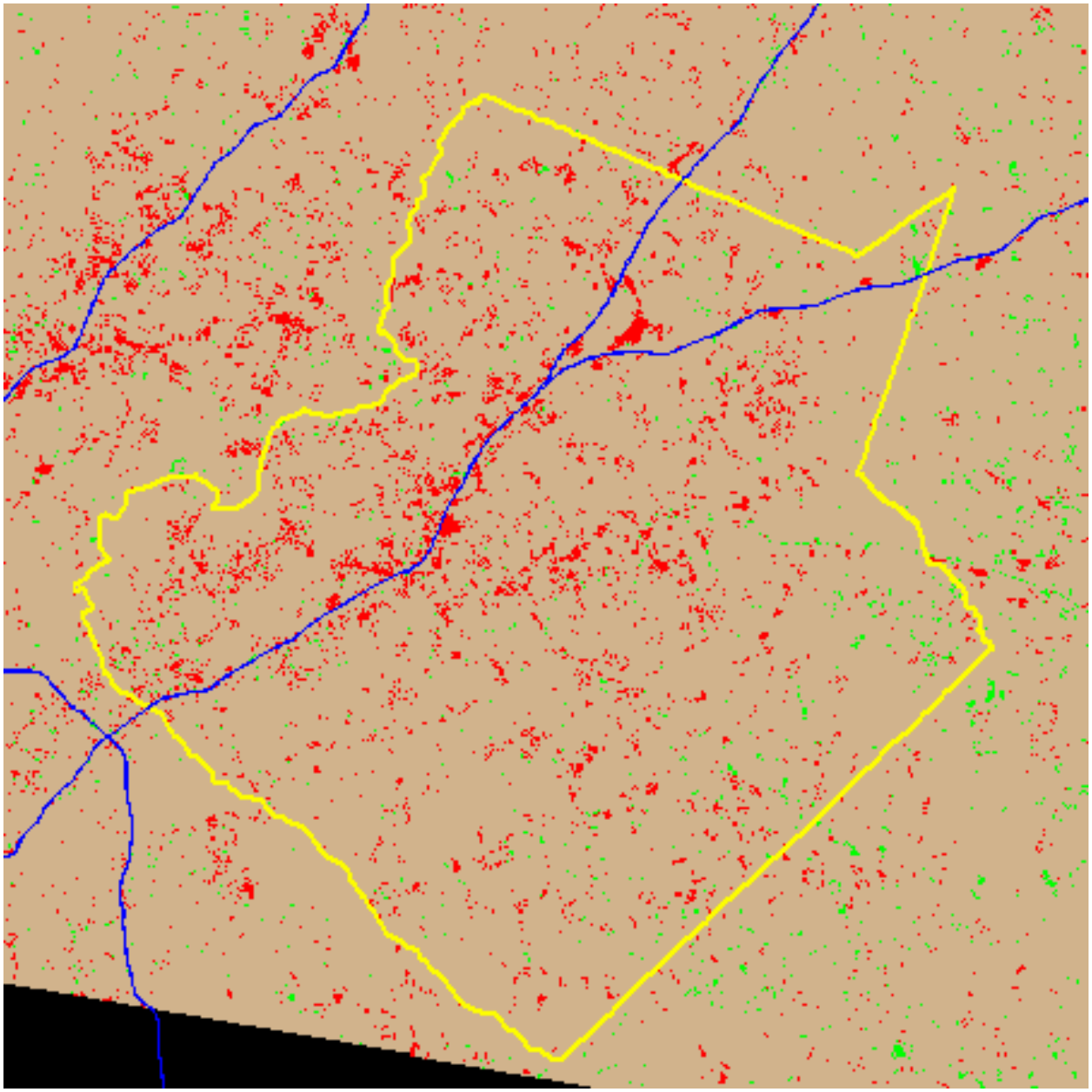

Figure 3.19. Tasseled Cap highlight change image with ± 2.0z threshold. Red pixels indicate areas of significant vegetation loss, green areas indicate increase, and tan areas indicate no change. The Gwinnett County boundary and interstates are included for reference. The large red area in the fork of I-85 and I-985 is the footprint of the Mall of Georgia.

Figure 3.20 shows the distribution of this new set of 102 accuracy assessment checkpoints. The same assessment procedures were used with this new set of points, and the results are shown below in tables 3.10 through 3.12.

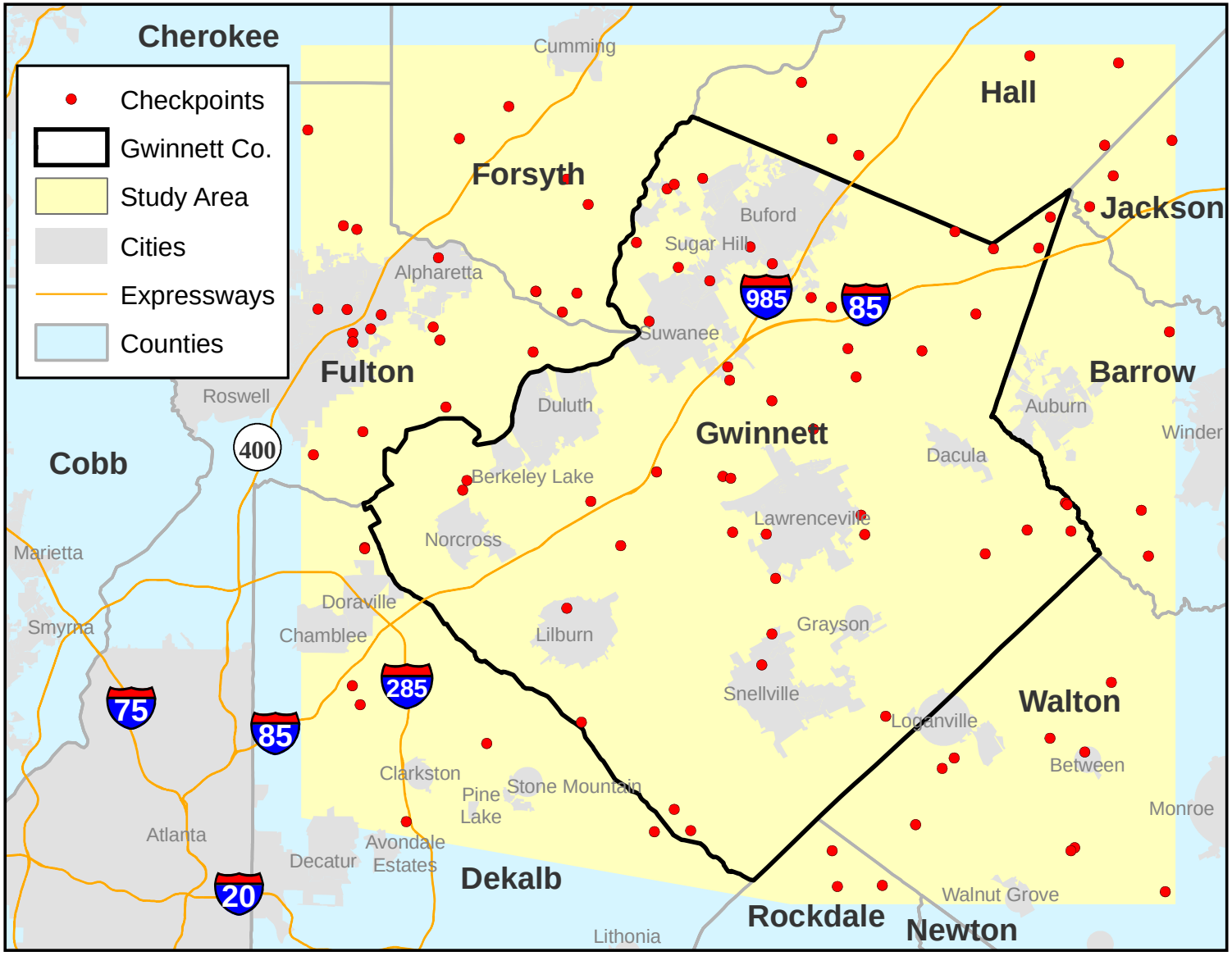

Figure 3.20. The distribution of the 102 random check points used in the accuracy assessment of the ± 2.0 z change images. Also shown are the study area subset extent and the Gwinnett County boundary.

Table 3.10. Error matrix and accuracies for NDVI differencing with a ± 2.0 z value change threshold.

Count of NDVI CLASS	GROUND TRUTH				
NDVI CLASS	**Decreased**	**Increased**	**Unchanged**	**Grand Total**	
Decreased	27	0	1	28	
Increased	0	2	23	25	
Unchanged	6	0	43	49	
Grand Total	33	2	67	102	
Producer's Accuracy		**User's Accuracy**			
Decreased	81.82%	**Decreased**	96.43%	**Overall Accuracy**	**70.59%**
Increased	100.00%	**Increased**	8.00%		
Unchanged	64.18%	**Unchanged**	87.76%		

Table 3.11 Error matrix and accuracies for PCA differencing with a ± 2.0 z value change threshold.

Count of PCA CLASS	GROUND TRUTH				
PCA CLASS	**Decreased**	**Increased**	**Unchanged**	**Grand Total**	
Decreased	13	0	2	15	
Increased	0	2	19	21	
Unchanged	20	0	46	66	
Grand Total	33	2	67	102	
Producer's Accuracy		**User's Accuracy**			
Decreased	39.39%	Decreased	86.67%	**Overall Accuracy**	**59.80%**
Increased	100.00%	Increased	9.52%		
Unchanged	68.66%	Unchanged	69.70%		

Table 3.12. Error matrix and accuracies for TCT differencing with a ± 2.0 z value change threshold.

Count of TASCAP CLASS	GROUND TRUTH				
TASCAP CLASS	**Decreased**	**Increased**	**Unchanged**	**Grand Total**	
Decreased	23	0	1	24	
Increased	0	1	20	21	
Unchanged	10	1	46	57	
Grand Total	33	2	67	102	
Producer's Accuracy		**User's Accuracy**			
Decreased	69.70%	Decreased	95.83%	**Overall Accuracy**	**68.63%**
Increased	50.00%	Increased	4.76%		
Unchanged	68.66%	Unchanged	80.70%		

It is clear that this higher change threshold did not improve the results; in fact the accuracies are similar to the results of the full set of 300 points for ± 1.25 z. It was hoped that increasing the threshold would improve the Producer's accuracy for the Unchanged classes, which it did slightly. But the User's accuracy for the Increased class is actually worse; in fact it is not above 10% in any of the methods with the ± 2.0 z threshold. Of equal or greater significance is the fact that the Producer's accuracy for the Decreased class declined significantly with the higher threshold, particularly with PCA. In other words, the higher threshold makes the analysis less sensitive to decreased vegetation cover due to clearing and development, and results in some areas that have in reality been cleared or deforested not being detected as such, while it does not improve the performance in the agricultural areas that are showing an increase in vegetation despite no change in landuse. It should be emphasized that relative to the spectral reflectance signatures in the Landsat data itself the classifications appeared correct, but with regard to actual landuse or land cover change perceptible in the high resolution aerial photographs, there was a discrepancy that could not be readily reconciled using the methods examined in the present study. In other words, these methods were effective in identifying improvements in vegetation conditions or vegetative changes, but less so from the perspective of land use/land cover changes.

This may be due in large part to the different natures of the Landsat imagery and the aerial photographs used for ground truthing. The Landsat images contain spectral information, particularly the near-infrared reflectance in Band 4, which is sensitive to changes in vegetative state as well as vegetation cover. The aerial photographs on the other hand, with the exception of the 1999 color infrared DOQQs, do not contain this information and are not as suitable for detecting changes in vegetative state, though they are sufficient for detecting changes in

vegetation cover and land uses. If a set of color-infrared aerial photographs had been available for the 1991 timeframe as well as the 1999, it is possible that the ground truthing may have been better able to take into account more subtle vegetative changes that were not discernible from the monochromatic or true color aerial photographs that were used in this study.

Nevertheless, in either case it is clear that NDVI and TCT image differencing are effective methods of change detection, while PCA is in both cases the worst of the three methods and based on these results, should not be the method of choice when pursuing further change detection research. While TCT and NDVI have similar accuracies, NDVI has an advantage over TCT for its ease to calculate, the index formula being a simpler calculation than the Tasseled Cap matrix transformation, and it is also more intuitive to understand and therefore to explain to non-scientific readers interested in change detection analysis.

Results for Kappa coefficients (KHAT)

Table 3.13 shows the Kappa coefficients calculated for each of the nine error matrices in the previous section, including those for all 300 check points with a threshold at ± 1.25 z, the 223 check points at ± 1.25 z threshold with those pixels of agricultural and open space areas removed, and the 102 checkpoints at ± 2.0 z threshold.

Table 3.13. Kappa Coefficient (KHAT) statistics for the nine errors matrices.

Checkpoint Group	NDVI	PCA	Tasseled Cap
All 300 checkpoints for ± 1.25 z change threshold	0.53	0.42	0.52
223 Checkpoint w/ Ag, Open Space Removed	0.83	0.68	0.84
102 Checkpoints for ± 2 z change threshold	0.50	0.23	0.43

These Kappa coefficients further reinforce the conclusion that the agricultural areas showing increased vegetative reflectance are introducing errors into the analysis from a landuse perspective, and that the higher threshold does not mitigate the problem but in fact reduces the effectiveness of the analysis for other classes. The best results were obtained from the lower ± 1.25 z change threshold with the agricultural and open space areas removed, and the results from this subset of points are the only ones that show a classification significantly better than one based on random pixel assignment. NDVI and TCT again had the best performance, while PCA performed the worst of the three methods in every case.

Summary of Vegetation Change within Gwinnett County, GA from 1991-2000

Table 3.14 shows the summary of the vegetation changes that took place in Gwinnett County during the 1991-2000 study period. This summary is based on the results using the ± 1.25 z change threshold. It is notable that differencing of the PCA transformed images resulted in significantly fewer pixels in the Decreased class, indicating that this method is less sensitive to such changes and classified the most pixels as Increased, introducing additional errors as described above. TCT resulted in the fewest pixels in the Increased class, while remaining sensitive to decreases in vegetation, contributing to its high level of overall accuracy. NDVI appears to be the most sensitive to decreasing vegetation which offsets the error introduced by the high number of pixels classified as Increased. While the majority of land area within Gwinnett County remained unchanged during the study period, an average of NDVI and TCT results for the Decreased class shows that approximately 13, 643 hectares (136.43 square km) of land was deforested or cleared, which is approximately 12.04% of the total land area.

Table 3.14. Summary of pixels in each change class for each method and conversion to area using hectares.

	Pixels by Method			Hectares by Method		
Class	**NDVI**	**PCA**	**TCT**	**NDVI**	**PCA**	**TCT**
Decreased	159,488	103,016	143,683	14,353.9	9,271.4	12,931.5
Unchanged	1,041,957	1,090,514	1,069,587	93,776.1	98,146.3	96,262.8
Increased	57,298	65,213	45,473	5,156.8	5,869.2	4,092.6

Tables 3.15 and 3.16 show the range of 1991 NDVI values for the lands undergoing vegetation change during the study period, based on the results of NDVI and TCT image differencing and a ± 1.25 z change threshold. Results were calculated for both of these methods due to the fact that they performed similarly well based on accuracy assessments and Kappa coefficients. Figure 3.21 shows the thematic image of 1991 NDVI values divided into four classes based on the ranges of values in tables 3.15 and 3.16.

Table 3.15. Range of 1991 NDVI values for the Decreased and Increased classes resulting from NDVI image differencing at a ± 1.25 z change threshold.

Range of 1991 NDVI Values	**Decreased**		**Percent of Total**	**Increased**		**Percent of Total**
	Pixels	**Hectares**		**Pixels**	**Hectares**	
-0.69 to -0.2	1,888	169.9	1.18	7,156	644.0	12.49
-0.2 to 0.0	11,395	1,025.6	7.14	28,533	2,568.0	49.80
0.0 to 0.25	127,799	11,501.9	80.13	21,591	1,943.2	37.68
0.25 to 0.64	18,406	1,656.5	11.54	18	1.6	0.03
Totals	159,488	14,354	100	57,298	5,157	100

Table 3.16. Range of 1991 NDVI values for the Decreased and Increased classes resulting from TCT image differencing at a ± 1.25 z change threshold.

Range of 1991 NDVI Values	**Decreased**		**Percent of Total**	**Increased**		**Percent of Total**
	Pixels	**Hectares**		**Pixels**	**Hectares**	
-0.69 to -0.2	7,135	642.2	4.97	8,294	746.5	18.24
-0.2 to 0.0	13,983	1,258.5	9.73	21,453	1,930.8	47.18
0.0 to 0.25	106,997	9,629.7	74.47	15,312	1,378.1	33.67
0.25 to 0.64	15,568	1,401.1	10.83	414	37.3	0.91
Totals	143,683	12,931	100	45,473	4,093	100

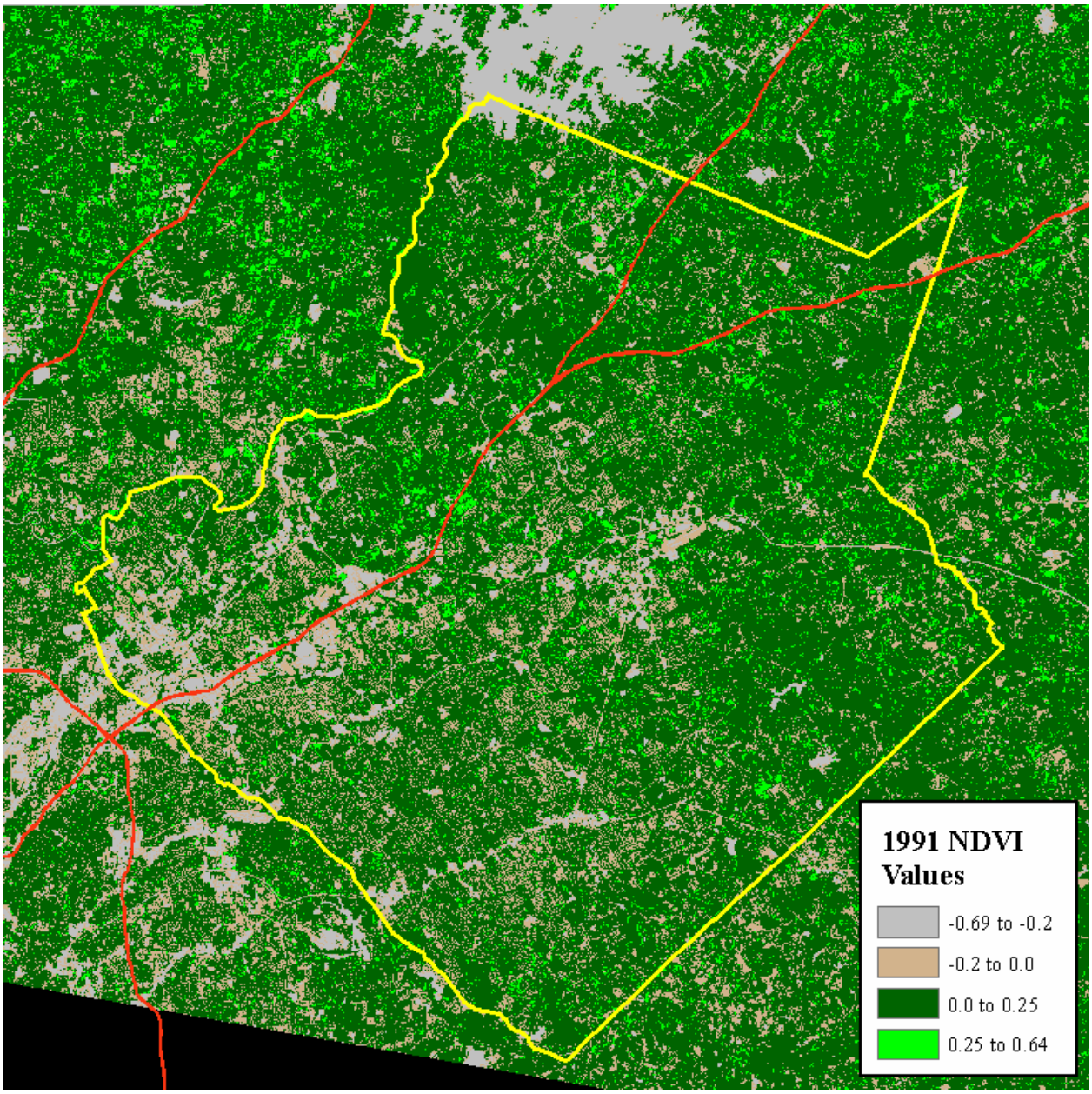

Figure 3.21. Thematic images showing four classes of 1991 NDVI values. Generally speaking, grey pixels represent paved urban surfaces or water, tan pixels represent bare soil, sparse vegetation or mixed pixels of urban and vegetation, dark green pixels represent forest, and bright green pixels represent agricultural areas or areas of healthy grass cover.

These results provide some interesting insight into the nature of the land use change that took place in Gwinnett County from 1991-2000. Recall that the ranges of NDVI values correspond roughly to certain land cover types, but not in every case. However, for purposes of discussion it can generally be said that values from -0.69 to -0.2 represent urban surfaces or

water, values from -0.2 to 0 represent bare soil or very sparse vegetation, values from 0 to 0.25 represent forest, and values from 0.25 to 0.69 represent agricultural or open grassy areas. From this it can be seen that the vast majority of land area showing a decrease in vegetation cover was originally forested (80.13% from NDVI, 74.47% from TCT), while a much smaller proportion of the decreased vegetation area came from agricultural or grassy areas with higher NDVI values (11.54% from NDVI, 10.83% from TCT). There are a moderately large number of Decreased pixels in the second class (7.14 % from NDVI, 9.73% from TCT) which correspond to bare soil or very sparse vegetation, which likely indicates these transitional areas being developed into concrete, asphalt, and other urban surface types. There are a surprising number of pixels with low original NDVI values showing decrease, particularly from TCT (1.18% from NDVI, 4.97% from TCT). This may be partly due to mixed pixels of predominantly urban area with some grass being further developed, and may also be due to decreases in NDVI over water areas between the 1991 and 2000 images, probably as the result of variations in suspended sediment, some of which exceed the ± 1.25 z change threshold.

Overall the number of pixels showing increased vegetation cover is much smaller than those showing decrease, with the ratio of Decreased to Increased pixels being approximately 3:1. Most of the increased areas are in the second class of NDVI values (49.8% from NDVI, 47.18% from TCT), indicating vegetation growth on areas of bare soil, or increased density and/or health in sparsely vegetated areas. There are also a considerable number of increased pixels in the third class of NDVI values (37.68% from NDVI, 33.67% from TCT), most likely indicating improvements to marginal or fallow agricultural lands or increases in forest health and/or density. There are surprisingly few pixels showing increase in the fourth class of highest NDVI values (0.03% from NDVI, 0.91% from TCT), presumably because these values were very high

to begin with which likely indicates well-maintained agricultural lands or grass surfaces (golf courses and lawns) that may not vary as much over time. The first class of values shows a moderate number of pixels with considerable increase as well (12.49% from NDVI, 18.24% from TCT); these are most likely urbanized areas experiencing a regrowth of tree canopy or grass cover, cleared areas being left to re-vegetate, or other moderate "greenings" of largely urban areas.

Again, this summary is based on rough generalizations of land cover types from observed ranges of NDVI values. This information may help understand some of the nature of the land cover changes that took place during the study period. It would be quite interesting to pursue this further using more advanced image analysis techniques and extensive photo interpretation, but for the purposes of this study it is sufficient to provide a "best-guess" interpretation of the nature of the changes, based on the results from these change detection methods. Suffice it to say that while one can use NDVI and TCT differencing to accurately determine broad classes of Decreased, Unchanged, or Increased vegetation cover, it is much more difficult to further sub-divide those classes into types of land cover based on NDVI values alone.

CHAPTER FOUR: CONCLUSIONS

1. Summary of Results and Discussion of Findings

In this study, three different methods to represent vegetation cover were evaluated in change detection by direct differencing. After geometric rectification (georeferencing) and radiometric normalization, Landsat images of 1991 and 2000 in Gwinnett County, Georgia, were used to calculate the normalized difference vegetation index (NDVI), Tasseled Cap transformation (TCT), and principal component analysis (PCA) transformation. Then thematic change images were produced by differencing between the two years and applying a threshold of the standardized differencing pixel values.

From the results of this research, it can be concluded that for change detection using image differencing, the NDVI and Tasseled Cap transformations provide more accurate and reliable results than principal components analysis in every scenario examined. PCA performed the least accurately and reliably of the three methods assessed, and should not be used in favor of NDVI or TCT for change detection studies of this nature. The primary difference between the three methods was the lower sensitivity of PCA to decreases in vegetation, resulting in a Producer's accuracy for the Decreased class significantly lower than the other two methods. NDVI and TCT performed approximately equally well, with a slight advantage perhaps given to NDVI based on ease of calculation, lack of the need for sensor-specific coefficients, and a more intuitive understanding of the transformation. Either of these two methods would be suitable for change detection analysis in this study area and in other areas with similar climate and vegetation cover. Further research would be required to determine whether these methods would perform equally well in study areas differing from the Southern Piedmont in terms of climate, vegetation cover, topography, and other variables.

It is important to note that these methods seem to perform well in detecting changes in vegetative state (health of plants and other phenological characteristics such as leaf browning, chlorotic spotting, and branch dieback), and density of vegetation cover. This is due to the fact that the Band 4 near-infrared reflectance that is closely related to the physical structure of healthy leaves is of primary importance in each of the three image transformation methods used in this study. However, such changes in vegetative reflectance and density of vegetation cover do not always correspond to visible changes in land cover and/or landuse. If the goal of a change detection study is primarily to assess the extent of changes in vegetation cover and vegetative reflectance, NDVI and TCT differencing would perform very well for that task. However, it cannot be assumed that decreases or increases in vegetative reflectance always correspond to changes in land use as was previously believed by this researcher. Raising the change threshold did not improve the results in this case, and in fact was detrimental as it resulted in areas of true changes being misclassified as unchanged. In the case of this study area, ancillary data sources provided information on the landuse history of this area as being characterized by high population growth, rapid urbanization, loss of tree cover and agricultural lands, and increased impervious surfaces. For this study, based on interpretation of high resolution aerial photos and the ancillary data mentioned above, it can be concluded that areas of decreased vegetative reflectance almost always corresponded to changes in landuse and land cover due to deforestation and urbanization, while areas of increased vegetative reflectance usually corresponded with increased density or health of crops or grass in agricultural and open space areas undergoing no change in landuse. Under different circumstances, decreases in vegetative reflectance could also be due to various other causes such as disease or drought and increase could result either from healthier growth or regeneration. Therefore it would be important to

bring in other data on the study area before any conclusions about land use change could be made from the results of a change detection study such as this one. This confusion was further compounded by the lack of high resolution color infrared aerial photos for the earlier time period, and a necessary reliance on panchromatic black and white photographs to determine the original land cover for the accuracy assessment. While it was relatively easy to determine changes in land use and land cover from these black and white images, it was very difficult to determine more subtle changes in vegetative state. The same was true, although to a lesser extent, for the true color aerial photographs available for the later dates. One must also take into account the inherently subjective nature of the interpretation of the ground truth data from aerial photographs, and the possibility of introducing errors in this step of the analysis. For this reason careful radiometric calibration between the two images used in the differencing becomes even more important, to ensure that there are no errors introduced from spectral mismatches and that all observed changes over time can ultimately be explained by other causes.

In addition to issues discussed above, during the accuracy assessment, the difficulty of interpretation in urban and fringe areas became apparent. This is largely due to the high spatial frequency of land cover changes in these areas, and the relatively low spatial resolution of the Landsat imagery. For example, individual households with relatively large land lots create a juxtaposition of rooftops, driveways, lawns and shrubs, and patches of original and planted tree cover, displaying different spectral signatures and textures on images as compared to large, contiguous and relatively uniform patches of commercial and residential developments. This in turn points to the fundamental difficulty of performing automated change detection in urban and fringe areas, which ironically is often where it is most needed and most valuable. Classifiers based on spatial patterns and textural characters may prove to be valuable in these cases. This

issue further emphasizes the need for excellent geometric registration between all images particularly in fringe areas in order to achieve accurate change detection results. It was observed that even with an RMSE of close to 0.2 pixels between the two study area Landsat subsets, slight misregistration could still be observed in some cases along roads and the edges of cleared areas, particularly towards the outer edges of the study area subset images. Similarly, it was noticed that errors of omission (photos showing a decrease in vegetation cover, which is missed by the change detection methods) are most common around the edges of cleared vegetation, particularly next to roads.

Finally, in several instances there were unexplained errors of commission over deep water areas in the study area for this project, which should show no change in vegetative reflectance but in fact did, probably as the result of variations in suspended sediment. There was also at least one instance of forested area being flooded for a reservoir, an interesting situation showing extensive decrease in vegetation cover. Another interesting example was the removal of forest to put in a golf course actually showing up as an increase in vegetative reflectance on the greens areas, presumably due to the rapid growth and constant maintenance of these bright green and vibrant grassy areas as compared to the darker foliage of established forest.

Overall, it was realized that while automated change detection methods correctly performed and rigorously applied can provide a large amount of valuable information, the inherent difficulties and pitfalls of this approach must be recognized. These shortcomings can be ameliorated or overcome by the researcher with extensive knowledge of the study area. In addition, the best reference data available for ground truthing and accuracy assessment, and ancillary data related to the land use in the area must be consulted as thoroughly as possible.

This research could be improved in the future in several ways. First and foremost, the availability of high resolution color infrared aerial photographs for the earlier 1991 timeframe that corresponded with those from 1999 would have made it possible to detect subtle changes in vegetative state not visible in the panchromatic and true color aerial photographs. This would very possibly have reduced the errors introduced by the disconnection between increased vegetative reflectance detected by the Landsat sensor, and the static land use perceptible in the aerial photographs. Secondly, an even better geometric registration between the two Landsat images may have reduced the errors introduced by the high spatial resolution of land use changes along edge areas and urban fringes. Even though the RMSE of 0.23 pixels for the registration in this study was well below the 0.5 maximum acceptable value, it did not quite reach the 0.2 pixel RMS recommended by Dai and Khorram (1998). Achieving an RMSE of 0.2 or even less could possibly mitigate a certain amount of error resulting from the high resolution of land use changes in an urban area and the relatively low spatial resolution of the Landsat data.

It may also be beneficial to convert the digital numbers stored in the Landsat image pixels to top of atmosphere at-satellite reflectance values prior to image transformation and differencing. While the relative radiometric calibration of the two images and the nature of the subsequent image transformations undoubtedly removed much of the influence of differences in sensor type and performance and atmospheric conditions, converting to at-satellite reflectance takes this correction one additional step and may further minimize any differences in spectral characteristics that could introduce error into the analysis. Furthermore, by converting to at-satellite reflectance it would be possible to use the updated Tasseled Cap coefficients for the Landsat 7 ETM+ sensor developed by Huang et al. (2002). Finally, additional classifiers, such as those based textural characters and pattern recognition, can be experimented with in addition

to those based solely on spectral signatures, especially in areas of complex land use patterns along the urban-rural interface.

2. Implications of Research

While acknowledging the issues discussed above, the results of this study do indicate the effects and extent of the rapid urbanization that took place within Gwinnett County, GA, the 17th fastest growing U.S. county during the 1991-2000 study period. These changes corresponded closely with the known high population growth rate and land-intensive development characteristic of urban sprawl. According to a recent article in the Atlanta Journal-Constitution, a study just completed by the Natural Resources Spatial Analysis Laboratory at the University of Georgia (UGA), Institute of Ecology, led to similar conclusions (Shelton, 2005). Using analysis of Landsat imagery researchers found that the sixteen county area surrounding the City of Atlanta and its suburbs lost an average of fifty-four acres of trees every day during 1992-2000, and replaced this natural surface with twenty-eight acres of concrete, asphalt, rooftops and other impervious surfaces every day. Gwinnett County lost an average of eight acres of tree cover per day and added five acres of impervious urban surface each day during 1992-2000. In fact, Gwinnett County was second only to Hall County (9 acres/day) for tree loss in the UGA study, and tied with Fulton County for most added impervious surfaces (Shelton, 2005). Recall from the results of this study that approximately 12% of the total land area of Gwinnett County was cleared of vegetation during 1991-2000, a large percentage considering the urbanization that occurred prior to the beginning of the study period and has since continued.

The environmental and ecological consequences of urban sprawl have been well documented. Increased impervious surface results in increased pollutant runoff to streams and

impacts on drinking water quality, and increased risk of flooding. Loss of tree cover results in a reduction of air quality, increased heat island effect, siltation of streams, and loss of wildlife habitat and recreation areas. The increased reliance on the automobile in low density, land intensive development that characterizes urban sprawl results in greatly increased air pollution and noise pollution (Sierra Club, 1998). The National Wildlife Federation (NWF) has stated that within the United States as many as 1,200 species of plants and animals are endangered or threatened with extinction due to loss of habitats from urban sprawl (Heilprin, 2005). Blair (2004) found that urban sprawl resulted in extinction of some bird species followed by invasion of "urban exploiter" species and had the overall effect of reducing species richness and biodiversity. Michael Klemens of the Wildlife Conservation Society claims that habitat fragmentation is the primary threat to biological diversity in the United States, and that "sprawl creates a legacy of homogenized, dysfunctional ecosystems; reducing biodiversity, increasing biomass of a comparatively small number of adaptable species, and diminishing vital ecosystem services upon which all life depends" (Klemens, 2005).

With so much at risk, tools for assessing the impact of urban sprawl are crucial to understanding and ultimately mitigating its negative effects. Remote sensing data and change detection methods are powerful tools for quantifying and analyzing the degree and extent of landscape changes due to urbanization, and for presenting the results of such analyses to decision-makers and the general public in a visually compelling and effective manner. Remote sensing data covering vast areas are relatively inexpensive, easily obtainable, consistent, and easy to process and analyze. There are libraries of remote sensing data going back for decades, which provide an invaluable source of information for global and regional monitoring of the environment. It is hoped that studies such as this one will go some small way towards increasing

the understanding, accuracy and usefulness of change detection methods using remote sensing data. Ultimately it is hoped that such studies will improve the ability of researchers to assess and comprehend the effects of urban sprawl on the landscape its and natural communities, thereby providing a foundation for reducing and mitigating the negative effects that often accompany such changes.

REFERENCES

Blair, Robert (2004). The effects of urban sprawl on birds at multiple levels of biological organization. *Ecology and Society*, vol. 9 no. 5. http://www.ecologyandsociety.org/vol9/iss5/art2/

Boyd, D.S., G.M. Foody, W.J. Ripple (2002). Evaluation of approaches for forest cover estimation in the Pacific Northwest, USA, using remote sensing. *Applied Geography*, vol. 22 no. 4, pp.375-392.

Braswell, B.H., S.C. Hagen, S.E. Frolking, W.A. Salas (2003). A multivariable approach for mapping sub-pixel land cover distributions using MISR and MODIS: Application in the Brazilian Amazon region. *Remote Sensing of Environment*, vol. 87 no. 2-3, pp. 243-256.

Brivio, P.A., M. Maggi, E. Binaghi, I. Gallo (2003). Mapping burned surfaces in sub-Saharan Africa based on multi-temporal neural classification. *International Journal of Remote Sensing*, vol. 24 no. 20 , pp. 4003-4018.

Chen, Z.J., J. Chen, P.J. Shi, M. Tamura (2003). An IHS-based change detection approach for assessment of urban expansion impact on arable land loss in China. *International Journal Of Remote Sensing*, vol. 24 no. 6, pp.1353-1360.

Cohen, J. (1960) A coefficient of agreement for nominal scales. *Educational and Psychological Measurement*, vol. 20, pp. 37-46.

Cohen, W.B., M. Fiorella, J. Gray, E. Helmer, K. Anderson (1998). An efficient and accurate method for mapping forest clearcuts in the Pacific Northwest using Landsat imagery. *Photogrammetric Engineering And Remote Sensing*, vol. 64 no. 4, pp.293-300.

Cohen, W.B., T.A. Spies, R.J. Alig, D.R. Oetter, T.K. Maiersperger, M. Fiorella (2002). Characterizing 23 years (1972-95) of stand replacement disturbance in western Oregon forests with Landsat imagery. *Ecosystems*, vol. 5 no. 2, pp.122-137.

Collins J.B., C.E. Woodcock (1996). As assessment of several linear change detection techniques for mapping forest mortality using multitemporal Landsat TM data. *Remote Sensing of Environment*, vol. 56, pp. 66-77.

Coppin, P.R., M.E. Bauer (1996). Digital change detection in forest ecosystems with remote sensing imagery. *Remote Sensing Reviews*, vol. 13, pp. 207-234.

Crist, E.P., R.J. Kauth (1986). The tasseled cap de-mystified. *Photogrammetric Engineering and Remote Sensing*, vol. 52 no. 1, pp. 81-86.

Crist, E.P., R.C. Cicone (1984). Application of the tasseled cap concept to simulated Thematic Mapper data. *Photogrammetric Engineering and Remote Sensing*, pp. 343-352.

Crist, E.P., R.C. Cicone, (1984). A physically-based transformation of Thematic Mapper data--the tm tasseled cap. *IEEE Transactions on Geoscience and Remote Sensing*, vol. 22 no. 3, May, pp. 256-263.

Dai, A., K. E. Trenberth, and T. Karl (1998). Global variations in droughts and wet spells: 1900-1995. Geophysical Research Letters, vol. 25, pp. 3367-3370.

Dai, X., S. Khorram (1998). The effects of image misregistration on the accuracy of remotely sensed change detection. *IEEE Transactions on Geoscience and Remtote Sensing*, vol. 36 no. 5, September 1998. pp. 1566-1577.

Dall'Olmo, G., A. Karnieli (2002). Monitoring phonological cycles of desert ecosystems using NDVI and LST data derived from NOAA-AVHRR imagery. *International Journal of Remote Sensing*, vol. 23 no. 19, pp. 4055-4071.

Defries, R., J.R.G. Townshend, C. Dimiceli, M. Hansen, C. Huang, R. Sohlberg (2000). The 250 m global land cover change product form the Moderate Resolution Imaging Spectroradiometer of NASA's Earth Observing System. *International Journal of Remote Sensing*, vol. 21 no. 6-7, pp. 1433-1460.

Defries, R.S., J.R.G Townshend (1999). Global land cover characterization from satellite data: from research to operational implementation? *Global Ecology and Biogeography*, vol. 8 no. 5, pp. 367-379.

Diuk-Wasser, M.A., M. Bagayoko, N. Sogoba, G. Dolo, M.B. Toure, S.F. Traore, C.E. Taylor (2004). Mapping rice field anopheline breeding habitats in Mali, West Africa, using Landsat ETM+ sensor data. *International Journal of Remote Sensing*, vol. 25 no. 2, pp. 359-376.

Du, Y., P.M. Teillet, J. Cihlar (2002). Radiometric normalization of multitemporal high-resolution satellite images with quality control for land cover change detection. *Remote Sensing of Environment*, vol. 82, pp. 123-134.

Flanigan, J.C. (1943). History of Gwinnett Co., GA 1818-1943 Vol. I. Moreno Press, Inc., Buford, GA.

Fuller, D.O., M. Fulk (2001). Burned area in Kalimantan, Indonesia mapped with NOAA-AVHRR and Landsat TM imagery. *International Journal Of Remote Sensing*, vol. 22 no. 4, pp.691-697.

Fung T., W. Siu (2000). Environmental quality and its changes, an analysis using NDVI. *International Journal of Remote Sensing*, vol. 21 no. 5, pp. 1011-1024.

Gillies, R.R., J.B. Box, J. Symanzik, E.J. Rodemaker (2003). Effects of urbanization on the aquatic fauna of the Line Creek watershed, Atlanta – a satellite perspective. *Remote Sensing Of Environment*, vol. 86 no. 3, pp. 411-422.

Giri, C., P. Defourny, S. Shrestha (2003). Land cover characterization and mapping of continental Southeast Asia using multi-resolution satellite sensor data. *International Journal of Remote Sensing*, vol. 24 no. 17, 4181-4196.

Guild, L.S., W.B. Cohen, J.B. Kaufmann (2004). Detection of deforestation and land conversion Rondonia, Brazil using change detection techniques. *International Journal of Remote Sensing*, vol. 25 no. 4, pp.731-750.

Hall, F. G., D.E. Strebel, J.E. Nickeson, S.J. Goetz (1991). Radiometric rectification: toward a common radiometric response among multidate, multisensor images. *Remote Sensing of Environment*, vol. 35, pp. 11-27.

Haralick, R. M., K. Shanmugan, I. Dinstein (1973). Texture features for image classification. *IEEE Transactions on System, Man and Cybernetics*, SMC-3, no. 6, pp. 610-621.

Hayes, D.J., S.A. Sader (2001). Comparison of Change-Detection Techniques for Monitoring Tropical Forest Clearing and Vegetation Regrowth in a Time Series. *Photogrammetric Engineering & Remote Sensing*, vol. 67, no. 9, pp. 1067-1075.

Heo, J., T.W. FitzHugh (2000). A standardized radiometric normalization method for change detection using remotely sensed imagery. *Photogrammetric Engineering & Remote Sensing*, vol. 66 no. 2, February 2000, pp. 173-181.

Huang, C., B. Wylie, L. Yang, C. Homer, G. Zylstra (2002). Derivation of a tasseled cap transformation based on Landsat 7 at-satelite reflectance. *International Journal of Remote Sensing*, vol. 23 no. 8, pp. 1741-1748.

Indrabudi, H., A. DeGier, L.O. Fresco (1998). Deforestation and its driving forces: A case study of Riam Kanan watershed, Indonesia. *Land Degradation & Development*, vol. 9 no. 4, pp.311-322.

Jantzen, D.T. (2004). A comparison of radiometric correction methods for Landsat TM data: radiometric correction with no atmospheric data or ground targets. Online paper by M.Sc. Candidate, Natural Resources and Environmental Studies, University of Northern British Columbia. http://www.gis.unbc.ca/projects/radio/introduction.html

Jensen, J. (1986). Introductory Digital Image Processing: A Remote Sensing Perspective. Prentice-Hall, Englewood Cliffs NJ. ISBN 0-13-500828-X.

Kauth, R. J., G.S. Thomas (1976). The tasseled cap -- a graphic description of the spectral-temporal development of agricultural crops as seen by Landsat. *Proceedings of the Symposium on Machine Processing of Remotely Sensed Data*, Purdue University of West Lafayette, Indiana, pp. 4B-41 to 4B-51.

Kuntz, S., F. Siegert (1999). Monitoring of deforestation and land use in Indonesia with multitemporal ERS data. International Journal Of Remote Sensing, vol. 20 no. 14, pp. 2835-2853.

Lambin, E.F. (1999). Monitoring forest degradation in tropical regions by remote sensing: some methodological issues. *Global Ecology and Biogeography*, vol. 8, pp. 191-198.

Lefsky, M.A., W.B. Cohen, S.A. Acker, G.G. Parker, T.A. Spies, D. Harding (1999). Lidar remote sensing of the canopy structure and biophysical properties of Douglas-fir western hemlock forests. *Remote Sensing Of Environment*, vol. 70 no. 3, pp.339-361.

Li, XB, Y.H. Chen, P.J. Shi, J. Chen (2003). Detecting vegetation fractional coverage of typical steppe in northern China based on multi-scale remotely sensed data. *Acta Botanica Sinica*, vol. 45 no. 10, pp.1146-1156.

Lillesand, T.M., R.W. Kiefer (2000). Remote Sensing and Image Interpretation, Fourth edition. John Wiley & Sons, Inc. NYC. ISBN 0-471-25515-7.

Liu, J.Y., D.F. Zhuang, D. Luo, X. Xiao (2003). Land-cover classification of China: integrated analysis of AVHRR imagery and geophysical data. *International Journal Of Remote Sensing*, vol. 24 no. 12, pp.2485-2500.

Lo, C.P., X.J. Yang (2002). Drivers of land-use/land-cover changes and dynamic modeling for the Atlanta, Georgia Metropolitan Area. *Photogrammetric Engineering And Remote Sensing*, vol. 68 no. 10, pp. 1073-1082.

Lu, D.S., E. Moran, M. Batistella (2003). Linear mixture model applied to Amazonian vegetation classification. *Remote Sensing of Environment*, vol. 87 no. 4, pp. 456-469.

Lu, J. (2003). Marine oil spill detection, statistics and mapping with ERS SAR imagery in south-east Asia. *International Journal Of Remote Sensing*, vol. 24 no. 15, pp. 3013-3032.

Lutgens, F.K., E.J. Tarbuck (1995). The Atmosphere: An Introduction to Meterology. Prentice Hall, Englewood Cliffs, NJ.

Lyon, J.G., D. Yuan, R.S. Lunetta, C.D. Elvidge (1998). A change detection experiment using vegetation indices. *Photogrammetric Engineering and Remote Sensing*, vol. 64 no. 2, pp. 143-150.

Mayaux, P., Y. Rauste, A. Rosenquist, M. Simard, S.S. Saatchi (2000). The Global Rain Forest Mapping Project JERS-1 radar mosaic of tropical Africa: Development and product characterization aspects. *IEEE Transactions on Geoscience and Remote Sensing*, vol. 38 no. 5, pp. 2218-2233.

Melack, J.M., E.M.L.M. Novo, C.C.F. Barbosa, M. Gastil (2003). Dual-season mapping of wetland inundation and vegetation for the central Amazon basin. *Remote Sensing of Environment*, vol. 87 no. 4, pp. 404-428.

Morisette , J.T. (1997). Satellite Based Change Detection. Ch. 4 from 'Using Generalized Linear Models to Enhance Satellite Based Land Cover Change Detection' (Doctoral Dissertation, North Carolina State University, 1997).
http://www.lib.ncsu.edu/etd/public/etd-151111139751001/chap-4.pdf

Nonomura, A., K. Sanga-Ngoie, K. Fukuyama (2003). Devising a new digital vegetation model for eco-climatic analysis in africa using GIS and NOAA AVHRR data. *International Journal of Remote Sensing*, vol. 24 no. 18, pp. 3611-3633.

Odum, E. P. (1971). Fundamentals of ecology, 3rd ed. W. B. Saunders, Philadelphia.

Pelkey, N.W., C.J. Stoner, T.M. Caro (2003). Assessing habitat protection regimes in Tanzania using AVHRR NDVI composites: comparisons at different spatial and temporal scales. *International Journal of Remote Sensing*, vol. 24 no. 12, pp. 2533-2558.

Potter, C., P.N. Tan, M. Steinbach, S. Klooster, V. Kumar, R. Myeni, V. Genovese (2003). Major disturbance events in terrestrial ecosystems detected using global satellite data sets. *Global Change Biology*, vol. 9 no. 7, pp. 1005-1021.

Ridd, M.K., J. Liu (1998). A comparison of four algorithms for change detection in an urban environment. *Remote Sensing of Environment*, vol. 63, pp. 95-100.

Roberts, D.A., M. Keller, J.V. Soares (2003). Studies of land-cover, land-use, and biophysical properties of vegetation in the Large Scale Biosphere Atmosphere experiment in Amazonia. *Remote Sensing of Environment*, vol. 87 no. 4, pp. 377-388.

Runnstrom, M.C. (2003). Rangeland development of the Mu Us sandy land in semiarid China: An analysis using landsat and NOAA remote sensing data. *Land Degradation & Development*, vol. 14 no. 2, pp.189-202.

Sabol, D.E., A.R. Gillespie, J.B. Adams, M.O. Smith, C.J. Tucker (2002). Structural stage in Pacific Northwest forests estimated using simple mixing models of multispectral images. *Remote Sensing Of Environment*, vol. 80 no. 1, pp.1-16.

Seto, K.C., R.K. Kaufmann (2003). Modeling the drivers of urban land use change in the Pearl River Delta, China: Integrating remote sensing with socioeconomic data. Land Economics, vol. 79 no. 1, pp.106-121.

Siegert, F., A.A. Hoffmann (2000). The 1998 forest fires in East Kalimantan (Indonesia): A quantitative evaluation using high resolution, multitemporal ERS-2 SAR images and NOAA-AVHRR hotspot data. *Remote Sensing Of Environment*, vol. 72 no. 1, pp.64-77.

Shelton, S. (2005). Study: 54 Acres of Trees Lost Daily. Atlanta Journal-Constitution, Issues Section, Physical Environment, April 15 2005.

Smith, C., N. Brown (1999). ERDAS Field Guide, Fifth Edition. ERDAS Inc, Atlanta, GA.

Song, C., C.E. Woodcock, K.C. Seto, M.P. Lenney, S.A. Macomber (2001). Classification and change detection using Landsat TM data: when and how to correct atmospheric effects? *Remote Sensing of Environment*, vol. 75, pp. 230-244.

Souza, C., L. Firestone, L.M. Silva, D. Roberts (2003). Mapping forest degradation in the Eastern Amazon from SPOT 4 through spectral mixture models. *Remote Sensing of Environment*, vol. 87 no. 4, pp. 494-506.

Stibig, H.J., R. Beuchle, F. Achard (2003). Mapping of the tropical forest cover if insular Southeast Asia from SPOT4-Vegetation images. *International Journal Of Remote Sensing*, vol. 24 no. 18, pp. 3651-3662.

Stow, D.A. (1998). Reducing the effects of misregistration on pixel-level change detection. *International Journal of Remote Sensing*, vol. 20 no. 12, pp. 2477-2483.

Symeonakis, E., N. Drake (2004). Monitoring desertification and land degradation over sub-Saharan Africa. *International Journal of Remote Sensing*, vol. 25 no. 3, pp. 573-592.

Tobler, M.W., R. Cochard, P.J. Edwards (2003). The impact of cattle ranching on large-scale vegetations patterns in a coastal savanna in Tanzania. *Journal of Applied Ecology*, vol. 40 no. 3, pp. 430-444.

Wang, R.H., Z.L. Fan, H.Z. Zhang, Y.P. Chen, Y.J. Ma (2002). Remote sensing analysis of desert vegetation and its landscape changes: The case in middle reaches of Tarim, River Basin, Xinjiang, China. *Science In China Series D-Earth Sciences*, vol. 45 supp. D, pp.54-58.

Wharton, C.H. (1977). The Natural Environments of Georgia. Georgia Department of Natural Resources Office of Planning & Research, Atlanta, GA.

Wilson, C. (1997). A comparison of multispectral change detection methods; principal componentsanalysis, principal components analysis on difference, normalized difference vegetation index, and kauth thomas transformation using multitemporal landsat mss data. *Project for Course 45.583,Professor Doug King, Carlton Univ., CA.*

Wilson, H.G., T. Nelson, B. Boots, M.A. Wulder (2004). Using a spatial statistic threshold technique for defining change in a forested environment. Waterloo Laboratory for Earth Observations (WatLEO), Department of Geography, University of Waterloo, Ontario Canada.

Wimberly, M.C., T.A. Spies (2001). Modeling landscape patterns of understory tree regeneration in the Pacific Northwest, USA. *Applied Vegetation Science*, vol. 4 no. 2, pp.277-286.

Yang, X.J. (2002). Satellite monitoring of urban spatial growth in the Atlanta metropolitan area. *Photogrammetric Engineering And Remote Sensing*, vol. 68 no. 7, pp. 725-734.

Yang, X., C.P. Lo (2002). Using a time series of satellite imagery to detect land use and land cover changes in the Atlanta, Georgia metropolitan area. *International Journal of Remote Sensing*, vol. 23 no. 9, pp. 1775-1798.

Yang, X., C.P. Lo (2000). Relative radiometric normalization performance for change detection from multi-date satellite images. *Photogrammetric Engineering & Remote Sensing*, vol. 66 no. 8, August 2000, pp. 967-980.

Yu, F., K.P. Price, J. Ellis, J.J. Feddema, P. Shi (2004). Interannual variations of the grassland boundaries bordering the eastern edges of the Gobi Desert in central Asia. *International Journal Of Remote Sensing*, vol. 25 no. 2, pp. 327-346.

Yu, F.F., K.P. Price, J. Ellis, P. Shi (2004). Response of seasonal vegetation development to climatic variations in eastern central Asia. *Remote Sensing of Environment*, vol. 87 no. 1, pp. 42-54.

Yuan D., C. Elvidge (1998). NALC land cover change detection pilot study: Washington D.C. area experiments. *Remote Sensing of Environment*, vol. 66, pp. 166-178.

Zhu, Z.L. (2003). Global forest cover mapping for the United Nations Food and Agriculture Organization Forest Resources Assessment 2000 program. *Forest Science*, vol. 49 no. 3, pp. 369-380.

Zhu, Z.L., J. Cihlar, C. Giri, I. Olthof (2004). Land cover mapping of north and central America – Global Land Cover 2000. *Remote Sensing of Environment*, vol. 89 no. 1, Jan. 15 2004, pp. 116-127.

ONLINE REFERENCES

Atlanta Regional Commission (2005), accessed 6/04. Regional Data.
http://www.atlantaregional.com/regionaldata/regionaldata.html

American Heritage® Dictionary of the English Language, Fourth Edition
Copyright © 2000 by Houghton Mifflin Company. Accessed 6/04. www.dictionary.com

Buckhead Civic Association, (2005), accessed 6/04. Fort Peachtree.
http://www.buckhead.net/history/fort-peachtree/

Bureau of Land Management (2004), accessed 6/04. Southern Piedmont Executive Summary.
http://www.blm.gov/wildlife/pl_11sum.htm

Global Land Cover Facility Earth Science Data Interface.
http://glcfapp.umiacs.umd.edu:8080/esdi/index.jsp

Heilprin, John (2005), accessed 5/05. Groups: sprawl threatens plants, animals. Duluth News Tribune, January 11 2005. http://www.duluthsuperior.com/mld/duluthsuperior/news/politics/10619970.htm

Klemens, Michael W. (2005), accessed 5/05. Nature in fragments: the legacy of urban sprawl. Metropolitan Conservation Alliance, Wildlife Conservation Society. http://research.amnh.org/biodiversity/symposia/archives/sprawl/presenterbios/bioklemens.html

Minnesota Department of Natural Resources (1999), accessed 6/04. Change Detection Methods. http://www.ra.dnr.state.mn.us/changeview/change_tech.html

NASA, (1997), accessed 6/04. High Spatial Resolution Airborne Multispectral Thermal Infrared Data to Support Analysis and Modeling Tasks in EOS IDS Project ATLANTA http://www.ghcc.msfc.nasa.gov/atlanta/

National Oceanic and Atmospheric Administration (NOAA), (2005), accessed 6/04. Palmer Drought Severity Index (PDSI) information. http://www.drought.noaa.gov/palmer.html

NOAA Coastal Services Center, Land Cover Analysis Technical FAQs page (2005), accessed 5/05. http://www.csc.noaa.gov/crs/lca/faq_tech.html

Sabin, Pat (2004), accessed 6/04. Gwinnett historical data. http://patsabin.com/gwinnett/history.htm http://patsabin.com/gwinnett/index.htm http://patsabin.com/gwinnett/text.htm

Sierra Club (1998). 1998 Sierra Club Sprawl Report: 30 Most Sprawl-Threatened Cities http://www.sierraclub.org/sprawl/report98/atlanta.asp

Sierra Club (1998), accessed 6/04. Club Exposes the Dark Side of Sprawl. The Planet Newsletter, October 1998, Vol. 5, No. 8. http://www.sierraclub.org/planet/199808/sprawl.asp

Taulman, James F. (2005), accessed 5/05. Partners In Flight Bird Conservation Plan Habitat Map Site, University of Arkansas Center for Advanced Spatial Technologies. http://www.cast.uark.edu/pif/main/maincont.htm

US Census Bureau (2003), accessed 6/04. 4 of 10 fastest growing counties. http://www.census.gov/Press-Release/www/2003/cb03-65.html

US Census Bureau (2004), accessed 6/04. County and City Data Book http://www.census.gov/statab/www/ccdb.html

US Census Bureau (2004), accessed 6/04. Five Georgia Counties Among the Top 10 Fastest-Growing; Loudoun, Va., Ranks First. http://www.census.gov/Press-Release/www/releases/archives/population/001758.html

US Census Bureau (2005), accessed 6/04. Georgia Quickfacts. http://quickfacts.census.gov/qfd/states/13000.html

US Census Bureau (2005), accessed 6/04. Georgia Quicklinks. http://quickfacts.census.gov/qfd/states/13000lk.html

US Census Bureau (2001), accessed 6/04. Metropolitan Area Rankings List. http://www.census.gov/Press-Release/metrolis.htm

US Census Bureau (2004), accessed 6/04. State and Metropolitan Area Data Book 5th Edition. http://www.census.gov/statab/www/smadb.html

United States Geological Survey (USGS), (2004), accessed 5/05. Apalachicola-Chattahoochee-Flint River Basin NAWQA Study. http://ga.water.usgs.gov/nawqa/basin3.html

University of Georgia College of Agricultural and Environmental Sciences, (2000), accessed 5/05. http://georgiafaces.caes.uga.edu/getstory.cfm?storyid=968

Appendix: Piedmont Environments found in Gwinnett County, GA, and the Dominant Tree Species Found There

Tree Species		Environments							
Common Name	**Latin Binomial**	**Bluff and Ravine Forests of northern affinities (Miner Mtn.)**	**Bluff, slope and ravine forests**	**Evergreen Heath bluffs**	**Oak-Hickory Climax forest**	**Xeric bluffs**	**Mixed Pine-Hardwood colluvial forests**	**Pine-Hardwood Xeric ridge and slope forests**	**Rock Outcrops**
Ash, White	*Fraxinus americana*		X						
Basswood	*Tilia americana*				X		X		
Beech	*Fagus*	X	X				X		
Cedar, Red	*Juniperus virginiana*		X			X			X
Chestnut, American	*Castanea dentata*				X				
Dogwood	*Cornus*		X		X			X	
Elm, American	*Ulmus americana*				X				
Elm, Winged	*Ulmus alata*				X				
Gum, Black	*Nyssa sylvatica*		X		X	X	X		
Gum, Sweet	*Nyssa ????*		X		X		X		
Hickory, Mockernut	*Carya tomentosa*		X		X			X	
Hickory, Pale	*Carya pallida*				X				
Hickory, Pignut	*Carya glabra*		X		X		X		
Hickory, Red	*Carya ovalis*				X			X	
Hickory, Shagbark	*Carya ovata*				X		X		
Hickory, Southern Shagbark	*Carya carolinae septentrionales*				X				
Ironwood	*Carpinus caroliniana*						X		
Magnolia, Bigleaf	*Magnolia macrophylla*	X					X		
Magnolia, Umbrella	*Magnolia tripetela*	X					X		
Maple, Florida	*Acer floridanum*		X						
Maple, Red	*Acer rubrum*		X		X		X		
Maple, Southern Sugar	*Acer saccharum*				X				
Oak, Black	*Quercus velutina*	X	X		X			X	
Oak, Blackjack	*Quercus marilandica*				X	X		X	

Common Name	Latin Binomial	Bluff and Ravine Forests of northern affinities (Miner Mtn.)	Bluff, slope and ravine forests	Evergreen Heath bluffs	Oak-Hickory Climax forest	Xeric bluffs	Mixed Pine-Hardwood colluvial forests	Pine-Hardwood Xeric ridge and slope forests	Rock Outcrops
Oak, Chestnut	*Quercus prinus; Quercus montana*	X	X				X	X	
Oak, Northern Red	*Quercus borealis*	X	X		X				
Oak, Post	*Quercus stellata*				X	X			
Oak, Scarlet	*Quercus coccinea*		X		X			X	
Oak, Southern Red	*Quercus falcata*		X	X	X	X		X	
Oak, White	*Quercus alba*	X	X	X	X	X	X	X	
Pine, Loblolly	*Pinus taeda*						X	X	X
Pine, Longleaf	*Pinus palustris*						X		
Pine, Shortleaf	*Pinus echinata*				X	X	X	X	
Poplar, Tulip	*Liriodendron tulipfera*	X	X				X	X	
Poplar, Yellow	*Liriodendron tulipfera*				X				
Sourwood	*Oxydendrum arboreum*	X	X		X	X	X	X	